Evaluating small unmanned aerial systems for detecting drought stress in turfgrass

by

Mu Hong

B.S., South China Agricultural University, 2016

A THESIS

submitted in partial fulfillment of the requirements for the degree

MASTER OF SCIENCE

Department of Horticulture and Natural Resources
College of Agriculture

KANSAS STATE UNIVERSITY
Manhattan, Kansas

2019

Approved by:

Major Professor
Dale Bremer

Copyright

Abstract

Recent advances in small unmanned aerial systems (sUAS) may provide rapid and accurate methods for turf research and management. The study was to evaluate early drought detection ability of ultra-high resolution remote sensing with sUAS technology, and compare it with traditional techniques on fairway-height 'Declaration' creeping bentgrass (*Agrostis stolonifera* L.) treated from severe deficit to well-watered irrigation (15, 30, 50, 65, 80, and 100% evapotranspiration replacement). Airborne measurements with a modified digital camera mounted on a hexacopter included reflectance from broad bands (near infrared [NIR, 680-780 nm], and green and blue bands [overlapped, 400-580 nm]), from which eight vegetation indices (VIs) were derived for evaluation. Canopy temperature was measured only in the final year with a thermal infrared camera mounted on a drone. Traditional measurements were volumetric water content (VWC), visual quality (VQ), percentage green cover (PGC), and VIs from handheld devices. Declines in VWC in irrigation-deficit treatments were consistently detected by the NIR band and six VIs from sUAS, and NDVI and red band from a handheld device, before drought stress was evident in VQ. These bands and indices predicted drought stress at least one week before symptoms appeared in VQ. Canopy temperature predicted drought stress as early as the best VIs and NIR, 16 days before symptoms appeared in VQ in 2017. Only the NIR and GreenBlue VI [(green-blue)/(green+blue)] consistently predicted drought stress throughout three years. Results indicate using ultra-high resolution and thermal remote sensing with sUAS can detect drought stress before it is visible to the human eye and may prove viable for irrigation management on turfgrass.

Table of Contents

List of Figures

List of Tables

Acknowledgements

I would like to thank my advisor, Dr. Dale Bremer, and committee members Drs. Steve Keeley, Jared Hoyle, and Catherine Lavis, as well as Drs. Jack Fry and Deon van der Merwe for their advising, patience, and encouragement. I couldn't make it without you!

I appreciated lots of help and cooperation from Trevor Witt and Drs. Brian McCornack and Ganesh Bhattarai for calibration events, insect consultations from Dr. Raymond Cloyd, and statistical consultations and knowledge from Jia Liang.

Grateful thanks to Cliff Dipman for maintaining plots and facilitating field work at the Rocky Ford Turfgrass Research Center, and helps from student workers Kalli Morland, Justin Jones, Gage Knudson, Lydia Fry, Slade Loewen, and Joel Marker.

I appreciated friendships and support of fellow graduate students Drs. Ross Braun and Mingying Xiang, as well as Wes Dyer and Nick Mitchell.

Thanks to the United States Golf Association and the Kansas Turfgrass Foundation for providing funding for this research, and Lebanon Turf Inc. for seed supply. Thanks to all the faculty, staff, and fellow graduate students in the Department of Horticulture and Natural Resources.

Dedication

I dedicated this work to my loving father and mother.

Chapter 1 - Early Drought Stress Detection in Turfgrass Utilizing Spectral Reflectance Imaging via Small Unmanned Aircraft Systems

Abstract

Recent advances in small unmanned aircraft system (sUAS) may provide a rapid and accurate method for turfgrass research and management with less labor. We evaluated the ability to detect drought stress early utilizing sUAS technology combined with ultra-high remote sensing. Results were compared with traditional, ground-based techniques in creeping bentgrass (*Agrostis stolonifera* L.) treated with irrigation levels from well-watered to severe deficit [100% to 15% evapotranspiration (ET) replacement]. Airborne measurements of three broadband reflectances [near infrared (NIR, 680-780 nm), and green (G) and blue (B) bands (overlapped, 400-580 nm)] and eight derived vegetation indices (VIs) were evaluated during the summers of 2015-2017. Traditional measurements included volumetric water content (VWC), visual quality (VQ), percentage green cover (PGC), soil temperature, and remote sensing with handheld optical sensors. Declines in VWC in deficit-irrigation treatments were consistently detected with the NIR broadband and six of eight VIs from sUAS, and the normalized difference vegetation index (NDVI) and red narrowband from a handheld optical sensor, before drought stress was visible. These bands and indices predicted drought stress one-to-two weeks before symptoms appeared in VQ and PGC in 2016 and 2017, but the most consistent and sensitive parameters of sUAS throughout the three-year study were the NIR and GreenBlue VI [(G-B)/(G+B)]. Results

indicated ultra-high spatial resolution remote sensing with sUAS detects drought stress before it is visible and may prove viable for irrigation management in turfgrass.

Introduction

There are an estimated 13 to 20 million hectares of turfgrass in the United States (Milesi et al., 2005). Climate change with increased temperatures and more variable precipitation will potentially incur more stresses on turfgrasses (Hatfield, 2017). Drought stress may increase with evapotranspiration in regions under rising temperatures (Asadi-Zarch et al., 2015). Various strategies have been investigated to conserve limited water resources in turfgrass management including deficit irrigation, breeding and selecting cultivars with better drought resistance and recovery abilities, maintaining acceptable quality with deficit irrigation, and using recycled water (Su et al., 2007; Harivandi et al., 2008; Lewis et al., 2012; Goldsby et al., 2015). Nevertheless, to increase the efficiency of irrigation management while maintaining acceptable turfgrass quality, rapid and accurate methods of detecting turfgrass water status are needed to evaluate drought stress. This is particularly true for turfgrass managers who may be required to make prompt decisions about irrigation timing, amounts, and other management strategies.

Conventional sampling methods are labor and time consuming (e.g. gravimetric or volumetric water content sampling over large areas). Consequently, using conventional methods to measure time-sensitive parameters could be confounded by dynamic physiological changes that occur during sampling in the field. For example, relative levels of xanthophyll cycle pigments, indicators of photosynthetic light use efficiency, can change on a scale of minutes, which challenges conventional sampling methods (Sims and Gamon, 2002). To meet that challenge, a photochemical reflectance index was developed to rapidly estimate xanthophyll

cycle pigments. Thus, remoting sensing *in situ* is valuable in providing real-time and non-destructive methods of crop evaluation. Advancing applications of spectral reflectance for detecting plant stress, such as during early onset of drought, has the potential to increase accuracy and efficiency for turf research and management.

Spectral reflectance signatures from plants contain valuable information that may indicate their physical and physiological condition (Knipling, 1970). Remote sensing of turfgrass has been used to identify drought and other stressors of turfgrass (Bell et al., 2000; Jiang and Carrow 2005; Bremer et al., 2011b). However, remote sensing in turfgrass is typically conducted with handheld or ground vehicle-mounted devices, which can be cumbersome and time-consuming, especially for rough terrain or over large areas (Bell et al., 2002).

Vegetation indices from spectral reflectance measurements

To date, canopy spectral reflectance of turf has been extensively investigated as an objective method to evaluate turfgrass visual quality. Reflectance of the visible spectrum is highly affected by photosynthetic components, while NIR is influenced by leaf cell structures and water content (Knipling, 1970; Carter, 1991). Broadbands peaking at 710, 900 to 950, and 1200 nm were used to determine turf quality, and narrowbands peaking at 664 to 687 nm were used to determine turf quality and leaf firing (Jiang and Carrow, 2005). Hyperspectral radiometry of certain wavebands of red and near infrared reflectance (NIR) showed significant correlation with green leaf area index and has the potential to predict it, but the accuracy of these models was affected by seasonal environmental changes (An et al., 2015).

Derivatives from spectral reflectance such as the normalized difference vegetation index (NDVI), computed as (NIR-red)/(NIR+red), are popularly investigated as indicators of plant physiology because they capture reflectance differences between the visible and NIR spectrums. For a senescing canopy such as drought-stressed turfgrass, reflectance increases in the visible spectrum because of reduced absorption due to limited photosynthesis. Conversely, reflectance in the NIR typically decreases with canopy senescence, with the overall result being a decline in NDVI (Huete et al., 2002; Bremer et al., 2011b). Thus, NDVI typically has strong and positive relationships with tissue N, shoot density, green percent coverage, and aboveground biomass (Huete et al., 2002; Bell et al., 2004; Bremer et al., 2011b). However, these relationships may be affected or confounded by species and environmental and cultural factors such as seasonality, nitrogen fertility, mowing height and irrigation (Xiong et al., 2007; Bremer et al., 2011a; Lee et al., 2011). It was recommended that turfgrass evaluations with NDVI be conducted under homogenous conditions such as within species and within mowing heights when comparing among treatments (Bremer et al., 2011a; Lee et al., 2011). Therefore, there are still difficulties for wide applications of NDVI in golf course management under various field conditions with uncontrolled factors.

Small unmanned aircraft systems in turfgrass

With recent advances in remote sensing platforms, specifically small unmanned aircraft systems (sUAS) technology, remote sensing equipment can be deployed extensively and rapidly over large areas. For example, a fixed-wing sUAS can cover about 4.6 ha per minute (Ireland-

Otto et al., 2016). Consequently, sUAS can cover areas the size of an 18-hole golf course much more quickly than conventional handheld or ground-vehicle-based platforms.

Other advantages of applying sUAS include flexibility and simple operational requirements, relatively low cost, reliability and safety, and excellent performance for qualified data acquisition in low altitude environments (Rango et al., 2006; Pajares, 2015). For example, an sUAS was safely deployed over a green roof structure to measure its vegetative properties in a densely-populated university campus in an urban area (Van der Merwe et al., 2017). That study revealed correlations between vegetative cover and surface temperature and NDVI values using colored-infrared (modified Canon S100) and thermal sensors mounted on the sUAS. Multispectral and thermal sensors have also been mounted on the sUAS for plant stress observations over agricultural fields and rangelands to determine optimal combinations of spatial and spectral resolution, measurement frequencies, and costs compared to satellite sensors (Rango et al., 2006; Berni et al., 2009; Wang et al., 2014).

Although applications of sUAS have been advanced in agricultural fields and rangelands and tallgrass prairie, little research has been conducted in turfgrass (Rango et al., 2006; Berni et al., 2009; Wang et al., 2014). Fenstermaker-Shaulis et al. (1997) conducted a pioneer irrigation study using a fixed wing sUAS, and found that NDVI was influenced by the irrigation uniformity and amount on tall fescue. Small UAS and spectral remote sensing applications in turfgrass positively detected different nitrogen statuses of ‘Patriot’ bermudagrass, ‘Zeon’ zoysiagrass and ‘Salam’ seashore paspalum (Caturegli et al., 2016). Finally, video imagery obtained from sUAS,

combined with new algorithms, may hold promise in mapping and classifying turfgrass to differentiate it from surrounding land use with a goal to more precisely determine the area that needs irrigation (Perea-Moreno et al., 2016).

Real-time measurements covering large areas in a short period (e.g., over golf courses or turfgrass sod farms) and acquiring synchronous data across the field is critical for detecting dynamic conditions of turfgrass stress, such as during drought. Furthermore, such timely and non-destructive measurements may increase management efficiency of golf courses, including irrigation management.

Therefore, our objectives were to evaluate the ability of sUAS technology to detect early drought stress in turfgrass across a gradient of irrigation regimes from well-watered to severe deficit irrigation and compare results with traditional (handheld) techniques. Specifically, our goal was to determine whether drought stress in turfgrass could be detected before it became visible to the human eye. Presumably, such an ability would allow more precise scheduling of water applications with an overall goal of maintaining plant health while conserving water.

Methods and Materials

Research was conducted over three summers under an automatic rainout shelter at the Rocky Ford Turfgrass Research Center near Manhattan, Kansas (39°13''53''N, 96°34'51''W). The rainout shelter covered the whole study area (66 m^2) when precipitation reached 0.25 mm

and retracted an hour after rainfall ceased. The soil was a Chase silty clay loam (fine, smectitic, mesic Aquertic Argiudoll).

Irrigation treatments were applied to 'Declaration' creeping bentgrass (*Agrostis stolonifera* L.) in 24 plots (1.7 by 1.5 m^2 each) in a randomized complete block design rearranged every year (29 June to 31 Aug 2015; 1 July to 29 Aug 2016; 9 June to 31 Aug 2017). Irrigation amount was calculated from daily reference evapotranspiration (ET_o, hereafter referred to as ET) using on-site weather data (http://mesonet.k-state.edu/) and the American Society of Civil Engineers (ASCE) standardized reference ET equation (Walter et al., 2000). Six deficit-irrigation treatments were included to induce a gradient of drought stress symptoms within each of the four blocks: 15, 30, 50, 65, 80 and 100% ET replacement. Irrigation was applied three times per week by hand with a wand attached to a meter (Model 03N31, GPI, Inc.) and hose. The rainout shelter malfunctioned on 5 Aug 2017, permitting 19 mm of precipitation.

Maintenance

Creeping bentgrass was initially seeded at 48.8 kg/ha on 18 Sept. 2014. After the first year of irrigation-deficit treatments, plots fully recovered before the second-year experiment. After the second summer, due to severe damage by irrigation-deficit treatments, plots were reestablished by verticutting, seeding at 40 kg/ha and topdressing on 22 Sept. 2016. Plots were not cultivated during the dry-down periods to avoid damage to the turfgrass canopy during drought stress. In 2017, plots were aerified to promote growth four days before the dry down began. This slightly disrupted the turf canopy during the first week of measurements, but those

effects diminished rapidly thereafter. Plots were mowed three times a week at 15.9 mm and clippings were removed. Turfgrass plots were fertilized with 48.9 kg N ha^{-1} in May 2015, on 22 Sept. 2016, on 20 Apr., and 12 May 2017; 38.4 kg P ha^{-1} on 22 Sept. 2016 and 3.1 kg P ha^{-1} on 12 May 2017; 73.1 kg K ha^{-1} on 22 Sept. 2016 and 40.6 kg K ha^{-1} on 12 May 2017.

For preventative insect control, chlorantraniliprole (Acelepryn, Syngenta Crop Protection LLC) was applied at 0.26 kg a.i. ha^{-1} on 26 May 2017. For preventative weed control, dithiopyr (Dimension, Dow AgroSciences LLC) at 0.56 kg a.i. ha^{-1} and a mixture of propionic acid, 2,4-D acid and dicamba (Trimec bentgrass formula, PBI Gordon Corporation) at 0.76 kg a.i. ha^{-1} was applied in mid-April over 2015-2017. For preventative control of dollar spot and other diseases in 2017, triticonazole (Triton FLO, Bayer Environmental Science) and tetrachloroisophthalonitrile (Syngenta) was applied at 1.1 kg a.i. ha^{-1} on 28 May and 6.9 kg a.i. ha^{-1} on 23 June, respectively.

Data collection

All measurements were taken weekly (weather permitting) on cloud-free days with wind speed below 24 km/h and within 2.5 hours of local solar noon. On each measurement day, a series of ultra-high spatial resolution images (< 1-cm ground resolution) were collected with a modified Canon PowerShot S100 camera (MaxMax.com) identical to that used by Van der Merwe et al. (2017). The camera sensor was equipped with filters blocking visible red light and NIR above 780 nm while allowing visible blue (B) and green bands (G) (overlapped, 400-570 nm), and the transition of visible red edge to NIR band (690-780 nm) to pass to the sensor. The

camera was mounted on a hexacopter (DJI S800 EVO) flown at 15–25 m above ground level to achieve image overlap of at least 75%. The camera was set to manual mode with autofocus and ISO at 100, and the exposure level was set to be two stops below the standard while facing straight down towards turfgrass on the ground by adjusting shutter speed or f-stop. In 2015 and 2016, shutter speed was set to 1/2000 and only the f-stop was adjusted as described above. In 2017, f-stop was set to f/2.2 and only shutter speed was adjusted accordingly for the same exposure level. The same firmware on this camera was used throughout three years.

The resulting JPEG images were processed into averaged orthomosaics using Agisoft Photoscan Professional (v. 1.3.4 build 5067, Agisoft LLC). The image processing procedure involved the following steps: photo alignment using high accuracy and referenced pair preselection, building a surface mesh using a high polygon count, building texture using the average blending mode, and exporting an orthophoto in TIF format.

Treatment effects were analyzed from the orthophoto by extracting a square that included the center 60% of each plot surface using AgVISR (v. 2.1.6, AgVISR Services LLC). The three reflectance broadbands and eight vegetation indices (VIs, calculated from the three bands) were then evaluated for their ability to detect drought stress among treatments. According to AgVISR, the eight vegetation indices included NDVI Enhanced1 [(NIR+G-2B)/(NIR+G+2B)], NDVI Enhanced2 [(NIR+G-B)/(NIR+G+B)], NDVI Enhanced3 [(NIR-G-B)/(NIR+G+B)], Blue NDVI [(NIR-B)/(NIR+B)], Green NDVI [(NIR-G)/(NIR+G)], GreenBlue [(G-B)/(G+B)], NIR Blueratio (NIR-B), NIR GreenDiff [(NIR-G-B)/(NIR-G+B)].

The absolute scales of NDVI in the study are not directly comparable to a traditional 0 to 1 scale derived from calibrated sensors. Apparent band-intensities in images from converted cameras are influenced by specific camera sensor characteristics and in-camera image processing algorithms, a Bayer array filter that selectively filters light entering "blue", "green" and "red" locations on the sensor array, and the replacement of the infrared cut filter with a filter that transmits light in the 400-570 and 690-780 nm wavelength ranges. The resulting band intensities, compared to a sensor that is calibrated to true energy levels, are reduced in the near-infrared band intensity compared to the visible light bands. This can result in apparent NDVI values from vegetation that are below 0, compared to vegetation NDVI values from traditional sensors that typically range between 0 and 1. However, differences in relative reflectance values, when comparing visible bands to near infrared bands, are effectively captured by modified cameras and results in the ability to detect differences in vegetation similar to the differences that are detectable using traditional NDVI approaches (Fenstermaker-Shaulis et al., 1997; Wang et al., 2014; Van der Merwe et al., 2017). Therefore, the relationship between digital numbers of our modified camera and reflectance was also checked (Appendix A).

Additional measurements included volumetric water content (VWC), visual quality ratings (VQ), soil temperature (T_{soil}), NDVI by two handheld optical sensors, and percentage green cover (PGC). During the three-year experiment, VWC was measured at 0 to 7.6 cm in two random locations within each plot using time domain reflectometry (FieldScout TDR 300 Soil Moisture Meter, Spectrum Technologies). Two personnel evaluated VQ of turfgrass to reduce

individual biases on a numeric scale from 1 to 9 (1 = dead turf, 9 = uniform, green and dense turf, and 6 = minimally acceptable turf for use in home lawns) according to color, texture, density, and uniformity (Morris and Shearman, 1999; Bell et al., 2002). Soil temperature was measured with digital soil thermometers (DT310LAB Lab Digital Stem Thermometer, General Tools & Instruments LLC), with one reading per plot at 7.6 cm. Traditional measurements of NDVI were obtained at three random locations within each plot with a handheld, passive remote sensor [FieldScout CM1000 NDVI meter (FS), Spectrum Technologies]. The latter sensed ambient light reflectance peaking at wavelengths of 660 and 840 nm, which was used for computing NDVI (hereafter labeled $NDVI_{FS}$ to denote FieldScout). Each reading was collected at handheld height (approximately 0.9 m) with a conical field of view of about 6.5 cm diameter on the ground.

In the latter two years, a handheld active optical sensor [RapidScan CS-45 (RS), Holland Scientific)] was also used to measure traditional NDVI. The latter used self-generated light reflectance peaking at wavelengths of 670 (Red_{RS}), 730 (red edge, RE_{RS}) and 780 (NIR_{RS}) nm (bandwidths are proprietary) which allowed for computing NDVI [$(NIR_{RS}-Red_{RS})/(NIR_{RS}+Red_{RS})$, hereafter labeled $NDVI_{RS}$ to denote RapidScan] as well as normalized difference red edge index [$NDRE_{RS} = (NIR_{RS}-RE_{RS})/(NIR_{RS}+RE_{RS})$]. Each measurement was obtained at handheld height (approximately 0.9 m) to scan about 80% of each plot, with readouts of the average value of $NDVI_{RS}$ and $NDRE_{RS}$, and the maximum, minimum, standard deviation and coefficient of variation of each. Images were collected in 2016 and 2017 for PGC analysis

using the method of Karcher and Richardson (2005) (SigmaScan Pro v. 5.0, SPSS Science Marketing Dept.). Images were taken with a Nikon D5000 digital camera (f-stop of 5.6, 1/125 sec exposure time, and 800 ISO-speed; Nikon Inc.) using a lighted camera box (51 cm x 61 cm x 56 cm).

Statistical analysis

All parameters measured during the study were analyzed in PROC MIXED (SAS 9.4, SAS Institute Inc.) with irrigation treatment as a fixed effect, year as a random effect, and date as a repeated measure. Different variance-covariance structures {compound symmetry [CS], autoregressive [AR(1)], toeplitz [TOEP], heterogenous compound symmetry [CSH], heterogeneous autoregressive [ARH(1)], and heterogeneous Toeplitz [TOEPH]} were investigated to find the best fitting model of which the Bayesian Information Criteria value is the lowest. Then, all parameters were analyzed with irrigation treatments as a fixed effect in PROC GLIMMIX of SAS for each measurement date ($P < 0.05$). Comprehensive results were recorded in Appendix B. Spearman correlations between parameters were conducted using PROC CORR of SAS ($P < 0.05$).

Results and Discussion

Drought stress detection: Deficit-irrigation main effects

Note: The main effects for traditional, ground-based measurements are presented in Tables 1.1 and 1.2, while the main effects for sUAS measurements are in Table 1.3. Table 1.1

presents a 3-year analysis of those variables measured over the entire study. Because some ground-based measurements were only obtained in the final two years (i.e., PGC, $NDVI_{RS}$, $NDRE_{RS}$, Red_{RS}, RE_{RS}, and NIR_{RS}), the main effects for all ground-based variables over those two years are presented in Table 1.2. This required separate analyses for those variables presented in both Table 1.1 (3-yr analysis) and Table 1.2 (2-yr analysis). All sUAS reflectance variables were measured over the three years and therefore, a 3-year analysis of all sUAS variables are presented in Table 1.3.

Ground-based measurements

Over the entire three years of the study, the strongest response to irrigation treatments was in VWC, followed by VQ, $NDVI_{FS}$, and finally T_{soil} (Table 1.1). In the final two years, the strongest responses to irrigation levels were also in VWC and VQ (Table 1.2). However, measurements in those two years indicated PGC and all variables measured with the handheld active optical sensor (i.e., $NDVI_{RS}$, Red_{RS}, NIR_{RS}, RE_{RS}, and $NDRE_{RS}$) were more strongly associated with irrigation treatments than $NDVI_{FS}$ and T_{soil} (Table 1.2). Interestingly, it was generally more difficult to differentiate among the upper (65 to 100% ET) than the lower (15 to 50% ET) ends of deficit-irrigation treatments, probably because of less water stress among 65 to 100% ET treatments during the dry-down periods.

Irrigation treatment levels were best correlated with VWC every year ($r = 0.60$ to 76, $P < 0.0001$; data for other variables not shown). This strong correlation, combined with VWC having the strongest response to irrigation among measured parameters, as mentioned above, confirms

that a gradient of drought stress was achieved across irrigation treatments. By design, this created opportunities for detection and prediction of drought stress with remote sensing data as the dry downs progressed.

Remote sensing measurements from sUAS

The NIR band and six VIs (NDVI Enhanced1, NDVI Enhanced2, Blue NDVI, GreenBlue, NIR Blueratio, and NIR GreenDiff) measured from the sUAS consistently detected differences between higher irrigation treatments (i.e., 65% and above) and lower irrigation treatments (i.e., 30% ET and below) across the three years (Table 1.3). Of those, all except Blue NDVI differentiated the 30% and 15% ET treatments distinctly from each other. The NIR band and NDVI Enhanced1, NDVI Enhanced2, and NIR GreenDiff VIs also differentiated between the lower irrigation treatments (30% ET and below) and 50% and higher ET treatments. The ability of these VIs and the NIR band to detect drought stress was validated by their patterns similar to VWC among treatments (Tables 1.1 and 1.2) and suggests they have greater ability to detect drought than the other VIs and reflectance bands.

Daily analysis of aerial remote sensing data for drought prediction

As the dry downs progressed, there were clear changes in soil, canopy, and spectral reflectance properties that corresponded strongly with irrigation gradients (Figs. 1.1-1.3). During the dry-down period in each of the three years, VWC and VQ generally declined with deficit-irrigation treatment, and with time the patterns in VWC and VQ diverged among treatments (Figs. 1.1-1.3, A, B). The same trends were true for remoting sensing parameters measured by

sUAS. For example, the NIR reflectance and the GreenBlue VI gradually decreased with deficit-irrigation, with greater skews for 15 to 50% ET treatments (Figs. 1.1-1.3, C, D). Color-enhanced images of the plot area using NIR reflectance and the NDVI Enhanced3 VI revealed negligible differences among treatment plots early in the study (Fig.1.4, A and Fig.1.5, A), but striking differences by the study's end in 2017 (Fig.1.4, B and Fig.1.5, B).

Lower NIR in less-irrigated turfgrass is in agreement with results from previous research. Taghvaeian et al. (2013) found that average NIR reflectance decreased from 38% to 28% when water application was reduced from 74% to 38% of the total grass-based reference ET. Reflectance in the NIR decreases with senescence because of reductions in green leaf area, which result in less NIR scattering among leaf cells (Guyot, 1990; Roberts et al., 2012). The GreenBlue VI may capture absorption differentials between the green and blue bands, which may indicate ratio changes of carotenoid and chlorophyll caused by stress (Sims and Gamon, 2002). Chlorophyll absorbance occurs in both blue and red bands, affecting the two shoulders of the green band, while carotenoids absorb in the blue band, affecting only one side (Jensen, 2009).

In 2015, there were never significant differences in VQ between 65 and 100% ET treatments, even at the end of the dry down (Fig.1.1, 31 Aug.); this was likely because the irrigation treatments were higher early in the summer. Nevertheless, soils were significantly drier in 65% than 100% plots on 31 Aug., and NIR and GreenBlue VI were the only spectral

reflectance parameters acquired from sUAS that detected differences between these two treatments (Fig.1.1; Appendix B).

In 2016 and 2017, when deficit irrigation plots were exposed to greater drought stress than 2015, decreases in VQ lagged behind corresponding decreases in VWC by one to two weeks (Figs. 1.2A, 1.2B, 1.3A, and 1.3B). Similarly, decreases in VQ in deficit-irrigated plots also lagged behind changes in reflectance parameters acquired from sUAS by one to two weeks before corresponding declines in VQ. This indicated spectral reflectance measurements detected early symptoms of drought stress in turfgrass before it was visible. Other researchers have also reported strong relationships between spectral reflectance parameters and VWC and VQ in deficit-irrigated turfgrass (Dettman-Kruse et al., 2006; Jiang et al., 2009).

The stronger gradients of drought stress across treatments in 2016 and 2017, combined with the lag time between changes in VWC and spectral reflectance parameters and VQ, allowed us to evaluate the number of days between initial detection of drought stress by VIs and NIR reflectance and subsequent declines in VQ. For example, in 2016, the NIR and six VIs (i.e., NDVI Enhanced1, NDVI Enhanced2, NDVI Enhanced3, Blue NDVI, GreenBlue, and NIR Blueratio VI) detected drought stress in 15% and 30% compared with 100% plots on 15 July, which was one week earlier than symptoms appeared in VQ and PGC on 22 July (Table 1.4).

In 2017, the abovementioned VIs (except NDVI Enhanced3) detected drought stress more than two weeks before subsequent declines in VQ. For example, five days into the dry down (15 June), VWC decreased in 15% and 30% compared with 100% ET plots (Table 1.5).

On the same day, NIR reflectance and the GreenBlue VI also decreased in 15% and 30% ET treatments, indicating they detected the drier soil conditions. This detection of initial drought stress by NIR and GreenBlue VI occurred 16 days before drought symptoms became evident in VQ in 15% and 30% ET plots on 1 July. The other four VIs (i.e., NDVI Enhanced1, NDVI Enhanced2, Blue NDVI, and NIR Blueratio) were able to detect drought stress in 15% but not 30% ET plots on 15 June, 16 days before VQ declined.

As the window narrowed in 2017 from two to 1.5 weeks before drought stress symptoms appeared, three additional VIs acquired from sUAS were able to detect early drought stress (Table 1.6). Specifically, NDVI Enhanced3, Green NDVI, and NIR GreenDiff detected drought stress in 15% ET compared with other irrigation treatments on 20 June, which was 11 days before symptoms appeared in VQ on 1 July. The NIR reflectance and GreenBlue VI also distinguished between 30% and 50% ET plots on 20 June (Table 1.6), which it hadn't five days earlier (Table 1.5; Fig.1.3).

In the discussion immediately above, regarding early drought detection in 2017, it is possible that drought symptoms became visible before 1 July because VQ was not evaluated on days between sUAS flights (e.g., between 20 June and 1 July). Thus, it is not certain that spectral reflectance parameters detected drought stress symptoms a full 16 days early. However, spectral reflectance parameters clearly detected drought stress before they were visible, as discussed above. This is supported by measurements of PGC, which also revealed no differences between 100% and 15% ET plots on 15 June, when spectral reflectance parameters detected lower VWC

in 15% plots (Table 1.5). Similarly, in 2016 there were no differences in PGC or VQ among irritation treatments on 15 July when spectral reflectance parameters detected lower VWC in 30% and 15% treatments (Table 1.4). Additional research is warranted to refine the window of time between initial drought stress detection by sUAS remote sensing and the appearance of drought stress symptoms.

Ground-based spectral reflectance measurements for drought prediction

Aligned with VWC, both $NDVI_{RS}$ and red reflectance measured with the handheld active optical sensor (RS) detected early drought stress in 15% and 30% ET compared with 100% ET treatments on 15 July, seven days before drought symptoms appeared in VQ and PGC in 2016 (Table 1.7). In 2017, $NDVI_{RS}$ and red reflectance also detected drought stress in 15% compared with 100% ET 16 days and five days before drought symptoms appeared in VQ and PGC, respectively (Table 1.8) (see also Appendix B).

At about one week in 2016 (22 July) and 1.5 weeks in 2017 (1 July) after drought was detected with $NDVI_{RS}$ and Red_{RS}, NIR_{RS}, RE_{RS}, and $NDRE_{RS}$ also detected drought stress in 15% compared with 100% ET plots (Tables 1.7 and 1.8; Appendix B). However, their drought stress detection was concurrent with the appearance of visual symptoms and thus, they did not detect drought earlier than VQ ratings. Similarly, the handheld passive optical sensor ($NDVI_{FS}$) detected drought stress on the same date drought symptoms appeared in VQ in 2015 (Appendix B) and 2016 (Table 1.7). However, in 2017 $NDVI_{FS}$ detected initial drought stress in 15% ET plots on 20 June, which was 11 days earlier drought symptoms were detected with VQ (Table

1.8). Therefore, among measured on-ground reflectance parameters, $NDVI_{RS}$ and Red_{RS} from the active optical sensor were best at predicting drought stress.

Comparisons between aerial- and ground-based spectral reflectance measurements

In 2016, spectral reflectance measurements with both sUAS (except blue and green bands) and handheld sensors were generally correlated strongly with PGC (|r| = 0.84-0.95) and VQ (|r| = 0.75-0.89), moderately with VWC (|r| = 0.53-0.59), and weakly with T_{soil} (|r| = 0.20-0.31) (Table 1.9). In 2017, the correlations of sUAS measurements with PGC (|r| = 0.68-0.84) and VQ (|r| = 0.65-0.77) decreased slightly from 2016, whereas correlations between handheld sensor measurements and PGC and VQ remained similar to 2016. Correlations between sUAS and handheld sensor measurements of spectral reflectance and VWC were similar between years, as were correlations between sUAS spectral reflectance and T_{soil}. However, in 2017 reflectance measurements with handheld sensors were not correlated with T_{soil}. The generally weak or negligible correlations between T_{soil} and spectral reflectance measurements were probably because T_{soil} was not even significantly correlated to irrigation treatments (data not shown).

Moderate to high correlations between ground-based measurements of NDVI and PGC, VQ, and VWC, such as those reported herein, have also been reported by others (Jiang and Carrow, 2005; Dettman-Kruse et al., 2008; Jiang et al., 2009; Bremer et al., 2011b). Our results further revealed that spectral reflectance measurements from sUAS have similar relationships with turfgrass canopy performance during drought stress as reflectance measurements from handheld sensors.

The data acquisition frequency in our study proved effective for detecting early drought stress in turfgrass. Remote sensing data from handheld optical sensors and sUAS were taken approximately weekly when weather permitted. The relatively low frequency we adopted for acquiring remote sensing data was adequate to predict drought stress in low irrigated areas distinguished from medium to well-irrigated ones. In fact, when VWC was measured twice a day, the daily fluctuation in VWC was difficult to differentiate from the actual dry down, which inhibited the time prediction of drought occurrence (Johnson et al., 2009). Those authors found that NDVI of creeping bentgrass with a handheld active spectral radiometer and a handheld optical sensor consistently detected dry downs 6-24 h and occasionally 30-48 h before drought stress became visible. Dettman-Kruse et al. (2008) used hyperspectral reflectance with auxiliary light, but ambient light blocked, to predict less VWC in perennial ryegrass and creeping bentgrass one day before the first sign of wilt symptoms (VQ > 6) ($r^2 = 0.49$ and $r^2 = 0.64$, respectively). As discussed above, additional research is required to better refine the time between early drought detection with sUAS remote sensing, but our results indicate drought can be detected five days or more in advance. Rapid, less frequent measurements with sUAS remote sensing techniques may be more practical and appropriate than ground-based measurements for scouting droughty turfgrass over large areas, such as in golf courses and sod farms.

Irrigation levels that maintained acceptable turf performance during the dry downs

Plots of 80% to 100% ET maintained the highest quality turfgrass longer than the other treatments during three years. For example, in 80% and 100% ET plots VQ was maintained

above minimally acceptable for more than 6, 6, and 11 weeks in 2015, 2016, and 2017, respectively (Table 1.10). Plots of 65% ET also maintained minimally acceptable VQ as long as 80% and 100% plots in 2015 and 2017, and 5 weeks in 2016, only shorter than 100% ET. This is similar to results from fairway-height creeping bentgrass in a sandy loam soil in New Jersey, which required 60 to 80% ET (determined with mini-lysimeters) to maintain acceptable turf performance during summer (DaCosta and Huang, 2006). Under the conditions of this study (Table 1.11), a soil-based (silty clay loam) creeping bentgrass fairway can be maintained acceptably with 65% ET for more than 5 weeks and with 50% ET for 4 weeks where water or rainfall is scarce and other stress factors (e.g. golf cart traffic) are not imposed. Turfgrass of acceptable VQ could be irrigated with 15% ET only for 1 to 3 weeks. However, because golf cart traffic is common on golf course fairways, periods of maintaining acceptable turf quality at those deficit irrigation levels would likely be diminished compared to our study.

Conclusions

In summary, NIR broadband reflectance and six VIs (NDVI Enhanced1, NDVI Enhanced2, NDVI Enhanced3, Blue NDVI, GreenBlue, and NIR Blueratio) acquired from sUAS as well as the $NDVI_{RS}$ and red narrowband reflectance (Red_{RS}) from the handheld active optical sensor detected drought stress one-to-two weeks before it became evident in VQ. Similarly, declines in PGC due to drought stress was predicted by sUAS-based NIR and the GreenBlue VI one-to-two weeks in advance, and by $NDVI_{RS}$ over one week in advance. The NIR and GreenBlue VI were the most sensitive spectral reflectance parameters from sUAS data that

consistently detected drought stress effects before they were observed in VQ and PGC throughout the three-year study. While NDVI has been widely used to detect plant stress, the NIR broadband also demonstrated a comparable ability to reveal turfgrass drought stress development.

To be noted, the GreenBlue VI uses bands that are present in regular, unmodified digital cameras (i.e., green and blue). Thus, although not evaluated in our study, regular digital cameras could be utilized if a modified camera such as ours, which measures NIR reflectance, is not available. This could make data collection cheaper and simpler, and deserves further study. For the handheld active optical sensor used in the latter two years, the $NDVI_{RS}$ and Red_{RS} predicted drought stress in VQ earlier than any other parameters from the two handheld sensors evaluated.

In this research, the ability of early drought stress detection by spectral reflectance parameters acquired from the sUAS-mounted sensor was the same or better than that by spectral reflectance parameters from ground-based sensors. Further research into accurate time prediction of drought stress occurrence in additional turfgrass species and cultivars is needed.

References

An, N., A.L. Goldsby, K.P. Price, and D.J. Bremer. 2015. Using hyperspectral radiometry to predict the green leaf area index of turfgrass. Int J Remote Sens. 36:1470–1483. doi: 10.1080/01431161.2015.1014971.

Asadi-Zarch, M.A., B. Sivakumar, and A. Sharma. 2015. Droughts in a warming climate: A global assessment of Standardized precipitation index (SPI) and Reconnaissance drought index (RDI). J Hydrol. 526:183–195. doi: 10.1016/j.jhydrol.2014.09.071.

Bell, G.E., D.L. Martin, R.M. Kuzmic, M.L. Stone, and J.B. Solie. 2000. Herbicide tolerance of two cold-resistant bermudagrass (Cynodon spp.) cultivars determined by visual assessment and vehicle-mounted optical sensing. Weed Technol. 14:635–641.doi: 10.1614/0890-037X(2000)014[0635:HTOTCR]2.0.CO;2.

Bell, G.E., D.L. Martin, S.G. Wiese, D.D. Dobson, M.W. Smith, M.L. Stone, and J.B. Solie. 2002. Vehicle-mounted optical sensing: An objective means for evaluating turf quality. Crop Sci. 42:197–201.

Bell, G.E., B.M. Howell, G.V. Johnson, W.R. Raun, J.B. Solie, and M.L. Stone. 2004. Optical sensing of turfgrass chlorophyll content and tissue nitrogen. HortScience. 39:1130–1132.

Berni, J., P.J. Zarco-Tejada, L. Suarez, and E. Fereres. 2009. Thermal and narrowband multispectral remote sensing for vegetation monitoring from an unmanned aerial vehicle. IEEE Trans Geosci Remote Sens. 47:722–738. doi: 10.1109/TGRS.2008.2010457.

Bremer, D.J., H. Lee, K. Su, and S.J. Keeley. 2011a.Relationships between normalized difference vegetation index and visual quality in cool-season turfgrass: I. Variation among species and cultivars. Crop Sci. 51:2212. doi: 10.2135/cropsci2010.12.0728.

Bremer, D.J., H. Lee, K. Su, and S.J. Keeley. 2011b.Relationships between normalized difference vegetation index and visual quality in cool-season turfgrass: II. Factors affecting NDVI and its component reflectances. Crop Sci. 51:2219. doi: 10.2135/cropsci2010.12.0729.

Carter, G.A. 1991.Primary and secondary effects of water content on the spectral reflectance of leaves. Am J Bot. 78:916–924. doi: 10.1002/j.1537-2197.1991.tb14495.x.

Caturegli, L., M. Corniglia, M. Gaetani, N. Grossi, S. Magni, M. Migliazzi, L. Angelini, M. Mazzoncini, N. Silvestri, M. Fontanelli, M. Raffaelli, A. Peruzzi, and M. Volterrani. 2016. Unmanned aerial vehicle to estimate nitrogen status of turfgrasses. PLoS One. 11:e0158268. doi: 10.1371/journal.pone.0158268.

Chaerle, L., and D. van der Straeten. 2001. Seeing is believing: imaging techniques to monitor plant health. Biochim Biophys Acta. 1519:153–166.

DaCosta, M., and B. Huang. 2006. Minimum water requirements for creeping, colonial, and velvet bentgrasses under fairway conditions. Crop Sci. 46:81.doi: 10.2135/cropsci2005.0118.

Dettman-Kruse, J.K., N.E. Christians, and M.H. Chaplin. 2008. Predicting soil water content through remote sensing of vegetative characteristics in a turfgrass system. Crop Sci. 48:763-770.

Fenstermaker-Shaulis, L.K., A. Leskys, and D.A. Devitt. 1997. Utilization of remotely sensed data to map and evaluate turfgrass stress associated with drought. Journal of Turfgrass Management. 2:65–81.doi: 10.1300/J099v02n01_06.

Goldsby, A.L., D.J. Bremer, J.D. Fry, and S.J. Keeley. 2015. Response and recovery characteristics of Kentucky bluegrass cultivars to extended drought. Crop, Forage & Turfgrass Manage. 1:0. doi: 10.2134/cftm2014.0087.

Guyot, G. 1990. Optical Properties of Vegetation Canopies. In: Applications of remote sensing in agriculture. Elsevier. p. 19–43.

Harivandi, M.A., K.B. Marcum, and Y.L. Qian. 2008. Recycled, gray, and saline water irrigation for turfgrass. In: J.B. Beard, Kenna, P. Michael, editors, Water quality and quantity issues for turfgrasses in urban landscapes. Council for Agric. Sci. and Technol., Ames, IA. p. 243-258

Hatfield, J. 2017. Turfgrass and climate change. Agron J. 109:1708. doi: 10.2134/agronj2016.10.0626.

Huete, A., K. Didan, T. Miura, E.P. Rodriguez, X. Gao, and L.G. Ferreira. 2002. Overview of the radiometric and biophysical performance of the MODIS vegetation indices. Remote Sens Environ. 83:195–213. doi: 10.1016/S0034-4257(02)00096-2.

Ireland-Otto, N., I.A. Ciampitti, M.T. Blanks, R.O. Burton Jr, and T. Balthazor. 2016. Costs of using unmanned aircraft on crop farms. Journal of ASFMRA:130–148.

Jensen, J.R. 2009. Remote sensing of the environment: An earth resource perspective. 2nd ed. Pearson Education, Delhi, India. p. 363.

Jiang, Y., and R.N. Carrow. 2005. Assessment of narrow-band canopy spectral reflectance and turfgrass performance under drought stress. HortScience. 40:242–245.

Jiang, Y.W., H.F. Liu, and V. Cline. 2009. Correlations of leaf relative water content, canopy temperature, and spectral reflectance in perennial ryegrass under water deficit conditions. Hortscience 44:459-462.

Johnsen, A.R., B.P. Horgan, B.S. Hulke, and V. Cline. 2009. Evaluation of remote sensing to measure plant stress in creeping bentgrass (*Agrostis stolonifera* L.) fairways. Crop Sci. 49: 2261-2274.

Karcher, D.E., and M.D. Richardson. 2005. Batch analysis of digital images to evaluate turfgrass characteristics. Crop Sci. 45:1536. doi: 10.2135/cropsci2004.0562.

Knipling, E.B. 1970. Physical and physiological basis for the reflectance of visible and near-infrared radiation from vegetation. Remote Sens Environ. 1:155–159. doi: 10.1016/S0034-4257(70)80021-9.

Lee, H., D.J. Bremer, K. Su, and S.J. Keeley. 2011.Relationships between normalized difference vegetation index and visual quality in turfgrasses: Effects of Mowing Height. Crop Sci. 51:323. doi: 10.2135/cropsci2010.05.0296.

Lewis, J.D., D.J. Bremer, S.J. Keeley, and J.D. Fry. 2012. Wilt-Based irrigation in Kentucky bluegrass: effects on visual quality and irrigation amounts among cultivars. Crop Sci. 52:1881.doi: 10.2135/cropsci2012.01.0033.

Milesi, C., S.W. Running, C.D. Elvidge, J.B. Dietz, B.T. Tuttle, and R.R. Nemani. 2005. Mapping and modeling the biogeochemical cycling of turf grasses in the United States. Environ Manage. 36:426–438. doi: 10.1007/s00267-004-0316-2.

Morris, K.N., and R.C. Shearman. 1999. NTEP turfgrass evaluation guidelines. National Turfgrass Evaluation Program, Beltsville, MD.

Pajares, G. 2015. Overview and current status of remote sensing applications based on unmanned aerial vehicles (UAVs). Photogramm Eng Rem S. 81:281–330. doi: 10.14358/PERS.81.4.281.

Perea-Moreno, A.J., M.J. Aguilera-Ureña, J.-E. Meroño-De Larriva, and F. Manzano-Agugliaro. 2016. Assessment of the potential of UAV video image analysis for planning irrigation needs of golf courses. Water. 8:584. doi: 10.3390/w8120584.

Rango, A., A. Laliberte, C. Steele, J.E. Herrick, B. Bestelmeyer, T. Schmugge, A. Roanhorse, and V. Jenkins. 2006. Using unmanned aerial vehicles for rangelands: Current applications and future potentials. Environmental Practice. 8:159–168. doi: 10.1017/S1466046606060224.

Roberts, D.A., K.L. Roth, and R. Perroy. 2012. Hyperspectral vegetation indices. In: P. S. Thenkabail, J. G. Lyon, and A. Huete, editors, Hyperspectral remote sensing of vegetation, CRC Press, Boca Raton, FL. p. 309–327.

Sims, D.A., and J.A. Gamon. 2002. Relationships between leaf pigment content and spectral reflectance across a wide range of species, leaf structures and developmental stages. Remote Sens Environ. 81:337–354. doi: 10.1016/S0034-4257(02)00010-X.

Su, K., D.J. Bremer, S.J. Keeley, and J.D. Fry. 2007. Effects of high temperature and drought on a hybrid bluegrass compared with Kentucky bluegrass and tall fescue. Crop Sci. 47:2152. doi: 10.2135/cropsci2006.12.0781.

Taghvaeian, S., J. Chávez, M. Hattendorf, and M. Crookston. 2013. Optical and thermal remote sensing of turfgrass quality, water stress, and water use under different soil and irrigation treatments. Remote Sensing. 5:2327–2347. doi: 10.3390/rs5052327.

Van der Merwe, D., L.R. Skabelund, A. Sharda, P. Blackmore, and D. Bremer. 2017. Towards characterizing green roof vegetation using color-infrared and thermal sensors. Proceedings of the CitiesAlive 15th Annual Green Roof and Wall Conference, Seattle, WA. 18-21 September.

Wang, H., C. Wang, K.P. Price, D. van der Merwe, and N. An. 2014. Modeling above-ground biomass in tallgrass prairie using ultra-high spatial resolution sUAS Imagery. Photogramm Eng Rem S. 80:1151–1159. doi: 10.14358/PERS.80.12.1151.

Xiang, H., and L. Tian. 2011.Method for automatic georeferencing aerial remote sensing (RS) images from an unmanned aerial vehicle (UAV) platform. Biosyst Eng. 108:104–113. doi: 10.1016/j.biosystemseng.2010.11.003.

Walter, I., R. Allen, R. Elliott, M. Jensen, D. Itenfisu, B. Mecham, T. Howell, R. Snyder, P. Brown, S. Echings, T. Spofford, M. Hattendorf, R. Cuenca, J. Wright, and D. Martin. 2001.ASCE's standardized reference evapotranspiration equation. p. 1-11.In Flug et al. (ed.) Watershed management and operations management 2000. doi: 10.1061/40499(2000)126

Xiong, X., G.E. Bell, J.B. Solie, M.W. Smith, and B. Martin. 2007. Bermudagrass seasonal responses to nitrogen fertilization and irrigation detected using optical sensing. Crop Sci. 47:1603. doi: 10.2135/cropsci2006.06.0400.

Zarco-Tejada, P.J., V. González-Dugo, and J.A.J. Berni. 2012. Fluorescence, temperature and narrow-band indices acquired from a UAV platform for water stress detection using a micro-hyperspectral imager and a thermal camera. Remote Sens Environ. 117:322–337. doi: 10.1016/j.rse.2011.10.007.

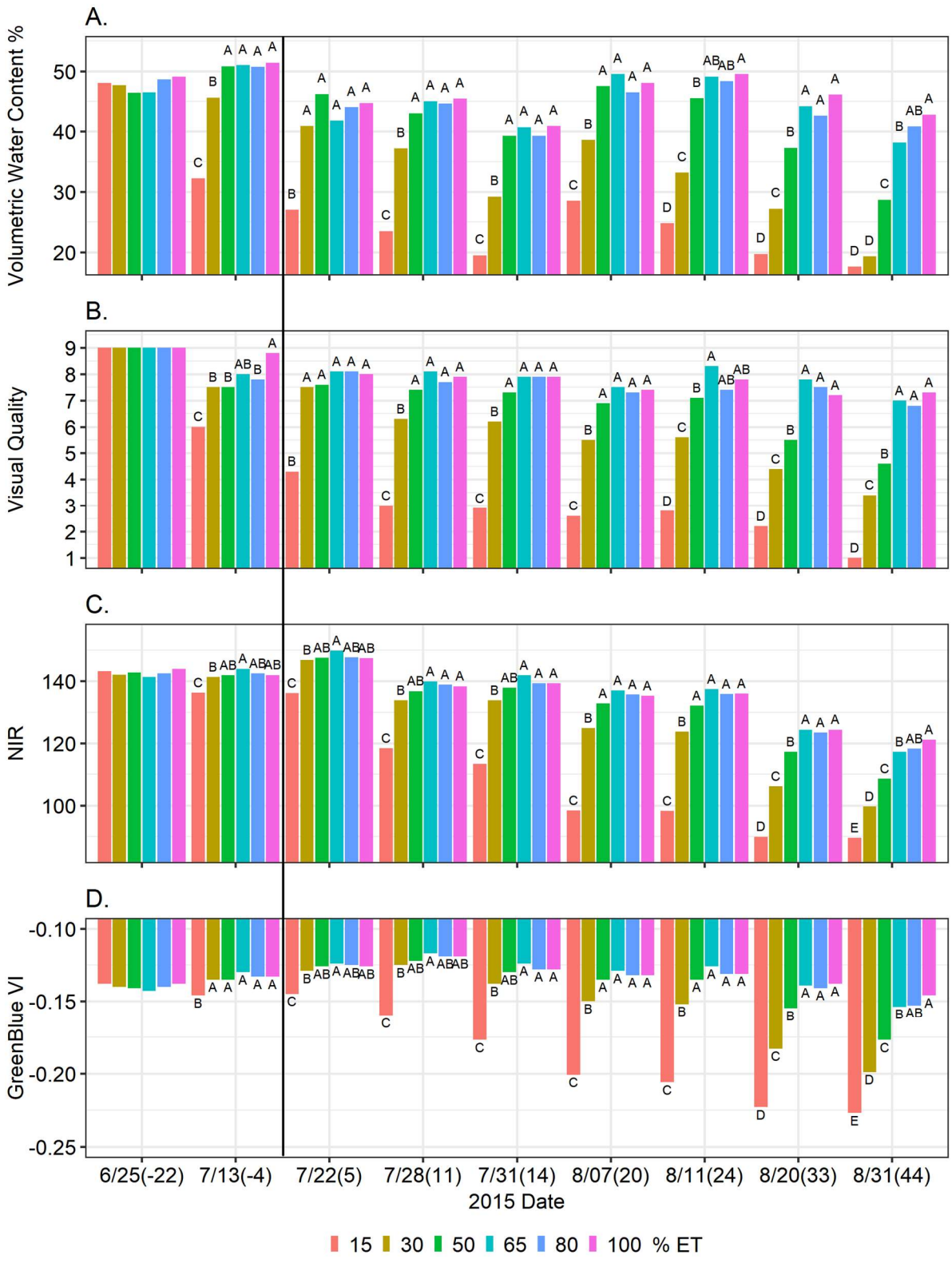

Figure 1.1. Analysis of irrigation effects on volumetric water content (A), visual quality (B), near infrared (NIR, C), and GreenBlue vegetation index (D) for 'Declaration' creeping bentgrass on

each measurement date in 2015 [number in parentheses on x-axis denotes days before (negative) or after (positive) the beginning of treatments]. Six irrigation treatments began as 25, 50, 75, 100, 125, and 150% evapotranspiration (ET) on 29 June, but because drought stress was negligible in all but 25 and 50% ET, treatments were decreased to 15, 30, 50, 65, 80 and 100% ET on 17 July denoted by a vertical line. Visual quality scale (1–9): 1 = dead, 6 = minimally acceptable, and 9 = uniform, green, dense turfgrass.

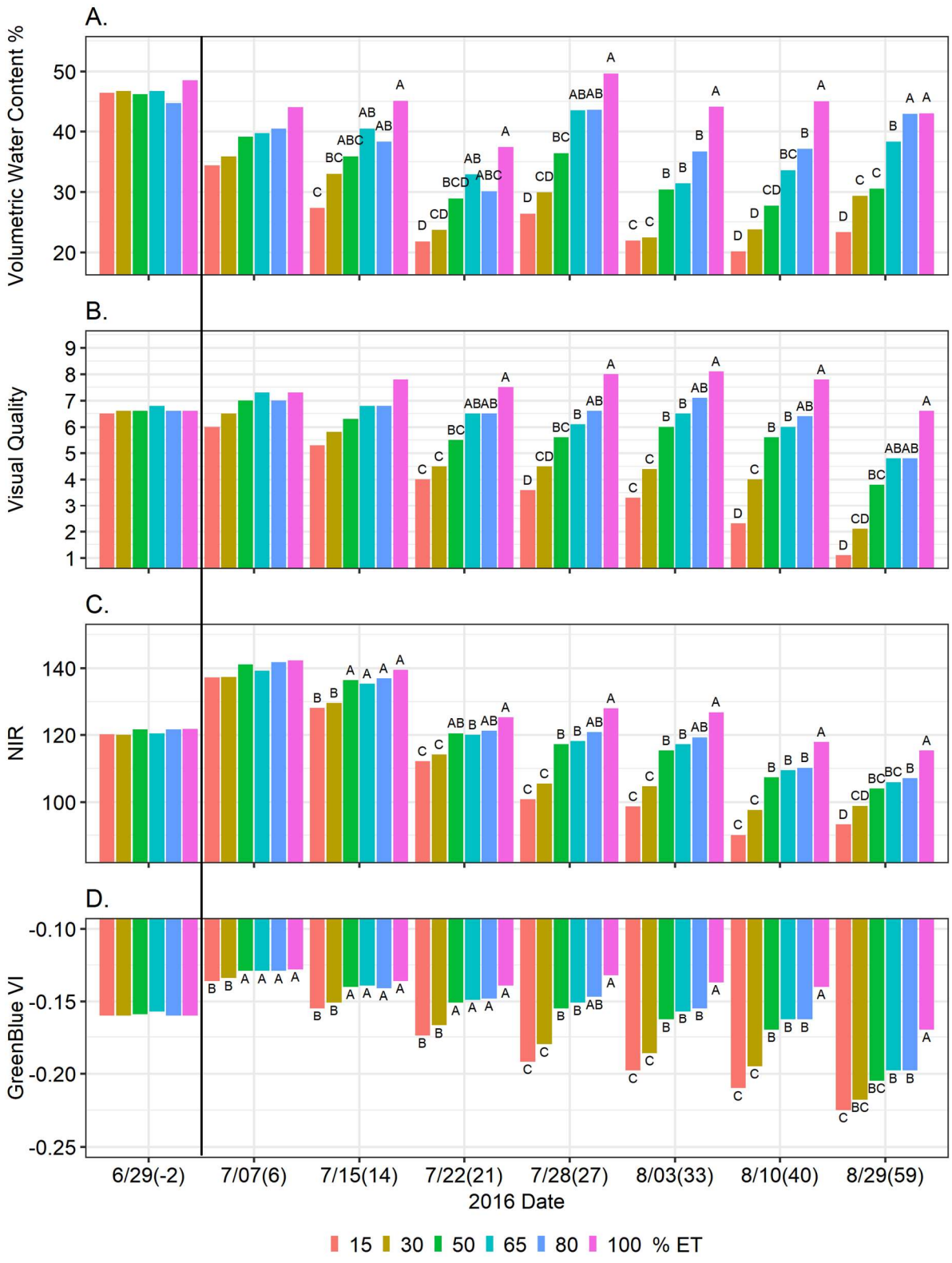

Figure 1.2. Analysis of irrigation effects on volumetric water content (A), visual quality (B), near infrared (NIR, C), and GreenBlue vegetation index (D) for 'Declaration' creeping bentgrass

watered with 15, 30, 50, 65, 80 and 100% evapotranspiration (ET) replacement on each measurement date in 2016 [number in parentheses on x-axis denotes days before (negative) or after (positive) the beginning of treatments]. Irrigation treatments began on 1 July denoted by a vertical line. Visual quality scale (1–9): 1 = dead, 6 = minimally acceptable, and 9 = uniform, green, dense turfgrass.

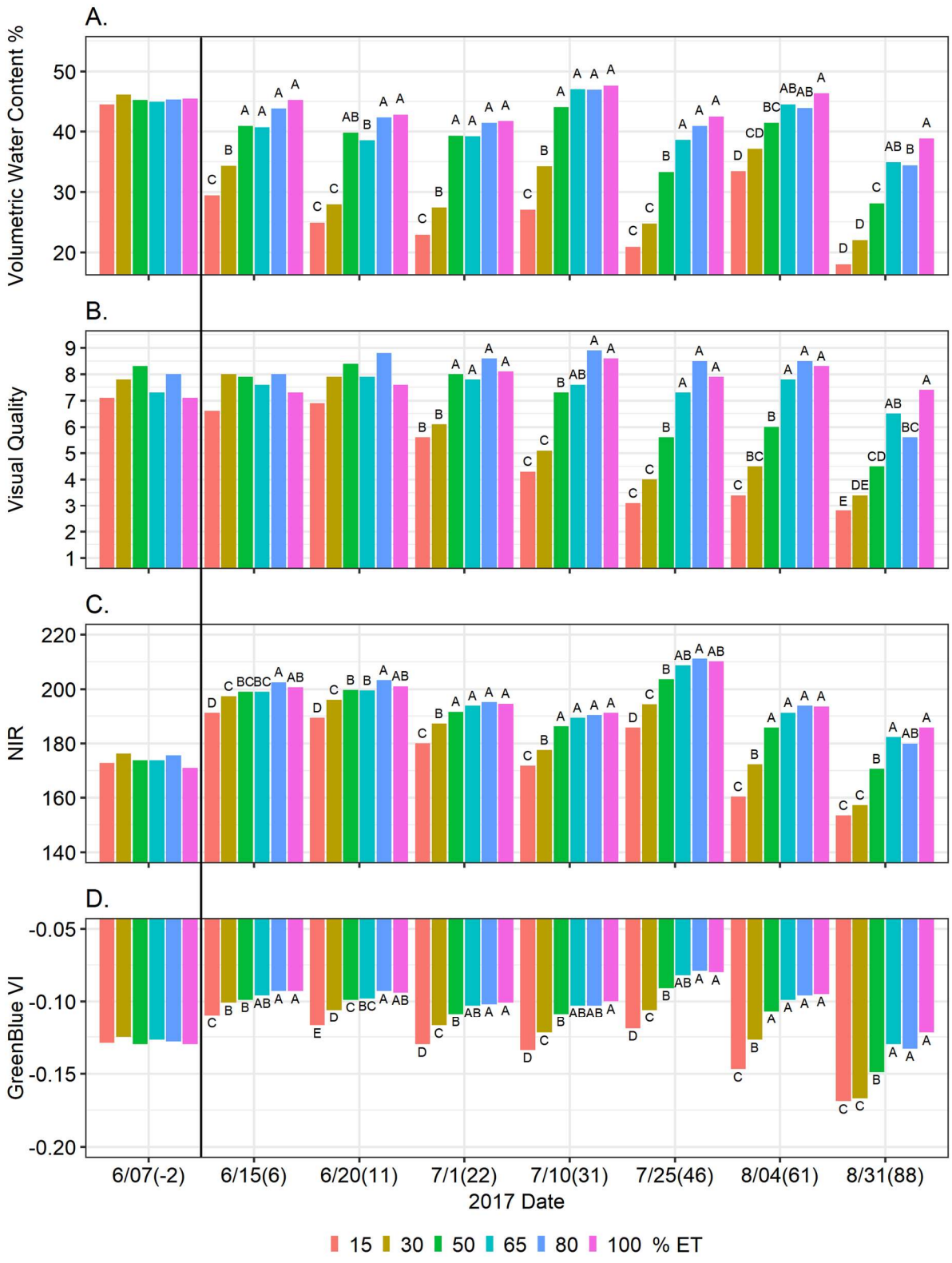

Figure 1.3. Analysis of irrigation effects on volumetric water content (A), visual quality (B), near infrared (NIR, C), and GreenBlue vegetation index (D) for 'Declaration' creeping bentgrass

watered with 15, 30, 50, 65, 80 and 100% evapotranspiration (ET) replacement on each measurement date in 2017 [number in parentheses on x-axis denotes days before (negative) or after (positive) the beginning of treatments]. Irrigation treatments began on 9 June denoted by a vertical line. Visual quality scale (1–9): 1 = dead, 6 = minimally acceptable, and 9 = uniform, green, dense turfgrass.

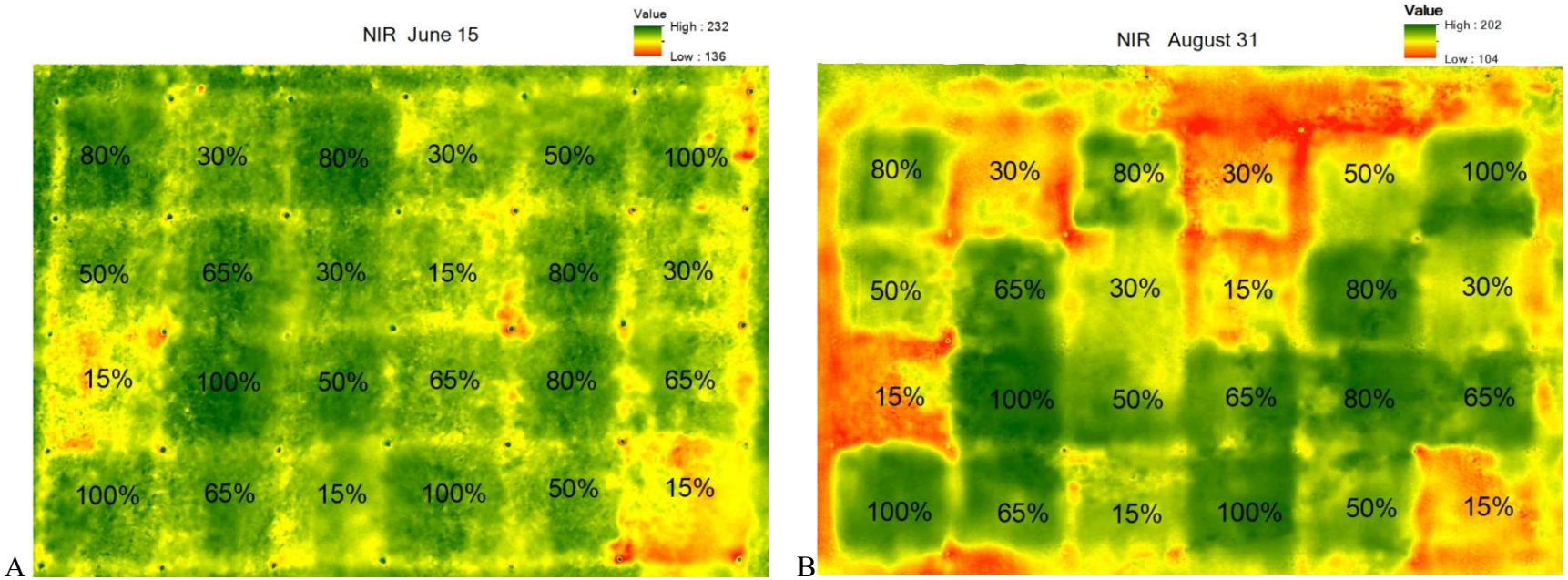

Figure 1.4. Near infrared (NIR) colored maps of 'Declaration' creeping bentgrass plots measured one week after irrigation treatments began (15 June 2017; A) and at the end of the study (31 Aug 2017; B). Percentages denote evapotranspiration (ET) replacement irrigation treatment.

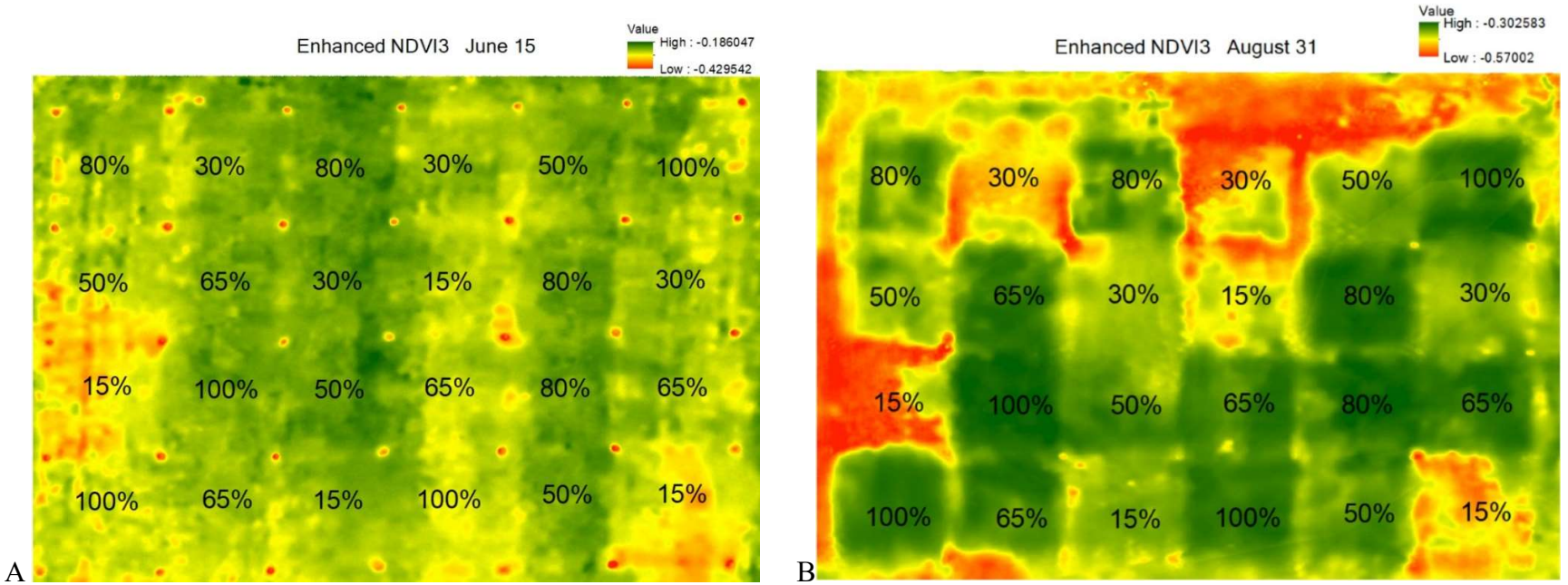

Figure 1.5. NDVI Enhance3 vegetation index colored maps of 'Declaration' creeping bentgrass plots measured one week after irrigation treatments began (15 June 2017; A) and at the end of the study (31 Aug 2017; B). Percentages denote evapotranspiration (ET) replacement irrigation treatment.

Table 1.1. Irrigation main effects on volumetric water content (VWC), visual quality (VQ), normalized difference vegetation index ($NDVI_{FS}$) from a handheld passive remote sensor, and soil temperature (T_{soil}) for 'Declaration' creeping bentgrass over drought periods of 2015-2017.

Treatment†	VWC‡	VQ§	$NDVI_{FS}$¶	T_{soil}#
100%	44.0A*	8.5A	0.81A	29.26BC
80%	42.6AB	8.3A	0.79A	29.17C
65%	40.9B	7.9AB	0.79A	29.23BC
50%	38.4C	7.5B	0.77A	29.23BC
30%	30.8D	5.9C	0.68B	29.48B
15%	23.9E	4.1D	0.60C	29.76A

* Treatment means were significantly different at $P < 0.05$ probability level, indicated by different letters; no letter presented when $P > 0.05$.
† Percentage of evapotranspiration (ET) replacement.
‡ Volumetric water content (cm^3cm^{-3}) measures the volume of water per unit bulk volume of soil across 7.6-cm depth.
§ Visual quality based on a 1 to 9 scale, with 1 = dead, 6 = minimally acceptable, and 9 = uniform, green, dense turfgrass.
¶ $NDVI_{FS} = (NIR_{FS}\text{-red})/(NIR_{FS}\text{+red})$ where red peaks at 660 and NIR_{FS} at 840 nm.
# Soil temperature averaged across 0-7.6-cm depth.

Table 1.2. Irrigation main effects on volumetric water content (VWC), visual quality (VQ), normalized difference vegetation index ($NDVI_{FS}$) from a handheld passive remote sensor, soil temperature (T_{soil}), percentage green cover (PGC), and variables [$NDVI_{RS}$, $NDRE_{RS}$, Red_{RS}, RE_{RS}, and NIR_{RS} band] from a handheld active remote sensor for 'Declaration' creeping bentgrass over drought periods in 2016 and 2017†.

Treatment‡	VWC§	VQ¶	T_{soil}#	PGC%	$NDVI_{FS}$††	$NDVI_{RS}$‡‡	$NDRE_{RS}$§§	Red_{RS}	RE_{RS}	NIR_{RS}
100%	42.8A*	8.8A	29.0BC	86.8A	0.79A	0.76A	0.29A	5.0D	19.72A	36.3A
80%	41.2A	8.4AB	28.7D	76.9AB	0.75A	0.73AB	0.28AB	5.7CD	19.45BC	35.8AB
65%	38.2B	7.6BC	29.0BC	78.2AB	0.76A	0.71AB	0.27AB	6.2CD	19.36B	35.2AB
50%	35.7B	7.4C	28.9C	74.2B	0.74A	0.69B	0.26B	6.6C	19.19CD	34.9B
30%	28.1C	5.6D	29.2B	56.0C	0.63B	0.61C	0.23C	8.3B	18.97D	33.5C
15%	24.1D	4.5E	29.5A	50.7C	0.60B	0.56D	0.22C	9.5A	18.96D	32.7C

* Treatment means were significantly different at $P < 0.05$ probability level, indicated by different letters; no letter presented when $P > 0.05$.
† Volumetric water content, VQ, $NDVI_{FS}$, and Tsoil were also measured in 2015.
‡ Percentage of evapotranspiration (ET) replacement.
§ Volumetric water content (cm^3cm^{-3}) measures the volume of water per unit bulk volume of soil across 7.6-cm depth.
¶ Visual quality based on a 1 to 9 scale, with 1 = dead, 6 = minimally acceptable, and 9 = uniform, green, dense turfgrass.
# Soil temperature averaged across 0-7.6-cm depth.
†† $NDVI_{FS}$ = (NIR_{FS}-red)/(NIR_{FS}+red) where red peaks at 660 and NIR_{FS} at 840 nm.
‡‡ $NDVI_{RS}$ = (NIR_{RS}-Red_{RS})/(NIR_{RS}+Red_{RS}). Red_{RS} peaks at 670nm and NIR_{RS} at 780nm.
§§$NDRE_{RS}$ = (NIR_{RS}-RE_{RS})/(NIR_{RS}+RE_{RS}). RE_{RS} peaks at 730nm.

Table 1.3. Irrigation main effects on reflectance of blue (B), green (G) and NIR, and vegetation indices [NDVI Enhanced1(NIR+G-2B)/(NIR+G+2B), NDVI Enhanced2 (NIR+G-B)/(NIR+G+B), NDVI Enhanced3 (NIR-G-B)/(NIR+G+B), Blue NDVI (NIR-B)/(NIR+B), Green NDVI (NIR-G)/(NIR+G), GreenBlue (G-B)/(G+B), NIR Green Diff (NIR-G-B)/(NIR-G+B), NIR Blueratio (NIR-B)] for 'Declaration' creeping bentgrass over drought periods of 2015-2017.

Trt† (%)	B	G	NIR	NDVI Enhanced1	NDVI Enhanced2	NDVI Enhanced3	Blue NDVI	Green NDVI	GreenBlue	NIR Blueratio	NIR Green Diff
100	158C	112B	145A	-0.078A	0.257A	-0.309A	-0.035A	0.098A	-0.131A	-9.7A	-0.69A
80	160BC	112B	144A	-0.088AB	0.247AB	-0.325AB	-0.056A	0.081AB	-0.136A	-12.8A	-0.71AB
65	158C	110BC	144A	-0.084A	0.253AB	-0.318A	-0.047A	0.090A	-0.135A	-14.9A	-0.71AB
50	160BC	110BC	141A	-0.102B	0.233B	-0.332AB	-0.067AB	0.079AB	-0.14AB	-18.4AB	-0.74B
30	164B	109C	135B	-0.126C	0.208C	-0.362BC	-0.106BC	0.051BC	-0.156B	-29.9B	-0.80C
15	170A	115A	124C	-0.155D	0.184D	-0.394C	-0.149C	0.021C	-0.170C	-42.5C	-0.91D

*Treatment means were significantly different at $P < 0.05$ probability level, indicated by different letters; no letter presented when $P > 0.05$.
† Percentage of evapotranspiration (ET) replacement.

Table 1.4. Daily irrigation treatment effects on visual quality (VQ), percentage green cover (PGC), volumetric water content (VWC), and reflectance data (GreenBlue, NIR [680-780 nm], NDVI Enhanced1, NDVI Enhanced2, NDVI Enhanced3, Blue NDVI, and NIR Blueratio) acquired from small unmanned aircraft (sUAS) one week before visual drought detection, over 'Declaration' creeping bentgrass on 15 and 22 July, 2016.

	15 July										22 July	
Trt† (%)	VQ‡	PGC	VWC	GreenBlue§	NIR	NDVI Enhanced 1¶	NDVI Enhanced 2#	NDVI Enhanced 3††	Blue NDVI‡‡	NIR Blueratio§§	PGC	VQ
100	7.8	93	45A*	-0.136A	139.5A	-0.080A	0.260A	-0.30A	-0.029A	-8.4A	94A	7.5A
80	6.8	83	38AB	-0.141A	136.9A	-0.089AB	0.252AB	-0.31AB	-0.041AB	-11.8AB	84A	6.5AB
65	6.8	85	41AB	-0.139A	135.3A	-0.085A	0.256A	-0.31AB	-0.036AB	-10.0AB	80A	6.5AB
50	6.3	79	36ABC	-0.140A	136.4A	-0.086AB	0.255AB	-0.31AB	-0.037AB	-10.5AB	79A	5.5BC
30	5.8	69	33BC	-0.151B	129.6B	-0.103BC	0.239BC	-0.32BC	-0.059BC	-16.3BC	43B	4.5C
15	5.3	76	27C	-0.155B	128.1B	-0.111C	0.231C	-0.33C	-0.069C	-19.1C	50B	4.0C

* Treatment means were significantly different at $P < 0.05$ probability level, indicated by different letters; no letter presented when $P > 0.05$.
† Percentage of evapotranspiration (ET) replacement.
‡ Visual quality based on a 1 to 9 scale, with 1 = dead, 6 = minimally acceptable, and 9 = uniform, green, dense turfgrass.
§ GreenBlue = (G-B)/(G+B); G, green reflectance, and B, blue reflectance are between 400-580 nm.
¶ NDVI Enhanced1 = (NIR+G-2B)/(NIR+G+2B).
# NDVI Enhanced2 = (NIR+G-B)/(NIR+G+B).
†† NDVI Enhanced3 = (NIR-G-B)/(NIR+G+B).
‡‡ Blue NDVI = (NIR-B)/(NIR+B).
§§ NIR Blueratio = NIR-B.

Table 1.5. Daily irrigation treatment effects on visual quality (VQ), percentage green cover (PGC), volumetric water content (VWC), and reflectance data (GreenBlue, NIR [680-780 nm], NDVI Enhanced1, NDVI Enhanced2, NDVI Enhanced3, Blue NDVI, and NIR Blueratio) acquired from small unmanned aircraft (sUAS) two weeks before visual drought detection, over 'Declaration' creeping bentgrass on 15 and 20 June, 1 July 2017.

Trt†	15 June									20 June		1 July	
(%)	VQ‡	PGC	VWC	GreenBlue§	NIR	NDVI Enhanced1¶	NDVI Enhanced2#	Blue NDVI††	NIR Blueratio‡‡	VQ	PGC	VQ	PGC
100	7.3	91AB*	45A	-0.093A	201AB	-0.055A	0.284A	-0.02A	-8A	7.6	91A	8.1A	98A
80	8.0	96A	44A	-0.093A	203A	-0.049A	0.289A	-0.01A	-3A	8.8	96A	8.6A	99A
65	7.6	93A	41A	-0.096AB	199BC	-0.056A	0.283A	-0.02A	-7A	7.9	94A	7.8A	98A
50	7.9	95A	41A	-0.099B	199BC	-0.055A	0.284A	-0.02A	-6A	8.4	96A	8.0A	99A
30	8.0	94A	34B	-0.101B	197C	-0.056A	0.282A	-0.02A	-6A	7.9	95A	6.1B	91B
15	6.6	85B	29C	-0.110C	191D	-0.073B	0.267B	-0.04B	-15B	6.9	83B	5.6B	85B

* Treatment means were significantly different at $P < 0.05$ probability level, indicated by different letters; no letter presented when $P > 0.05$.
† Percentage of evapotranspiration (ET) replacement.
‡ Visual quality based on a 1 to 9 scale, with 1 = dead, 6 = minimally acceptable, and 9 = uniform, green, dense turfgrass.
§ GreenBlue = (G-B)/(G+B); G, green reflectance, and B, blue reflectance are between 400-580 nm.
¶ NDVI Enhanced1 = (NIR+G-2B)/(NIR+G+2B).
# NDVI Enhanced2 = (NIR+G-B)/(NIR+G+B).
†† Blue NDVI = (NIR-B)/(NIR+B).
‡‡ NIR Blueratio = NIR-B.

Table 1.6. Daily irrigation treatment effects on visual quality (VQ), percentage green cover (PGC), volumetric water content (VWC), and reflectance data (GreenBlue, NIR [680-780 nm], NDVI Enhanced1, NDVI Enhanced2, NDVI Enhanced3, Blue NDVI, NIR Blueratio, Green NDVI, and NIR GreenDiff) acquired from small unmanned aircraft (sUAS) one week before visual drought detection, over 'Declaration' creeping bentgrass on 20 June and 1 July, 2017.

Trt† (%)	20 June												1 July	
	VQ‡	PGC	VWC	GreenBlue§	NIR	NDVI Enhanced 1¶	NDVI Enhanced 2#	NDVI Enhanced 3††	Blue NDVI‡‡	NIR Blue ratio§§	Green NDVI¶¶	NIR Green Diff##	VQ	PGC
100	7.6	91A*	43A	-0.094AB	201AB	-0.055AB	0.284AB	-0.31A	-0.02AB	-8AB	0.076AB	-0.76A	8.1A	98A
80	8.8	96A	42A	-0.093A	203A	-0.048A	0.290A	-0.30A	-0.01A	-3A	0.086A	-0.73A	8.6A	99A
65	7.9	94A	39B	-0.098BC	200B	-0.057AB	0.281AB	-0.31A	-0.02AB	-8AB	0.078A	-0.76A	7.8A	98A
50	8.4	96A	40AB	-0.099C	200B	-0.057AB	0.281AB	-0.31A	-0.02AB	-8AB	0.081A	-0.75A	8.0A	99A
30	7.9	93A	28C	-0.106D	196C	-0.064B	0.275B	-0.31A	-0.03B	-10B	0.080A	-0.75A	6.1B	91B
15	6.9	83B	25C	-0.117E	189D	-0.084C	0.256C	-0.33B	-0.05C	-21C	0.064B	-0.80B	5.6B	85B

* Treatment means were significantly different at $P < 0.05$ probability level, indicated by different letters; no letter presented when $P > 0.05$.
† Percentage of evapotranspiration (ET) replacement.
‡ Visual quality based on a 1 to 9 scale, with 1 = dead, 6 = minimally acceptable, and 9 = uniform, green, dense turfgrass.
§ GreenBlue = (G-B)/(G+B); G, green reflectance, and B, blue reflectance are between 400-580 nm.
¶ NDVI Enhanced1 = (NIR+G-2B)/(NIR+G+2B).
# NDVI Enhanced2 = (NIR+G-B)/(NIR+G+B).
†† NDVI Enhanced3 = (NIR-G-B)/(NIR+G+B).
‡‡ Blue NDVI = (NIR-B)/(NIR+B).
§§ NIR Blueratio = NIR-B.
¶¶ Green NDVI = (NIR-G)/(NIR+G).
NIR GreenDiff = (NIR-G-B)/(NIR-G+B).

Table 1.7. Daily irrigation treatment effects on on-ground measurements for 'Declaration' creeping bentgrass including visual quality (VQ), volumetric water content (VWC), percentage green cover (PGC), handheld active sensor ($NDVI_{RS}$, $NDRE_{RS}$, Red_{RS}, RE_{RS}, and NIR_{RS}), and handheld passive sensor ($NDVI_{FS}$) on 15 and 22 July, 2016 ($P < 0.05$). Variables except VQ are only shown on the first date of drought detection.

Trt†	15 July					22 July						
	VQ‡	PGC	VWC	$NDVI_{RS}$§	Red_{RS}	VQ	PGC	VWC	NIR_{RS}	RE_{RS}	$NDRE_{RS}$¶	$NDVI_{FS}$#
100%	7.8	93	45A*	0.78A	4.6A	7.5A	94A	37A	37.3A	19.6A	0.31A	0.80A
80%	6.8	83	39AB	0.753A	5.1A	6.5AB	84A	30ABC	35.9AB	20.0AB	0.29AB	0.77A
65%	6.8	85	41AB	0.745AB	5.2AB	6.5AB	80A	33AB	35.1BC	20.2BC	0.27BC	0.74AB
50%	6.3	79	36ABC	0.745AB	5.2AB	5.5BC	79A	29DBC	35.2BC	20.1ABC	0.27BC	0.76A
30%	5.8	69	33BC	0.700BC	6.2BC	4.5C	43B	24CD	33.5CD	20.6CD	0.24CD	0.68BC
15%	5.3	76	27C	0.690C	6.4C	4.0C	50B	22D	32.9D	20.7D	0.23D	0.62C

* Treatment means were significantly different at $P < 0.05$ probability level, indicated by different letters; no letter presented when $P > 0.05$.

† Percentage of evapotranspiration (ET) replacement.

‡ Visual quality based on a 1 to 9 scale, with 1 = dead, 6 = minimally acceptable, and 9 = uniform, green, dense turfgrass.

§$NDVI_{RS} = (NIR_{RS}-Red_{RS})/(NIR_{RS}+Red_{RS})$; NIR_{RS} peaks at 780nm, near infrared reflectance; Red_{RS} peaks at 670nm.

¶ $NDRE_{RS} = (NIR_{RS}-RE_{RS})/(NIR_{RS}+RE_{RS})$; RE_{RS}, red edge peaks at 730nm.

$NDVI_{FS} = (NIR_{FS}-red)/(NIR_{FS}+red)$; 660 (red) and 840 ($NIR_{FS}$) nm.

Table 1.8. Daily irrigation treatment effects on on-ground measurements for 'Declaration' creeping bentgrass including visual quality (VQ), volumetric water content (VWC), percentage green cover (PGC), handheld active sensor ($NDVI_{RS}$, $NDRE_{RS}$, Red_{RS}, RE_{RS}, and NIR_{RS}), and handheld passive sensor ($NDVI_{FS}$) on 15 and 20 June, 1 July 2017. Variables except VQ are only shown on the first date of drought detection.

Trt†	15 June					20 June				1 July					
(%)	VQ‡	PGC	VWC	$NDVI_{RS}$§	Red_{RS}	VQ	PGC	VWC	$NDVI_{FS}$¶	VQ	PGC	VWC	NIR_{RS}	RE_{RS}	$NDRE_{RS}$#
100	7.3	90.5AB*	45A	0.78A	4.5A	7.6	91A	43A	0.82A	8.1A	98A	42A	38.6AB	19.4BC	0.33AB
80	8	95.6A	44A	0.81A	4.0A	8.8	96A	42A	0.84A	8.6A	99A	41A	39.3A	19.2C	0.34A
65	7.6	92.5A	41A	0.78A	4.6A	7.9	94A	39B	0.82A	7.8A	98A	39A	38.3AB	19.4BC	0.33AB
50	7.9	94.9A	41A	0.80A	4.3A	8.4	96A	40AB	0.82A	8.0A	99A	39A	38.0AB	19.5BC	0.32AB
30	8	93.8A	35B	0.79A	4.4A	7.9	95A	28C	0.81A	6.1B	91B	27B	37.3B	19.7AB	0.31BC
15	6.6	84.5B	30C	0.75B	5.3B	6.9	83B	25C	0.74B	5.6B	85B	23C	35.5C	20.0A	0.28C

* Treatment means were significantly different at $P < 0.05$ probability level, indicated by different letters; no letter presented when $P > 0.05$.

† Percentage of evapotranspiration (ET) replacement.

‡ Visual quality based on a 1 to 9 scale, with 1 = dead, 6 = minimally acceptable, and 9 = uniform, green, dense turfgrass.

§ $NDVI_{RS} = (NIR_{RS}-Red_{RS})/(NIR_{RS}+Red_{RS})$; NIR_{RS} peaks at 780nm, near infrared reflectance; Red_{RS} peaks at 670nm.

¶ $NDVI_{FS} = (NIR_{FS}-red)/(NIR_{FS}+red)$; 660 (red) and 840 ($NIR_{FS}$) nm.

$NDRE_{RS} = (NIR_{RS}-RE_{RS})/(NIR_{RS}+RE_{RS})$; RE_{RS}, red edge peaks at 730nm.

Table 1.9. Pearson correlation coefficients (r) between visual quality (VQ), percentage green cover (PGC), volumetric water content (VWC), soil temperature (T_{soil}) and measurements of remote sensing data [small unmanned aerial system (sUAS), handheld passive sensor ($NDVI_{FS}$), and handheld active sensor (RE_{RS}, Red_{RS}, NIR_{RS}, $NDVI_{RS}$, and $NDRE_{RS}$)] for 'Declaration' creeping bentgrass under a gradient of irrigation treatments over 2016-2017 ($P < 0.05$).

	2016				2017			
	VQ	PGC (%)	VWC (%)	T_{soil} (°C)	VQ	PGC (%)	VWC (%)	T_{soil} (°C)
Ground-based measurements								
VQ	1.00	0.87	0.68	NS	1.00	0.86	0.71	NS
PGC	0.87	1.00	0.65	0.26	0.86	1.00	0.63	NS
VWC	0.68	0.65	1.00	0.17	0.71	0.63	1.00	NS
Remote sensing measurements								
sUAS-based								
Blue	-0.70	-0.68	-0.35	NS	-0.54	-0.61	-0.66	NS
Green	-0.33	-0.26	NS	NS	NS	NS	-0.26	0.18
NIR†	0.75	0.84	0.55	0.31	0.65	0.68	0.34	0.24
GreenBlue‡	0.86	0.91	0.56	0.23	0.76	0.81	0.59	0.24
NDVI Enhanced1§	0.87	0.93	0.56	0.27	0.76	0.82	0.59	0.24
NDVI Enhanced2¶	0.87	0.92	0.56	0.27	0.77	0.84	0.62	0.19
NDVI Enhanced3#	0.87	0.92	0.56	0.29	0.77	0.83	0.61	0.21
Blue NDVI ††	0.87	0.92	0.56	0.28	0.75	0.83	0.62	NS
Green NDVI ‡‡	0.86	0.91	0.54	0.29	0.68	0.71	0.50	0.31
NIR Blueratio§§	0.86	0.90	0.53	0.25	0.77	0.83	0.62	0.21
NIR Greendiff¶¶	0.87	0.91	0.55	0.29	0.76	0.84	0.62	0.15
Handheld optical sensors								
$NDVI_{FS}$##	0.88	0.92	0.58	0.20	0.87	0.94	0.62	NS
RE_{RS}†‡	-0.88	-0.94	-0.55	-0.23	-0.89	-0.91	-0.57	NS
Red_{RS}†§	-0.86	-0.94	-0.58	-0.30	-0.89	-0.92	-0.61	NS
NIR_{RS}†¶	0.89	0.94	0.57	0.24	0.91	0.90	0.60	NS
$NDVI_{RS}$†#	0.87	0.95	0.59	0.30	0.90	0.93	0.62	NS
$NDRE_{RS}$‡†	0.89	0.94	0.56	0.20	0.90	0.91	0.59	NS

† NIR, near infrared reflectance, peaks within 680-780 nm.

‡ GreenBlue = (Green-Blue)/(Green+Blue).

§ NDVI Enhanced1 = (NIR+Green-2Blue)/(NIR+Green+2Blue).

¶ NDVI Enhanced2 = (NIR+Green-Blue)/(NIR+Green+Blue).

NDVI Enhanced3 = (NIR-Green-Blue)/(NIR+Green+Blue).

†† Blue NDVI = (NIR-Blue)/(NIR+Blue).

‡‡ Green NDVI = (NIR-Green)/(NIR+Green).

§§ NIR Blueratio = NIR-Blue.

¶¶ NIR GreenDiff = (NIR-Green-Blue)/(NIR-Green+Blue).

$NDVI_{FS}$ = (NIR_{FS}-red)/(NIR_{FS}+red); 660 (red) and 840 (NIR_{FS}) nm.

†‡ RE_{RS}, red edge, peaks at 730nm.

†§ Red_{RS}, peaks at 670nm.

†¶ NIR_{RS} peaks at 780nm.

†# $NDVI_{RS}$ = (NIR_{RS}-Red_{RS})/(NIR_{RS}+Red_{RS}).

‡† $NDRE_{RS}$ = (NIR_{RS}-RE_{RS})/(NIR_{RS}+RE_{RS}).

Table 1.10. Estimated days to maintained visual quality above minimally acceptable over 2015-2017.

	2015		2016		2017	
Trt* (%)	Estimate Days	Standard Error	Estimate Days	Standard Error	Estimate Days	Standard Error
100	45A	2.6	59A	7.3	85A	5.2
80	45A	2.6	43AB	7.3	83A	5.2
65	45A	2.6	35BC	7.3	82A	5.2
50	37B	2.6	29BC	7.3	65B	5.1
30	20C	2.6	19C	7.3	30C	5.4
15	5D	2.6	15C	7.3	26C	5.2

* Treatment means were significantly different at $P < 0.05$ probability level.

Table 1.11. Daily averages of maximum and minimum air temperature, grass evapotranspiration (ET_o), and solar radiation from an on-site weather station per drought period (29 June to 31 Aug 2015; 1 July to 29 Aug 2016; 9 June to 31 Aug 2017).

Year	Air Temperature °C d^{-1}			ET_o	Solar Radiation
	Max	Min	Average	mm d^{-1}	MJ m^{-2} d^{-1}
2015	31.1	18.9	25.0	5.1	22.1
2016	31.2	20.3	25.8	5.0	21.1
2017	30.3	17.8	24.1	5.3	23.4

Chapter 2 - Early Drought Stress Detection in Turfgrass Utilizing Thermal Imaging via Small Unmanned Aircraft Systems

Abstract

Recent advances in aerial platforms and thermal imaging provide opportunities to improve turfgrass management, including early drought detection and water conservation, but research on this topic is limited. Our objectives were to: i) evaluate the ability of canopy temperature (Tc) imaging from small unmanned aircraft systems (sUAS) to detect drought stress early in turfgrass; ii) compare early drought-stress detection ability of Tc imaging with that of sUAS-mounted and handheld optical sensors; and iii) evaluate relationships between thermal data and spectral reflectance from sUAS-mounted and handheld sensors, soil volumetric water content (VWC), soil temperature, turfgrass visual quality (VQ), and percentage green cover (PGC). The study was conducted during summer 2017 on creeping bentgrass (*Agrostis stolonifera* L.) irrigated from 15% to 100% evapotranspiration (ET) replacements to impose a gradient of drought stress. Airborne spectral reflectance measurements included three individual broadbands [near infrared (NIR, 680-780 nm), green and blue bands (overlapped, 400-580 nm)] and eight derived vegetation indices. Results indicated thermal imaging via the sUAS detected rises of Tc in 15% and 30% compared to 100% ET plots, corresponding to declines in VWC, before drought stress became visible. This was comparable to the best spectral parameters (i.e., NIR band and GreenBlue VI) on companion flights, and Tc was closely correlated with spectral data from sUAS-mounted ($|r| = 0.52$-0.69) and handheld sensors ($|r| = 0.75$-0.82). Thermal data

were more strongly correlated with turfgrass VQ ($r = -0.60$ to -0.77) and PGC ($r = -0.58$ to -0.78) than with VWC ($r = -0.43$ to -0.63) and soil temperature ($|r| = 0.27$-0.41).

Introduction

There are estimated 13 to 20 million hectares of turfgrass in the U.S., including on roadsides, residences, golf courses, sports facilities, campuses, etc. (Milesi et al., 2005). Besides aesthetical and recreational benefits to the community, turfgrass also improves the environment by mitigating heat buildup, stabilizing soil and dust, sequestering carbon in the soil, reducing glare, noise and air pollution, etc. (Beard, 1973). Because water is increasingly a limited resource, wise irrigation management of large areas of turfgrass will be critical towards conserving water.

Recent advances in aerial remote sensing platforms, specifically small unmanned aircraft system (sUAS) technology, and remote sensing instrumentation provide a potentially efficient method for early detection of drought stress and conserving water in turfgrass management. The advantages of applying the sUAS include flexibility and increasingly user-friendly operational requirements, decreasing costs, improved reliability and safety, and excellent performance for high-quality data acquisition in low altitude environments, compared to expensive and time-inflexible satellite data (Pajares, 2015).

Other researchers have modeled soil moisture with canopy spectral reflectance on creeping bentgrass (*Agrostis stolonifera* L.) and perennial ryegrass (*Lolium perenne* L.) (Dettman-Kruse et al., 2008). Under drought stress, turfgrass visual quality decreases, mainly because soil moisture becomes limited. However, due to variability in drought resistance among turfgrass species and cultivars, and because other environmental factors besides soil moisture

(e.g., soil type, climate) may affect turf performance in response to drought stress, relationships between turfgrass visual performance and declines in soil moisture may vary. This could result in inaccurate timing of irrigation for the prevention of visible drought-stress symptoms. Therefore, site-specific remote sensing measurements that predict declines in turfgrass visual performance due to early drought stress may provide for a more accurate, timelier irrigation schedule.

Canopy temperature (Tc) is an important component of the turfgrass environment. As water stress occurs, transpiration and its cooling effects are reduced by stomatal closure, which results in an increase in Tc (Blonquist et al., 2009; Peterson et al., 2017). The application of using Tc and canopy-air temperature difference (Tc-Ta) to assess plant water stress and stomatal regulation has been documented for turfgrass (Martin et al., 1994; Blonquist et al., 2009; Ballester et al., 2017; Peterson et al., 2017). More recently, thermal infrared sensors have been incorporated with the sUAS for research over agricultural crops, vineyard and orchards (Berni et al., 2009; Zarco-Tejada et al., 2012; Zarco-Tejada et al., 2013; Ballester et al., 2017).

Thermal infrared imagery has begun to be used on turfgrass, such as in golf courses, and promoted by companies aimed at assisting superintendents and sport facility managers. Surprisingly, little research has investigated the utility of measuring Tc via sUAS for turfgrass management, not to mention the relationships between Tc and spectral reflectance or vegetation indices (VIs), in response to plant stresses (Fenstermaker-Shaulis et al., 1997; Taghvaeian et al., 2013; Van der Merwe et al., 2017).

Taghvaeian et al. (2013) compared the Grass Water Stress Index (crop water stress index for turfgrass using handheld thermometer measurements) with a surface energy balance model METRIC (using handheld multi-spectral radiometer measurements, surface temperature, etc.) on warm- and cool-season turfgrasses under varying irrigation treatments, and found evapotranspiration estimates from these two methods were similar. It indicated there might be relationships between spectral reflectance and canopy temperature of turfgrass under drought stress.

Our objectives were to i) evaluate the ability of thermal infrared imaging via sUAS platforms to detect drought stress early in turfgrass; ii) compare the early drought-stress detection ability of thermal imaging with that of spectral reflectance data obtained concurrently from sUAS-mounted and handheld optical sensors; and iii) evaluate relationships between thermal imaging data and spectral reflectance and other canopy and soil variables. We acquired a whole-season profile of Tc in response to drought stress in turfgrass using thermal imagery mounted on sUAS platforms, which provide a wide range of data for evaluations.

Methods and Materials

The research was conducted under an automatic rainout shelter at the Rocky Ford Turfgrass Research Center near Manhattan, Kansas (39º13’’53’’N, 96º34’51’’W). The rainout shelter covered the whole study area (about 66 m^2) when precipitation reached 0.25 mm and

retracted an hour after rainfall ceased. The soil was a Chase silty clay loam (fine, smectitic, mesic Aquertic Argiudoll).

From 7 June to 31 Aug. 2017, irrigation treatments were applied to 'Declaration' creeping bentgrass (Agrostis stolonifera L.) in 24 plots (1.7 by 1.5 m^2 each) arranged in a randomized complete block design. Irrigation amounts were calculated from daily reference evapotranspiration (ET_o, hereafter referred to as ET) using on-site weather data (http://mesonet.k-state.edu/) and the American Society of Civil Engineers (ASCE) standardized reference ET equation (Walter et al., 2000). Six deficit-irrigation treatments were included to induce a gradient of drought stress symptoms within each block: 15, 30, 50, 65, 80 and 100% ET replacement. Irrigation was applied three times per week by hand with a wand attached to a meter (Model 03N31, GPI, Inc.) and hose. The rainout shelter malfunctioned on 5 Aug, permitting 19 mm of precipitation.

Maintenance

Creeping bentgrass was initially seeded at 48.8 kg/ha on 18 Sept. 2014, and reestablished by verticutting, seeding at about 40 kg/ha and topdressing on 22 Sept. 2016. The creeping bentgrass was aerified on 5 June 2017. Plots were not cultivated during the dry-down periods to avoid damage to the turfgrass canopy during drought stress. In 2017, plots were aerified to promote growth four days before the dry down began. This slightly disrupted the turf canopy during the first week of measurements, but those effects diminished rapidly thereafter. Plots were

mowed three times a week at 15.9 mm and clippings were removed. Turfgrass was fertilized with 48.9 kg N ha^{-1}, 3.1 kg P ha^{-1}, and 40.6 kg K ha^{-1} on 12 May.

For preventative insect control, chlorantraniliprole (Acelepryn, Syngenta Crop Protection LLC) was applied at 0.26 kg a.i. ha-1 on 26 May 2017. Dithiopyr (Dimension, Dow AgroSciences LLC) at 0.56 kg a.i. ha-1 and a mixture of propionic acid, 2,4-D acid and dicamba (Trimec bentgrass formula, PBI Gordon Corporation) at 0.76 kg a.i. ha-1 was applied in mid-April over 2015-2017. For preventative control of dollar spot and other diseases in 2017, triticonazole (Triton FLO, Bayer Environmental Science) and tetrachloroisophthalonitrile (Syngenta) was applied at 1.1 kg a.i. ha-1 on 28 May and 6.9 kg a.i. ha-1 on 23 June, respectively.

Data collection

All measurements were taken weekly (weather permitting) on cloud-free days with wind speed below 24 km/h and within 2.5 hours of local solar noon. On each measurement day, a thermal camera (FLIR VUE PRO R 336), mounted on an IRIS+ (3D Robotics) flown at 25 m AGL, was used to attain Tc from 15 June to 31 Aug. The camera has 35º FOV (field of view) and 9 mm focal length with 4.7-cm ground resolution, as calculated from Mission Planner (v.1.3.56, ArduPilot). One thermal image containing the whole study area was selected for each measurement date. Average canopy temperatures were retrieved from the center 60% of each plot from the thermal images using the FLIR tool (v.5.13.), which also produced color-enhanced thermal maps. Average five-minute air temperatures at 2 m above ground level during the

acquisition period were obtained from the on-site weather station, and used to calculate rough estimates of Tc-Ta for each plot. Although irrigation treatments began on 7 June, airborne canopy temperature measurements were not acquired until 15 June due to technical issues.

A series of ultra-high spatial resolution images (< 1-cm ground resolution) were also collected on each measurement date with a modified Canon PowerShot S100 camera (MaxMax.com) identical to that used by Van der Merwe et al. (2017). The camera sensor was equipped with filters blocking visible red light (580-680 nm) and NIR above 780 nm while allowing visible blue (B) and green bands (G) (overlapped, 400-580 nm), and the transition of visible red edge to NIR band (680-780 nm), to pass to the sensor. The camera was mounted on a hexacopter (S800 EVO, DJI) flown 25 m above ground level (AGL) to achieve image overlap of at least 75%. The camera was set to manual mode with autofocus and ISO at 100, and the exposure level was set to be two stops below the standard while facing straight down towards the turfgrass surface by adjusting shutter speed with f-stop being fixed (f/2.2). The resulting JPEG images were stitched into averaged orthomosaics using Agisoft Photoscan Professional (version 1.3.4 build 5067).

Treatment effects were analyzed from the orthophoto using AgVISR (v. 2.1.6, AgVISR Services). The three individual band spectral reflectances contained in the extracted squares and eight vegetation indices (calculated from the three bands) were evaluated for their ability to detect drought stress. According to AgVISR, the eight vegetation indices included NDVI Enhanced1 [(NIR+G-2B)/(NIR+G+2B)], NDVI Enhanced2 [(NIR+G-B)/(NIR+G+B)], NDVI

Enhanced3 [(NIR-G-B)/(NIR+G+B)], Blue NDVI [(NIR-B)/(NIR+B)], Green NDVI [(NIR-G)/(NIR+G)], GreenBlue [(G-B)/(G+B)], NIR Blueratio (NIR-B), NIR Green Diff [(NIR-G-B)/(NIR-G+B)]. The absolute scales of NDVI in the study may not comparable to the traditional scale because calibration plates were not used, but it did not affect comparisons among treatments. Additional details about NDVI scales, as well as about image processing to develop the VIs, can be found in chapter 1.

Turfgrass performance was evaluated by visual quality ratings (VQ) and percentage green cover (PGC). Two personnel evaluated the VQ of turfgrass to reduce individual biases on a numeric scale from 1 to 9 (1 = dead or dormant turf, 9 = uniform, green and dense turf, and 6 = minimally acceptable turf for use in golf course fairways) according to color, texture, density, and uniformity (Morris and Shearman, 1999; Bell et al., 2002). Images were collected for PGC analysis using the method of Karcher and Richardson (2005) (SigmaScan Pro v. 5.0, SPSS Science Marketing Dept.). Images were taken with a Nikon D5000 digital camera (f-stop of 5.6, 1/125 sec exposure time, and 800 ISO-speed; Nikon Inc.) using a lighted camera box (51 x 61 x 56 cm).

Additional measurements included volumetric water content (VWC), soil temperature, and NDVI by two handheld optical sensors. The VWC was measured with time domain reflectometry (TDR; FieldScout TDR 300 Soil Moisture Meter, Spectrum Technologies) at 0 to 7.6 cm depth in two random locations within each plot. Soil temperature was measured with digital soil thermometers (DT310LAB Lab Digital Stem Thermometer, General Tools &

Instruments), with one reading per plot at 7.6 cm depth. Handheld measurements of NDVI were obtained with a passive optical sensor [FieldScout CM1000 NDVI meter (FS), Spectrum Technologies] in three random locations within each plot. It sensed ambient light spectral reflectance peaking at wavelengths of 660 and 840 nm for computing $NDVI_{FS}$. Each reading was collected at approximately 0.9 m AGL with a conical field of view (FOV) of approximately 6.5 cm diameter on the ground. Additional NDVI measurements were obtained with an active remote sensor [RapidScan CS-45 (RS), Holland Scientific), which measured self-generated light spectral reflectance peaking at narrowbands of 670 (red), 730 (red edge) and 780 (near infrared, NIR_{RS}) nm (bandwidths are proprietary), which allows for computing $NDVI_{RS}$ [(NIR_{RS}-red)/(NIR_{RS}+red)] as well as NDRE [(NIR_{RS}-RE)/(NIR_{RS}+RE)]. It was carried at approximately 0.9 m AGL to scan about 80% of each plot with readouts of the average, maximum, and minimum values of NDVI and NDRE across each plot, and the standard deviation and coefficient of variation of the average.

Statistical analysis

Analysis of irrigation treatment main effects on all variables on each measurement date was conducted in PROC GLIMMIX of SAS, with treatment being a fixed effect and date being a random effect ($P < 0.05$; SAS 9.4, SAS Institute). Pearson's correlations among variables were conducted by PROC CORR of SAS ($P < 0.05$).

Linear relationships were analyzed between Tc and VQ and PGC, grouped by irrigation treatments. Analysis-of-variance F -test ($P < 0.05$) and adjusted r^2 were calculated in PROC REG

of SAS. A significant relationship between PGC and Tc was detected among 15 to 50% ET irrigated plots, to which a sigmoid model developed by Karcher et al. (2008) was adopted to fit the data. The parameters of this model, slope and Tc where PGC equals 50%, were determined by Solver Parameter in Microsoft Excel (16.0.11001.20070) when the coefficient of determination (r^2) was the maximum.

Results and Discussion

Irrigation main effect on canopy temperature and turf visual performance

As mentioned earlier, Tc from the sUAS was not measured until one week after irrigation treatments began (15 June). By then, Tc was already greater in 15% and 30% than in 100% ET plots, and remained so throughout the study (Table 2.1). Greater Tc in 15% and 30% ET plots throughout the study was likely an ability of Tc to detect lower VWC in less-irrigated plots (Dettman-Kruse et al., 2008). Because turfgrass fully covered the soil throughout the study, higher Tc in less-irrigated plots was likely caused by reductions in canopy ET as the soils dried, which reduced evaporative cooling compared with higher irrigated treatments (Blonquist et al., 2009; Peterson et al., 2017). Color-enhanced images of creeping bentgrass revealed negligible differences in Tc among treatment plots early in the study (Fig. 2.1A), but striking differences by the study's end (Fig. 2.1B).

Early in the study, Tc increased in drier plots before drought stress became evident in VQ. For example, on 15 June there were no differences in VQ among treatments, nor significant

correlations between VQ and irrigation level, despite higher Tc in 15% and 30% than 100% ET plots (Tables 2.1 and 2.2). In fact, VQ didn't decrease in 15% and 30% ET plots until 1 July, which suggests Tc detected drought stress 16 days before it became visible. However, it is not certain that spectral reflectance parameters detected drought stress symptoms a full 16 days early, and it is possible that drought symptoms became visible before 1 July because VQ was not evaluated on days between sUAS flights (e.g., between 20 June and 1 July). By the end of the study, Tc was also greater in 50% ET than in 100% ET plots. Interestingly, Tc was similar among the highest three irrigation treatments (i.e., 65% to 100% ET) throughout the study.

Correlations between irrigation level and VWC were consistently strong ($r > 0.80$) during the dry down (Table 2.2). This, along with clear patterns of decreasing VWC with irrigation treatment level during the dry down (Table 2.1), indicated that a strong gradient of drought stress was achieved across the treatments. Not surprisingly, Tc was inversely correlated with irrigation level throughout the study, with correlation coefficients (r) ranging from -0.65 to -0.82. The strongest correlation with Tc was on the final day of the study, when differences among irrigation treatments were the greatest.

After three weeks into the study (1 July), VQ and PGC also became correlated with irrigation levels (Table 2.2). However, in contrast to Tc, neither VQ nor PGC were significantly correlated with irrigation level during the first two weeks of the study (i.e., through 20 June). Regarding VQ, insignificant correlations with irrigation treatment on those two dates were likely because of the slower response of VQ to drought stress than Tc, as discussed above. Conversely,

PGC was lower in 15% ET that the other treatments on 20 June, or about two weeks into the study (Table 2.1). This indicates PGC was more sensitive to early drought stress than VQ, although VQ could vary with different evaluators. Regardless, Tc was even more sensitive than PGC in detecting early drought stress, based on VWC patterns. For example, VWC was lower in 30% than 100% ET plots on 15 June, which was detected by Tc but not PGC.

Comparisons of drought-stress detection ability between canopy temperature and spectral reflectance data from sUAS-mounted and handheld optical sensors

One week into the study (June 15), before any differences in VQ emerged, early drought stress was detected in less-irrigated treatments by Tc, NIR, and five VIs from sUAS measurements, and $NDVI_{RS}$ and red reflectance (Red_{RS}) from the handheld active but not the handheld passive optical sensor ($NDVI_{FS}$) (Table 2.3). Moreover, Tc, NIR, and GreenBlue VI from the sUAS were more sensitive at detecting early drought stress in the lower irrigation levels than the other spectral reflectance measurements from the sUAS and RS. Specifically, Tc, NIR and GreenBlue VI all differentiated 100% from 15% and 30% ET plots, whereas the other measurements by the sUAS and RS only detected drought stress in 15% ET (Table 2.3). This observation is supported by stronger correlations between Tc, NIR, and the GreenBlue VI and irrigation levels than nearly all of the other VIs and reflectance bands (Table 2.2, June 15). Thus, the ability of Tc to detect early drought stress is comparable to the best spectral parameters (i.e., NIR and GreenBlue VI) on a companion flight.

Researchers of other plant systems have reported Tc to detect plant water stress better than other parameters, including spectral reflectance measurements. For example, in almond, lemon, and peach trees, airborne Tc was more sensitive to water stress than stem water potential, stomatal conductance, and VIs acquired by the same sUAS (Ballester et al., 2017). Thermal imagery on orange trees from an sUAS showed that Tc had a stronger relationship with stomatal conductance than did spectral reflectance and fluorescence indices conducted with hyperspectral radiance imagery, when xylem water potential ranged from -0.5 to -2 MPa (Zarco-Tejada et al, 2012).

The thermal images were single snapshots by the FLIR camera mounted on an sUAS (Fig. 2.1). In contrast, spectral reflectance measurements required the stitching together of multiple images to produce orthomosaics, meaning more data collection and processing, as well as software costs. Furthermore, VIs or reflectance bands (e.g., NIR) derived from single photos with the modified digital camera were not able to differentiate treatment differences across the study area (data not shown). Therefore, thermal imaging may require fewer aerial measurements to generate orthomosaics than spectral reflectance imaging over the same area. However, more thermal image collection may still be necessary for reducing errors, especially when short focal length lenses are used, the surface is rough, or the solar angle away from zenith is large (Van der Merwe et al., 2017).

Correlations between aerial thermal data and aerial and ground-based spectral reflectance data and ground-based canopy and soil measurements

Same-day measurements of Tc and spectral reflectance obtained aerially, spectral reflectance obtained by handheld optical devices, and of VQ, PGC, VWC, and T_{soil}, provided a unique opportunity to examine correlations between Tc and the other measurements. Although Tc provides a relative estimate of plant stress among irrigation levels, Tc-Ta was also examined because it adjusts for differences in meteorological conditions that affected Tc on a given day (Martin et al., 1994). Presumably, greater differences between Tc and Ta indicate greater drought stress, particularly in relation to non-water-stressed plants in 100% ET plots.

Over the entire study, thermal data (Tc and Tc-Ta) were better correlated with PGC and VQ than with VWC or T_{soil} (Table 2.4). This indicated that under varying drought conditions, thermal data were more directly associated with the turfgrass canopy properties than with soil properties. The reason is that Tc, which is a direct measure of the surface temperature of turfgrass covering the plots, increases as transpiration decreases and the leaves fire in response to drying soils in less-irrigated plots (Peterson et al., 2017). Strong correlations between Tc and canopy properties were a result of wide ranges in Tc and VQ and PGC across the season in lower irrigation treatments (15% to 50%) (Figs. 2.2 and 2.3). Correlations between Tc and canopy properties were not significant in 65%, 80%, and 100% ET plots probably because transpiration in each of those treatments remained relatively stable throughout the season.

A sigmoid curve was fitted in the relationship between PGC and Tc, especially among 15 to 50% ET irrigated plots (Fig. 2.4). The PGC declined relatively slowly when drought stress started to develop, as indicated by relatively low Tc. Then Tc increased dramatically with

decreasing PGC, and finally began to level out. This is supported by the relatively slow decline in turfgrass VQ during early drought stress development that allowed for early detections with remote sensing, as discussed in previous sections. Interestingly, similar sigmoid relationships were reported between PGC and the number of days after irrigation withheld in a turfgrass dry down study (Karcher et al., 2008).

Canopy temperature was also significantly correlated with VWC and T_{soil}, but the relationships were weaker than with VQ and PGC, as discussed above (Table 2.4). The correlation of Tc with VWC was stronger than with T_{soil}, probably because of the strong impact of irrigation treatments on VWC (Tables 2.1 and 2.2). In contrast to VWC, the effects of irrigation level on T_{soil} in less-irrigated plots did not appear until later in the experiment (Table 2.1, 1 July), and even then the correlations were weaker throughout the study (Table 2.2). Although T_{soil} typically increases as the soil dries, other factors such as shading by the turfgrass canopy may confound relationships between T_{soil} and Tc (Bremer and Ham, 1999; Bremer et al., 2001).

Overall, thermal data were significantly correlated with spectral reflectance data (with the exception of green reflectance from the sUAS) measured across the irrigation gradients ($|r|$ = 0.52 to 0.82 for Tc, and $|r|$ = 0.20 to 0.65 for Tc-Ta, Table 2.4). As for sUAS measurements, the correlations between Tc and VQ ($r = -0.77$, $P < .0001$) and PGC ($r = -0.78$, $P < .0001$) (Table 2.4) were as strong as between most VIs and VQ ($r = 0.77$ to 0.82, $P < .0001$) and PGC ($r = 0.77$ to 0.86, $P < .0001$) (Table 1.9, Chapter 1), which indicates comparable relationships between

sUAS remote sensing data (i.e., Tc and spectral reflectance variables) and turf canopy properties as varying drought stress developed across irrigation treatments (e.g., 15 June shown in Table 2.3).

Correlations of thermal data with spectral parameters obtained with handheld optical sensors (|r| = 0.59-0.82) were slightly higher than spectral parameters obtained with the sUAS (|r| = 0.20-0.69) (Table 2.4). This may have been an artifact of different reflectance signal processing between the camera sensor and the handheld optical sensors, as well as different VIs and reflectance bands that were used in these sensors. Also, spectral reflectance data from the sUAS were derived from broadbands, while handheld optical measurements were from narrowbands.

Interestingly, most VIs were better correlated with Tc than Tc-Ta. This may be explained by slight differences in the time between measurements of Tc and Ta. Specifically, Tc was measured aerially from the drone and Ta was obtained from a weather station within 50 m from the study area. While every effort was made to match the time of Tc measurements with Ta, they were likely separated by several minutes, which probably affected the accuracy the Tc-Ta estimates. However, it is notable that compared with sUAS data, Tc-Ta was significantly and best correlated with NIR and GreenBlue, which were also the best at predicting early drought stress (Table 2.4; Chapter 1). It may indicate these spectral parameters were more sensitive to initial increases in turfgrass Tc relative to Ta in response to early drought stress.

Conclusions

In this study, the Tc acquired by the sUAS predicted drought stress more than 5 days before drought symptoms were evident in either VQ or PGC. The ability of Tc to predict drought stress was also comparable to the best spectral parameters reported in Chapter 1 (NIR and GreenBlue VI on companion flights, and $NDVI_{RS}$ and Red_{RS} of the handheld active optical sensor). Results from this study suggest thermal imaging with sUAS provides an effective method for monitoring and predicting drought stress in turfgrass. Additional research using thermal imaging from sUAS is needed on different turfgrass species and cultivars in different locations.

Thermal data were more strongly associated with turfgrass visual performance (i.e., VQ and PGC) than with soil moisture or soil temperature. Relationships between thermal and spectral data and turfgrass canopy properties were nearly equivalent, demonstrating the potential for using one or both to detect early drought stress in turfgrass.

References

Beard, J.B. 1973. Turfgrass: Science and Culture. Prentice Hall, Englewood Cliffs, NJ. p. 1-2.

Ballester, C., P.J. Zarco-Tejada, E. Nicolás, J.J. Alarcón, E. Fereres, D.S. Intrigliolo, and V. Gonzalez-Dugo. 2017. Evaluating the performance of xanthophyll, chlorophyll and structure-sensitive spectral indices to detect water stress in five fruit tree species. Precision Agric. 19:178–193. doi: 10.1007/s11119-017-9512-y.

Bell, G.E., D.L. Martin, S.G. Wiese, D.D. Dobson, M.W. Smith, M.L. Stone, and J.B. Solie. 2002. Vehicle-mounted optical sensing: An objective means for evaluating turf quality. Crop Sci. 42:197–201.

Berni, J., P.J. Zarco-Tejada, L. Suarez, and E. Fereres. 2009. Thermal and narrowband multispectral remote sensing for vegetation monitoring from an unmanned aerial vehicle. IEEE Trans Geosci Remote Sens. 47:722–738. doi: 10.1109/TGRS.2008.2010457.

Blonquist, J.M., J.M. Norman, and B. Bugbee. 2009. Automated measurement of canopy stomatal conductance based on infrared temperature. Agricultural and Forest Meteorology. 149:2183–2197. doi: 10.1016/j.agrformet.2009.10.003.

Bremer, D.J., and J.M. Ham. 1999. Effect of spring burning on the surface energy balance in a tallgrass prairie. Agric. for. Meteorol. 97:43-54.

Bremer, D.J., L.M. Auen, J.M. Ham, and C.E. Owensby. 2001. Evapotranspiration in a prairie ecosystem: Effects of grazing by cattle. Agron. J. 93:338-348.

Dettman-Kruse, J.K., N.E. Christians, and M.H. Chaplin. 2008. Predicting soil water content through remote sensing of vegetative characteristics in a turfgrass system. Crop Sci. 48:763. doi: 10.2135/cropsci2006.01.0040.

Fenstermaker-Shaulis, L.K., A. Leskys, and D.A. Devitt. 1997. Utilization of remotely sensed data to map and evaluate turfgrass stress associated with drought. Journal of Turfgrass Management. 2:65–81. doi: 10.1300/J099v02n01_06.

Karcher, D.E., and M.D. Richardson. 2005. Batch analysis of digital images to evaluate turfgrass characteristics. Crop Sci. 45:1536. doi: 10.2135/cropsci2004.0562.

Karcher, D.E., M.D. Richardson, K. Hignight, and D. Rush. 2008. Drought tolerance of tall fescue varieties selected for high root:shoot ratios. Crop Sci. 48:771–777.

Martin, D.L., D.J. Wehner, and C.S. Throssell. 1994. Models for predicting the lower limit of the canopy-air temperature difference of two cool season grasses. Crop Sci. 34:192. doi: 10.2135/cropsci1994.0011183X003400010034x.

Milesi, C., S.W. Running, C.D. Elvidge, J.B. Dietz, B.T. Tuttle, and R.R. Nemani. 2005. Mapping and modeling the biogeochemical cycling of turf grasses in the United States. Environ Manage. 36:426–438. doi: 10.1007/s00267-004-0316-2.

Morris, K.N., and R.C. Shearman. 1999. NTEP turfgrass evaluation guidelines. National Turfgrass Evaluation Program, Beltsville, MD.

Pajares, G. 2015. Overview and current status of remote sensing applications based on unmanned aerial vehicles (UAVs). Photogramm Eng Rem S. 81:281–330. doi: 10.14358/PERS.81.4.281.

Peterson, K.W., D.J. Bremer, and J.M. Blonquist. 2017. Estimating transpiration from turfgrass using stomatal conductance values derived from infrared thermometry. Int. Turf. Soc. Res. J. 13:113-118. doi: 10.2134/itsrj2016.09.0788.

Taghvaeian, S., J. Chávez, M. Hattendorf, and M. Crookston. 2013. Optical and thermal remote sensing of turfgrass quality, water stress, and water use under different soil and irrigation treatments. Remote Sensing. 5:2327–2347. doi: 10.3390/rs5052327.

Van der Merwe, D., L.R. Skabelund, A. Sharda, P. Blackmore, and D. Bremer. 2017. Towards characterizing green roof vegetation using color-infrared and thermal sensors. Proceedings of the CitiesAlive 15th Annual Green Roof and Wall Conference, Seattle, WA. 18-21 September.

Walter, I., R. Allen, R. Elliott, M. Jensen, D. Itenfisu, B. Mecham, T. Howell, R. Snyder, P. Brown, S. Echings, T. Spofford, M. Hattendorf, R. Cuenca, J. Wright, and D. Martin. 2001. ASCE's standardized reference evapotranspiration equation. p. 1-11. In Flug et al. (ed.) Watershed management and operations management 2000. doi: 10.1061/40499(2000)126

Zarco-Tejada, P.J., V. González-Dugo, and J.A.J. Berni. 2012. Fluorescence, temperature and narrow-band indices acquired from a UAV platform for water stress detection using a

micro-hyperspectral imager and a thermal camera. Remote Sens Environ. 117:322–337. doi: 10.1016/j.rse.2011.10.007.

Zarco-Tejada, P.J., V. González-Dugo, L.E. Williams, L. Suárez, J.A.J. Berni, D. Goldhamer, and E. Fereres. 2013. A PRI-based water stress index combining structural and chlorophyll effects: Assessment using diurnal narrow-band airborne imagery and the CWSI thermal index. Remote Sens Environ. 138:38–50. doi: 10.1016/j.rse.2013.07.024.

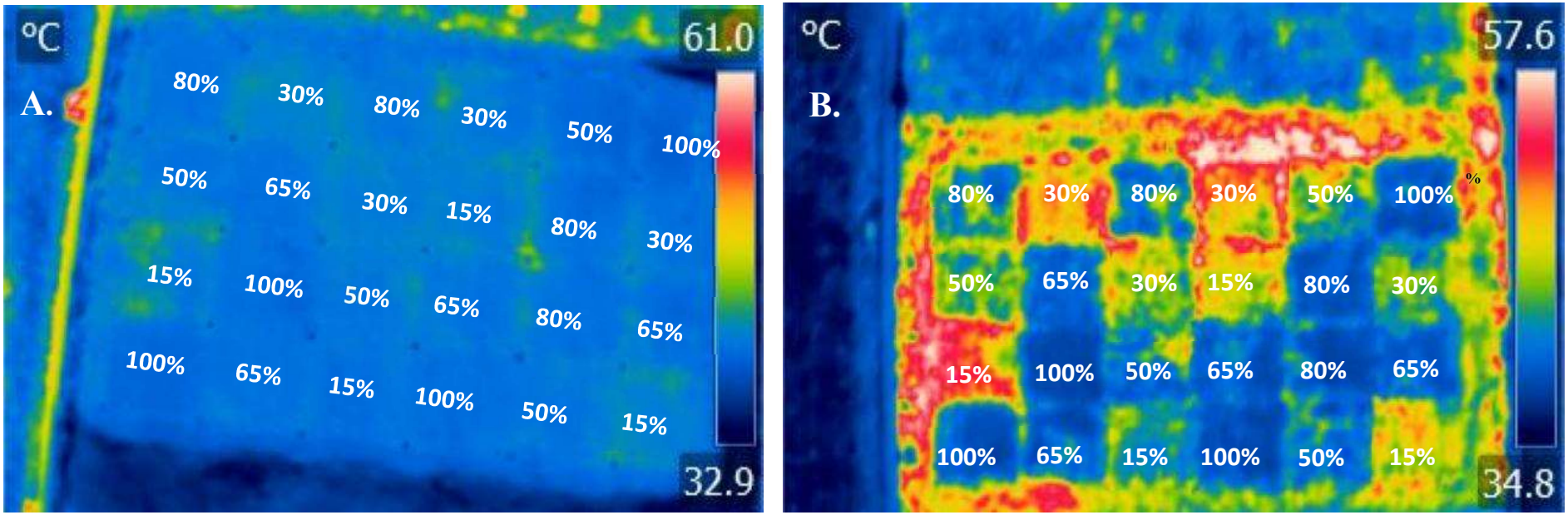

Figure 2.1. Color-enhanced thermal image of plots on 15 June (A) and 31 August (B). Percentages denote ET replacement irrigation treatment.

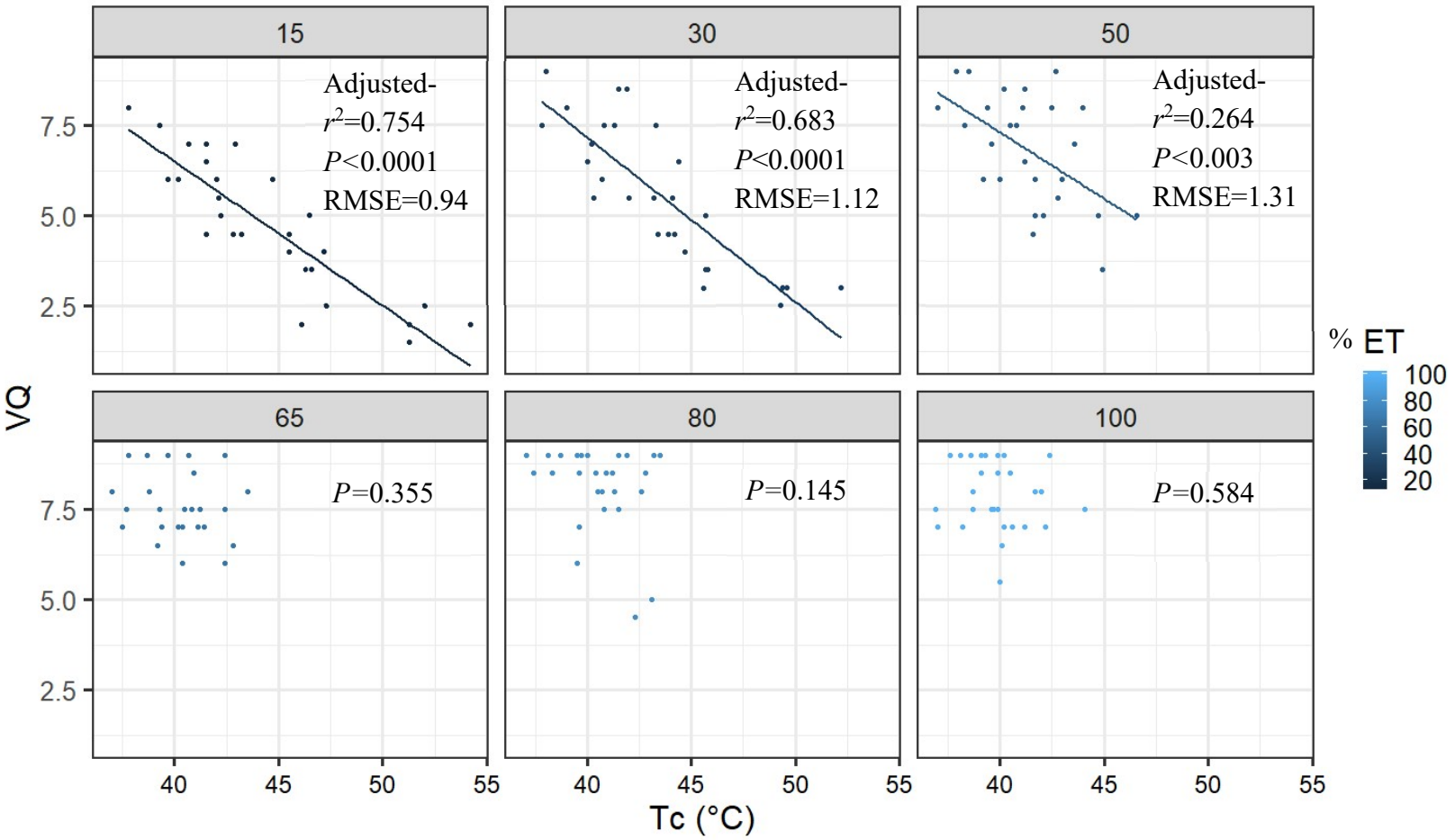

Figure 2.2. Linear relationships between visual quality (VQ) and canopy temperature (Tc) grouped by irrigation level (% ET).

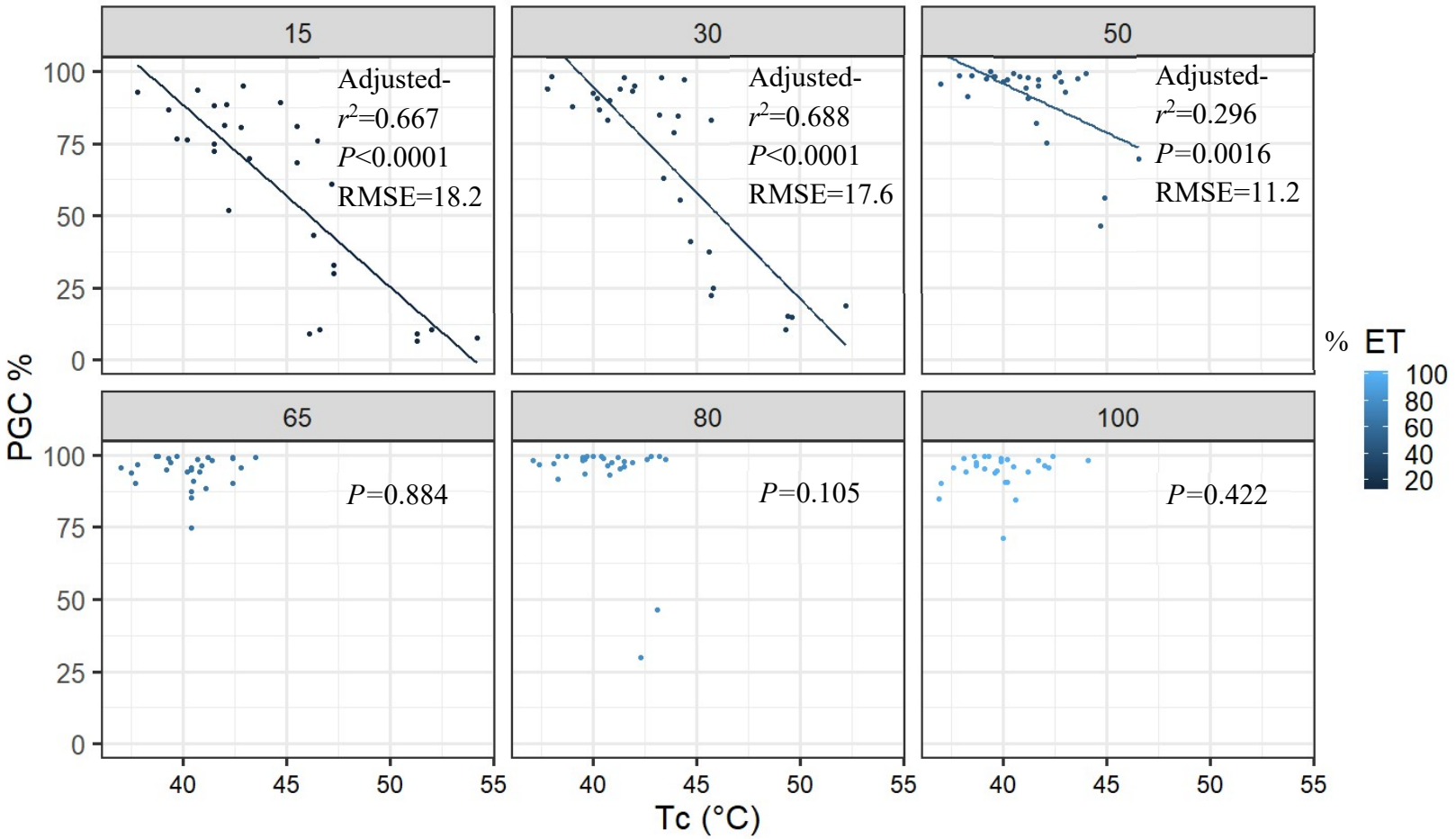

Figure 2.3. Linear relationships between percentage green cover (PGC) and canopy temperature (Tc) grouped by irrigation level (% ET).

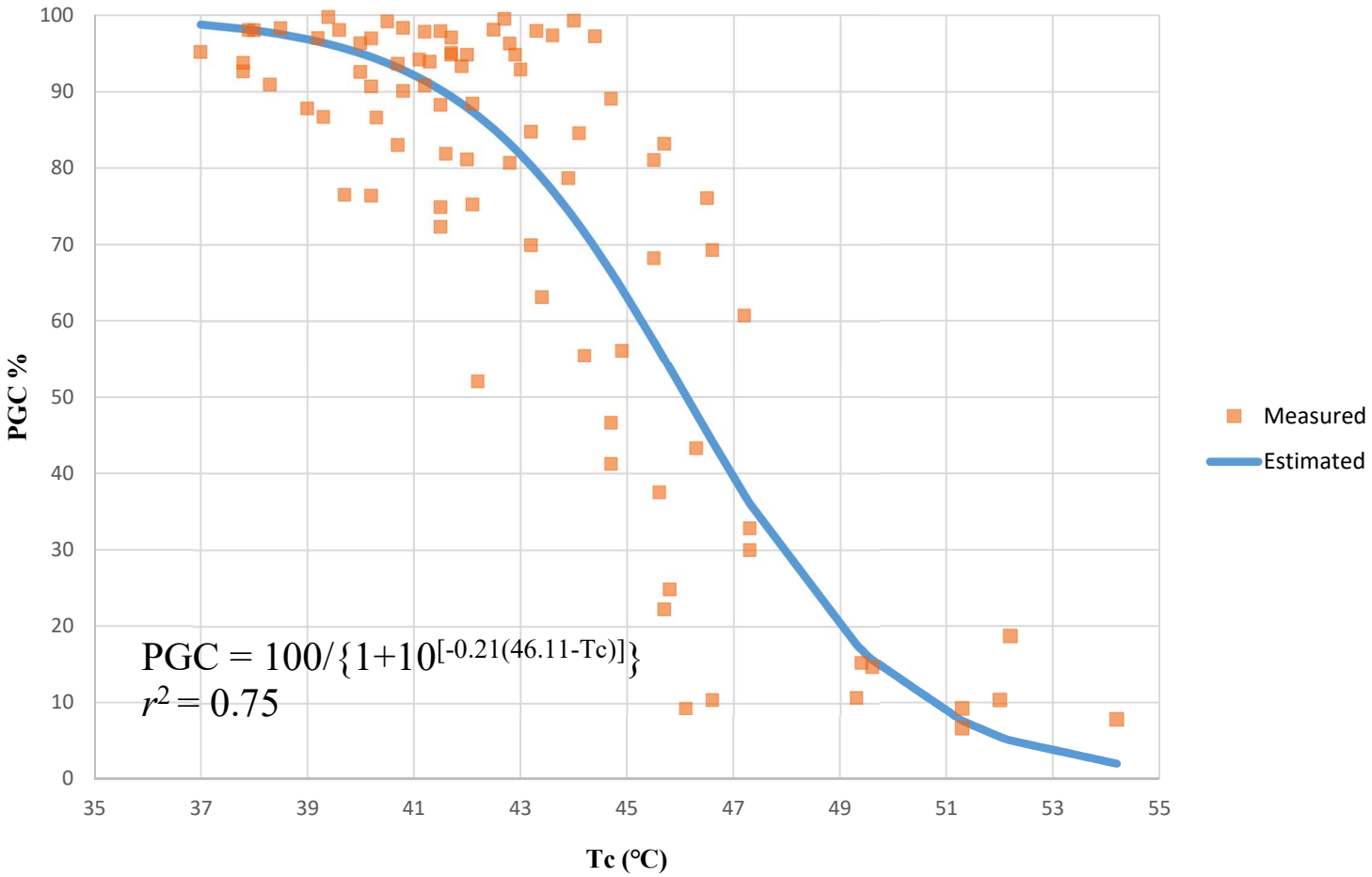

Figure 2.4. Scatterplot of percentage green cover (PGC) versus measured and estimated canopy temperature (Tc) among 15 to 50% ET irrigated plots.

Table 2.1. Irrigation main effect by date on canopy temperature (Tc), visual quality (VQ), percentage green cover (PGC), and volumetric water content (VWC), in 'Declaration' creeping bentgrass in 2017 ($P < 0.05$).

Treatment†	7-June	15-June	20-June	1-July	10-July	25-July	4-Aug	31-Aug
		Average air temperature for the same hour Tc was measured (°C)						
		33.5	32.9	28.3	35.5	34.1	23.5	26.6
				Tc (°C)				
100%	na‡	40.4A	37.4A	42.6A	39.1A	40.8A	39.3A	39.4A
80%	na	40.9ABC	37.7AB	43.0AB	39.7A	41.5A	39.5A	41.1AB
65%	na	40.8AB	37.5A	42.8A	39.9A	41.2A	39.3A	40.4A
50%	na	40.9ABC	37.9AB	43.2AB	40.2A	43.5AB	40.6AB	43.3B
30%	na	41.4BC	38.8BC	44.4BC	42.5B	47.2BC	43.1BC	47.2C
15%	na	41.4C	39.3C	44.9C	44.6C	49.7C	45.3C	47.2C
				VQ				
100%	7.1	7.3	7.6	8.1A	8.6A	7.9A	8.3A	7.4A
80%	8.0	8.0	8.8	8.6A	8.9A	8.5A	8.5A	5.6BC
65%	7.3	7.6	7.9	7.8A	7.6AB	7.3A	7.8A	6.5AB
50%	8.3	7.9	8.4	8.0A	7.3B	5.6B	6.0B	4.5CD
30%	7.8	8.0	7.9	6.1B	5.1C	4.0C	4.5BC	3.4DE
15%	7.1	6.6	6.9	5.6B	4.3C	3.1C	3.4C	2.8E
				PGC (%)				
100%	82.5	90.5AB	91.2A	98.0A	97.7AB	96.4A	98.8A	89.3A
80%	90.8	95.6A	95.8A	99.0A	99.1A	97.5A	99.5A	67.0AB
65%	87.5	92.5A	94.1A	98.2A	97.6AB	95.7A	98.3A	85.5A
50%	90.9	94.9A	95.6A	98.5A	98.4AB	88.3A	96.8A	64.9AB
30%	92.0	93.8A	92.5A	90.7B	72.9CB	49.3B	57.3B	26.4C
15%	83.0	84.5B	83.1B	85.2B	53.0C	36.8B	35.1B	38.2CB
				VWC (%)				
100%	45.4	45.2A	42.8A	41.7A	47.6A	42.5A	46.3A	38.8A
80%	45.3	43.8A	42.3A	41.4A	46.9A	40.9A	43.9AB	34.4B
65%	44.9	40.7A	38.5B	39.2A	47A	38.6A	44.5AB	34.9AB
50%	45.2	40.9A	39.8AB	39.3A	44A	33.3B	41.4BC	28.1C
30%	46.1	34.3B	27.9C	27.4B	34.2B	24.7C	37.1CD	22.0D
15%	44.5	29.4C	24.9C	22.9C	27C	20.9C	33.4D	18.0D
				T_{soil}(°C)				
100%	27.5	28.7ABC	25.7	27.0C	30.2C	30.8B	26.4B	25.0
80%	27.4	28.2C	25.9	26.8C	30.2C	30.5B	26.4B	25.0
65%	27.3	28.7AB	25.7	27.0BC	30.7BC	30.8B	26.3B	25.1
50%	27.4	28.4BC	26.0	26.8C	30.5BC	31.1B	26.3B	25.3
30%	27.4	28.9A	26.0	27.5AB	30.9B	31.7A	26.7A	25.4
15%	27.2	28.8AB	26.0	28.0A	31.8A	31.9A	26.9A	25.7

† Percentage of evapotranspiration (ET) replacement.

‡ Airborne canopy temperature wasn't available on 7 June.

Table 2.2. Pearson correlation coefficients (r) by date between irrigation treatment levels (% ET) and volumetric water content (VWC), visual quality (VQ), percentage green cover (PGC), soil temperature (T_{soil}), canopy temperature (Tc), spectral reflectance data acquired from small unmanned aerial system (sUAS), and handheld optical sensors [FieldScout ($_{FS}$), and RapidScan ($_{RS}$)], for 'Declaration' creeping bentgrass ($P < 0.05$).

Variable	15 June	20 June	1 July	10 July	25 July	4 Aug	31 Aug
Ground-based measurements							
VWC	0.83	0.88	0.85	0.83	0.92	0.81	0.92
VQ	NS	NS	0.72	0.87	0.87	0.85	0.84
PGC	NS	NS	0.65	0.64	0.72	0.73	0.66
T_{soil}	NS	NS	-0.65	-0.47	-0.67	-0.42	-0.53
Remote sensing measurements							
sUAS-based							
Thermal Imaging (Canopy Temperature)							
Tc	-0.68	-0.65	-0.67	-0.78	-0.77	-0.68	-0.82
Spectral Reflectance (modified digital camera)							
Blue	NS*	NS	-0.67	-0.66	-0.67	-0.65	-0.72
Green	0.75	0.66	NS	NS	NS	NS	NS
NIR†	0.70	0.78	0.80	0.84	0.84	0.84	0.84
GreenBlue‡	0.81	0.86	0.86	0.86	0.85	0.84	0.87
NDVI Enhanced1§	0.55	0.72	0.80	0.82	0.81	0.79	0.84
NDVI Enhanced2¶	0.55	0.72	0.80	0.81	0.81	0.79	0.83
NDVI Enhanced3#	NS	0.54	0.75	0.78	0.77	0.76	0.80
Blue NDVI††	NS	0.63	0.77	0.79	0.79	0.77	0.81
Green NDVI‡‡	NS	NS	0.69	0.73	0.73	0.73	0.75
NIR Blueratio§§	NS	0.62	0.77	0.79	0.79	0.77	0.80
NIR Greendiff¶¶	NS	NS	0.71	0.75	0.74	0.74	0.76
Handheld optical sensors							
$NDVI_{FS}$##	NS	0.51	0.56	0.71	0.76	0.75	0.77
$NDVI_{RS}$†‡	NS	0.49	0.74	0.75	0.81	0.78	0.76
Red_{RS}	-0.42	-0.57	-0.74	-0.75	-0.79	-0.77	-0.75
NIR_{RS}	NS	NS	0.68	0.75	0.86	0.85	0.78
NDRE†§	NS	NS	0.67	0.74	0.83	0.84	0.77
Red edge	NS	NS	-0.65	-0.73	-0.82	-0.81	-0.76

*Correlations were not significant at $P < 0.05$ probability level.

† NIR, near infrared spectral reflectance, peaks within 680-780 nm.

‡ GreenBlue = (Green-Blue)/(Green+Blue).

§ NDVI Enhanced1 = (NIR+Green-2Blue)/(NIR+Green+2Blue).

¶ NDVI Enhanced2 = (NIR+Green-Blue)/(NIR+Green+Blue).

NDVI Enhanced3 = (NIR-Green-Blue)/(NIR+Green+Blue).

†† Blue NDVI = (NIR-Blue)/(NIR+Blue).

‡‡ Green NDVI = (NIR-Green)/(NIR+Green).

§§ NIR Blueratio = NIR-Blue.

¶¶ NIR Green Diff = (NIR-Green-Blue)/(NIR-Green+Blue).

$NDVI_{FS}$ = (NIR_{FS}-red)/(NIR_{FS}+red); 660 (red) and 840 (NIR_{FS}) nm.

†‡ $NDVI_{RS}$ = (NIR_{RS}-Red_{RS})/(NIR_{RS}+Red_{RS}). NIR_{RS} peaks at 780nm. Red_{RS}, peaks at 670nm.
†§ NDRE = (NIR_{RS}-Red edge)/(NIR_{RS}+Red edge). Red edge, peaks at 730nm.

Table 2.3. Analysis of irrigation main effects on visual quality (VQ), canopy thermal infrared temperature (Tc), spectral reflectance data acquired from the small unmanned aerial system (sUAS), and the RapidScan handheld optical sensor ($NDVI_{RS}$ and Red_{RS})], for 'Declaration' creeping bentgrass on 15 June.

Treatment†	VQ	VWC	Tc (°C)	NIR	GreenBlue§	NDVI Enhanced1¶	NDVI Enhanced2#	Blue NDVI††	NIR Blueratio‡‡	$NDVI_{RS}$§§	Red_{RS}
100%	7.3	45.2A	40.4A*	201AB***	-0.093A***	-0.055A**	0.284A**	-0.019A**	-7.79A**	0.78A*	4.5A*
80%	8	43.8A	40.9ABC	203A	-0.093A	-0.049A	0.289A	-0.008A	-3.43A	0.81A	4.0A
65%	7.6	40.7A	40.8AB	199BC	-0.096AB	-0.056A	0.283A	-0.018A	-7.45A	0.78A	4.6A
50%	7.9	40.9A	40.9ABC	199BC	-0.099B	-0.055A	0.284A	-0.015A	-5.99A	0.80A	4.3A
30%	8	34.3B	41.38BC	197C	-0.101B	-0.056A	0.282A	-0.016A	-6.23A	0.79A	4.4A
15%	6.6	29.4C	41.43C	191D	-0.110C	-0.073B	0.267B	-0.038B	-15.13B	0.75B	5.3B

*Treatment means were significantly different at $P < 0.05$ probability level, indicated by different letters; no letter presented when $P > 0.05$.

** Treatment means were significantly different at $P < 0.01$ probability level, indicated by different letters.

*** Treatment means were significantly different at $P \leq 0.001$ probability level, indicated by different letters.

† Percentage of evapotranspiration (ET) replacement.

‡ Visual quality based on a 1 to 9 scale, with 1 = dead, 6 = minimally acceptable, and 9 = uniform, green, dense turfgrass.

§ GreenBlue = (G-B)/(G+B); G, green spectral reflectance, and B, blue spectral reflectance are between 400-580 nm.

¶ NDVI Enhanced1 = (NIR+G-2B)/(NIR+G+2B). NIR, near infrared spectral reflectance, peaks within 680-780 nm.

NDVI Enhanced2 = (NIR+G-B)/(NIR+G+B).

†† Blue NDVI = (NIR-B)/(NIR+B).

‡‡ NIR Blueratio = (NIR-B).

§§ $NDVI_{RS}$ = (NIR_{RS}-Red_{RS})/(NIR_{RS}+Red_{RS}); NIR_{RS} peaks at 780nm, near infrared spectral reflectance; Red_{RS} peaks at 670nm.

Table 2.4. Pearson correlation coefficients (r) of canopy temperature (Tc) and canopy-air temperature difference (Tc-Ta) with volumetric water content (VWC), visual quality (VQ), percentage green cover (PGC), soil temperature (Tsoil), spectral reflectance data acquired from small unmanned aerial system (sUAS), and handheld optical sensors [FieldScout ($_{FS}$), and RapidScan ($_{RS}$)], on 'Declaration' creeping bentgrass ($P < 0.05$).

	Tc (°C)	Tc-Ta (°C)
Ground-based measurements		
VWC	-0.63	-0.43
VQ	-0.77	-0.60
PGC	-0.78	-0.58
T_{soil}	0.27	-0.41
Remote sensing measurements		
sUAS-based		
Blue	0.52	0.20
Green	NS*	-0.34
NIR†	-0.58	-0.68
GreenBlue‡	-0.59	-0.66
NDVI Enhanced1§	-0.67	-0.60
NDVI Enhanced2¶	-0.67	-0.60
NDVI Enhanced3#	-0.68	-0.54
Blue NDVI††	-0.68	-0.57
Green NDVI‡‡	-0.68	-0.48
NIR Blueratio§§	-0.68	-0.57
NIR Greendiff¶¶	-0.69	-0.50
Handheld optical sensors		
$NDVI_{FS}$##	-0.79	-0.59
$NDVI_{RS}$†‡	-0.82	-0.64
Red	0.82	0.64
NIR_{RS}	-0.75	-0.64
NDRE†§	-0.77	-0.65
Red edge	0.77	0.65

* Correlation was not significantly different at $P < 0.05$ probability level.
† NIR, near infrared spectral reflectance, peaks within 680-780 nm.
‡ GreenBlue = (Green-Blue)/(Green+Blue).
§ NDVI Enhanced1 = (NIR+Green-2Blue)/(NIR+Green+2Blue).
¶ NDVI Enhanced2 = (NIR+Green-Blue)/(NIR+Green+Blue).
# NDVI Enhanced3 = (NIR-Green-Blue)/(NIR+Green+Blue).
†† Blue NDVI = (NIR-Blue)/(NIR+Blue).
‡‡ Green NDVI = (NIR-Green)/(NIR+Green).
§§ NIR Blueratio = NIR-Blue.
¶¶ NIR Green Diff = (NIR-Green-Blue)/(NIR-Green+Blue).
$NDVI_{FS}$ = (NIR_{FS}-red)/(NIR_{FS}+red); 660 (red) and 840 (NIR_{FS}) nm.
†‡ $NDVI_{RS}$ = (NIR_{RS}-R)/(NIR_{RS}+R). NIR_{RS} peaks at 780nm. Red, peaks at 670nm.
†§ NDRE = (NIR_{RS}-Red edge)/(NIR_{RS}+Red edge). Red edge, peaks at 730nm.

Appendix A - Calibration

Introduction

Calibration panels are typically used for calculating spectral reflectance, or normalizing spectral reflectance measurements to an invariant standard. However, this method is not effective under most practical conditions due to non-Lambertian spectral reflectance patterns from the panels, and the problem of deploying panels over time or over an entire flight area (D. van der Merwe, personal communication, Aug. 7, 2018). Therefore, in Chapter 1, relative values of spectral reflectance were assessed for the daily differences caused by irrigation treatments without deploying calibration panels, and we assumed that the sensor value was related to the intensity of spectral reflectance under field conditions (i.e. consistent angles of the sun and sensor, leveled surface, etc.). Here, the hypothesis was tested *that there is a simple linear correlation between the camera signal and spectral reflectance under proper exposure*.

Methods and Materials

The calibration experiment was conducted on a cloud-free day within 2.5 hours of local solar noon, using the same modified Canon PowerShot S100 camera and firmware as documented in Chapter 1. A series of calibration panels were used to evaluate relationships between digital number readings from the Canon S100 (i.e., the camera signal) and relative spectral reflectance as determined from a passive hyperspectral imaging sensor (Nano-Hyperspec VNIR, Headwall). The digital number of a pixel from the Canon S100 was extracted using AgVISR (v. 2.1.6, AgVISR Services).

The camera settings were the same as in the experiments of 2015 and 2016. Specifically, the camera was set to manual mode, autofocus, ISO at 100, shutter speed at 1/2000, and the exposure level adjusted to two stops below the standard using only the f-stop while facing the camera down, perpendicular towards the turfgrass surface. In 2017, one difference was the f-stop

was fixed at f/2.2 and the shutter speed was adjusted to achieve the abovementioned exposure. However, this calibration did not account for this difference.

The hyperspectral imaging sensor contained narrowbands (about 2.22 nm width) from 400 to 1000 nm. It was mounted on a leveled track with the speed of 0.02 m/s to scan an object. Exposure time and frame period were set to 82 ms. Relative spectral reflectance of a pixel was extracted using SpectralView (E60602 vs64 5.5.1).

Within half an hour of solar noon of a clear day on Sept. 20, 2018, both the camera (held by hand) and hyperspectral imaging sensor (mounted on a track) were faced downward (about 1m above ground) perpendicular to the surface to take measurements on seven panels (0.67m x 0.67m) of one white and 6 different grey tones (mixture of different proportions of pure white and black matt paint) on the level ground of an open field (Fig. A.1) (Iqbal et al., 2018). Panels were placed in the center of field of view of the camera and hyperspectral imaging sensor, and twenty random points within the 60% center of each panel were selected and measured. These twenty extracted readings of each board (grey tone) were averaged for the bands of both sensors (Fig. A.2). Although the locations of twenty random points on each panel were not exactly the same for each of the two instruments, results indicated they were homogenous because of very low standard deviations (less than 2% of the mean). Blue and green bands of the camera were integrated into single broadband due to the overlap between them. Averages of visible and NIR bands (400-580 and 680-780 nm) were then correlated between two sensors in Microsoft Excel (16.0.11001.20070).

Results and Discussion

Within both the visible (blue and green) and NIR portions of the spectrum, digital numbers from the modified camera and relative reflectance values from the hyperspectral

imaging sensor both increased across measurements from darker to lighter gray and finally white panels (Fig. A.3). However, there was a stronger logistic (non-linear) than linear relationship between measurements with the Canon S100 (digital numbers) and the hyperspectral sensor (relative reflectance), in both the visible and NIR. The logistic relationships between the digital camera and the hyperspectral measurements in the visible and NIR were due to the nonlinear use of sensor data by the camera to produce images that are optimized for viewing by people (D. van der Merwe, personal communication, Nov. 1, 2018).

The logistic relationship between measurements with the digital camera and the hyperspectral sensor was contrary to our hypothesis the relationship would be linear. However, linear relationships were strong within certain ranges of exposure. Namely, when the relative reflectance was low, digital numbers increased linearly within both the visible and NIR bands (r^2 = 0.97 and r^2 = 0.98, respectively) (Fig. A.3). The linearity is more likely to break down at the extremes of exposure, but the extremes were not relevant to field conditions (D. van der Merwe, personal communication, July 24, 2018). When linear relationships were applied to the whole range of exposure (Fig. A.3), digital numbers responded more linearly (r^2 = 0.96) in the NIR band than in the visible band (i.e., blue-green bands) (r^2 = 0.83). In other words, the linearity of NIR band was less affected by high exposure.

This calibration verified the linear correlation between the digital number of a modified camera and the spectral reflectance, when the exposure was not extreme. To be noted, image processing can differ between camera models, and it needs to be taken into account when using different sensors. Equivalence cannot be assumed when different camera models, or even different firmware versions or settings in the same camera, are used (D. van der Merwe, personal communication, Nov. 1, 2018).

Reference

Iqbal F., A. Lucieer, and K. Barry. 2018. Simplified radiometric calibration for UAS-mounted multispectral sensor. European Journal of Remote Sensing. 51:301-313, doi: 10.1080/22797254.2018.1432293.

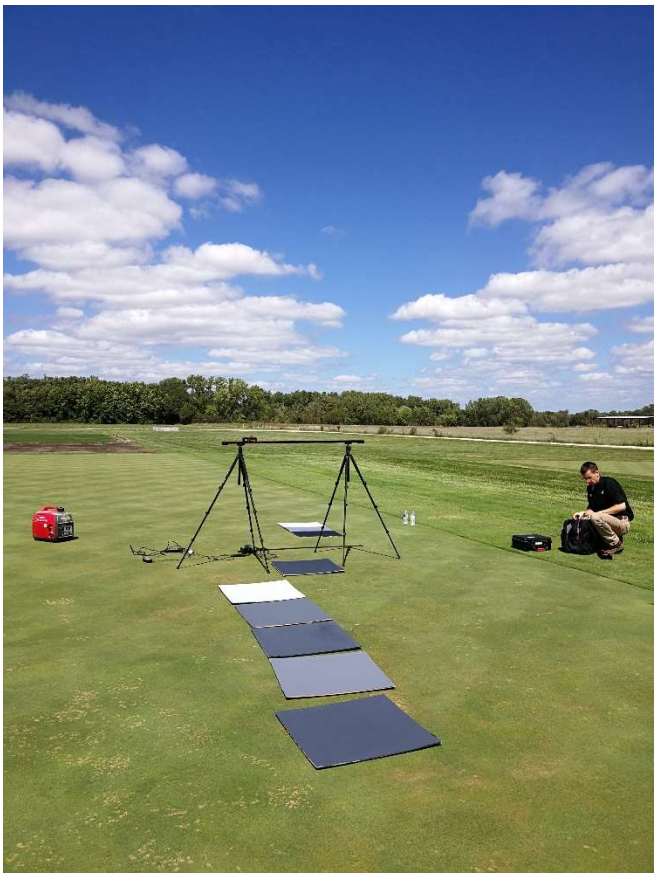

Figure A.1. A hyperspectral imaging sensor was mounted on a leveled track supported with two tripods. The hyperspectral imaging sensor faced perpendicularly downward to scan seven calibration panels individually. Trevor Witt, a UAS Data Analyst at Applied Aviation Research Center, Kansas State University, helped operate the hyperspectral imaging sensor.

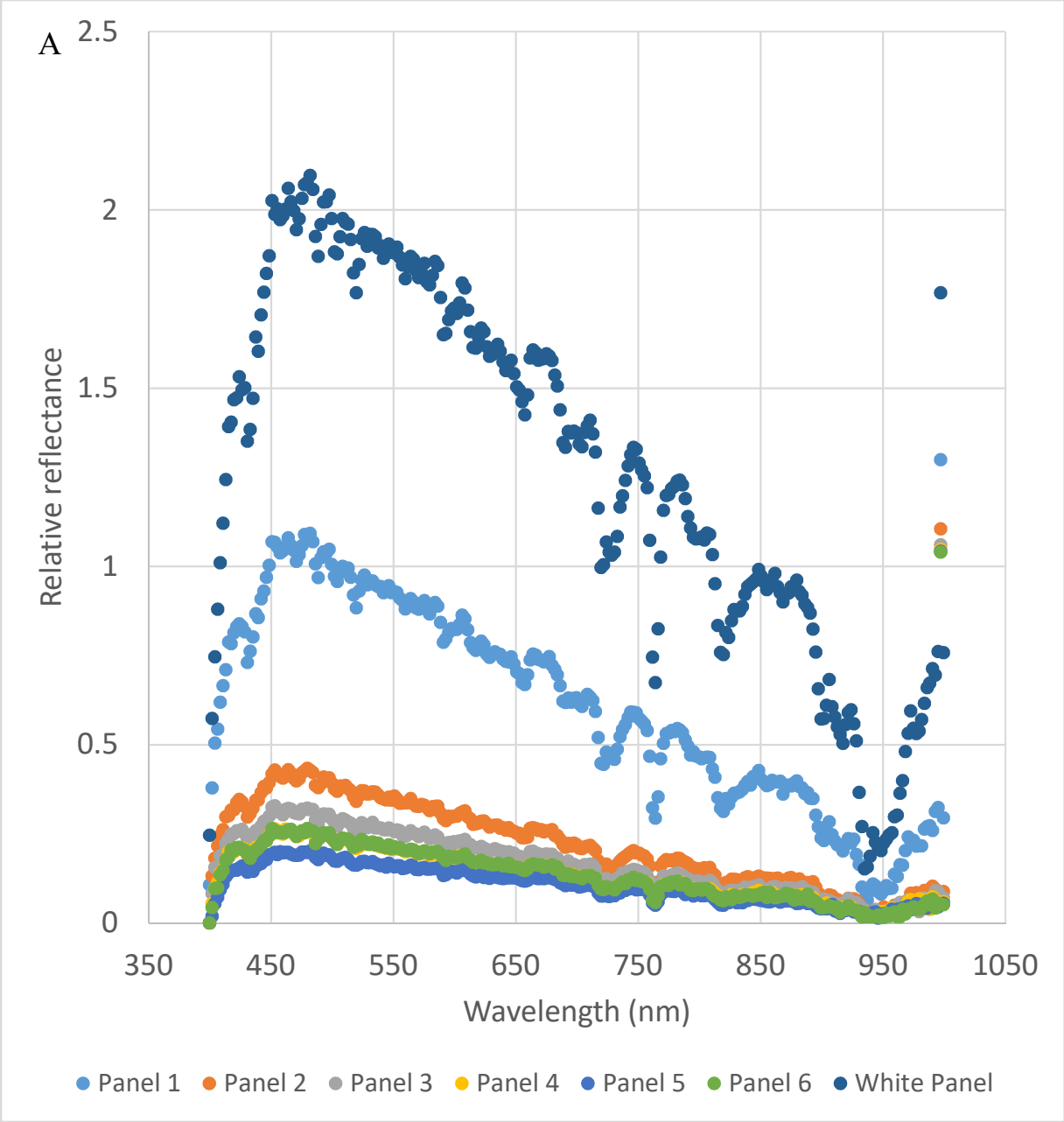
A
2.5
2
1.5
1
0.5
0
Relative reflectance
350
450
550
650
750
850
950
1050
Wavelength (nm)
Panel 1
Panel 2
Panel 3
Panel 4
Panel 5
Panel 6
White Panel

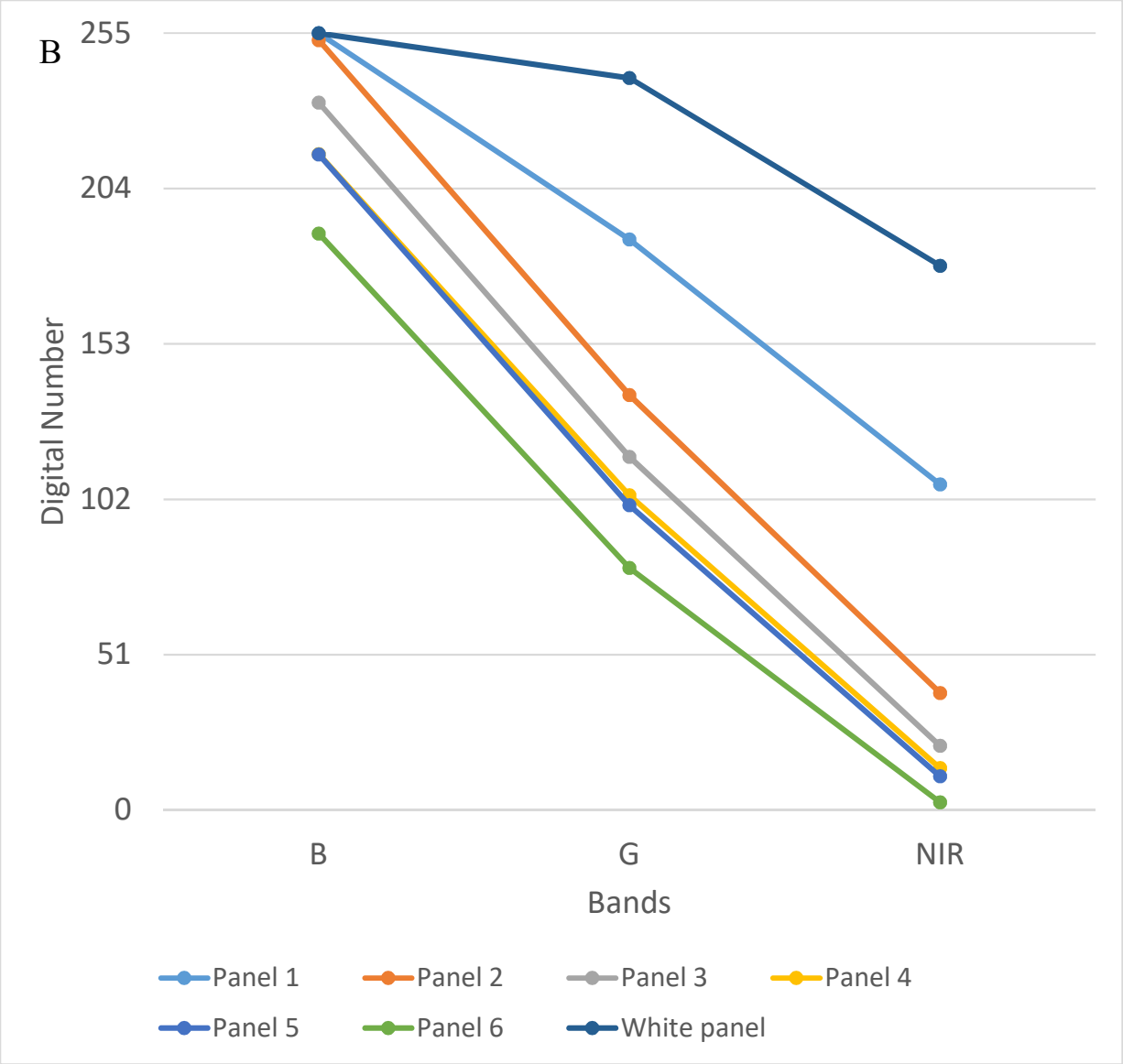

Figure A.2. Changes in relative spectral reflectance of a hyperspectral imaging sensor (A) and digital numbers of modified Canon S100 (B) from a white and a series of grey panels across bands (Panel 1 to 6: light to dark grey tones).

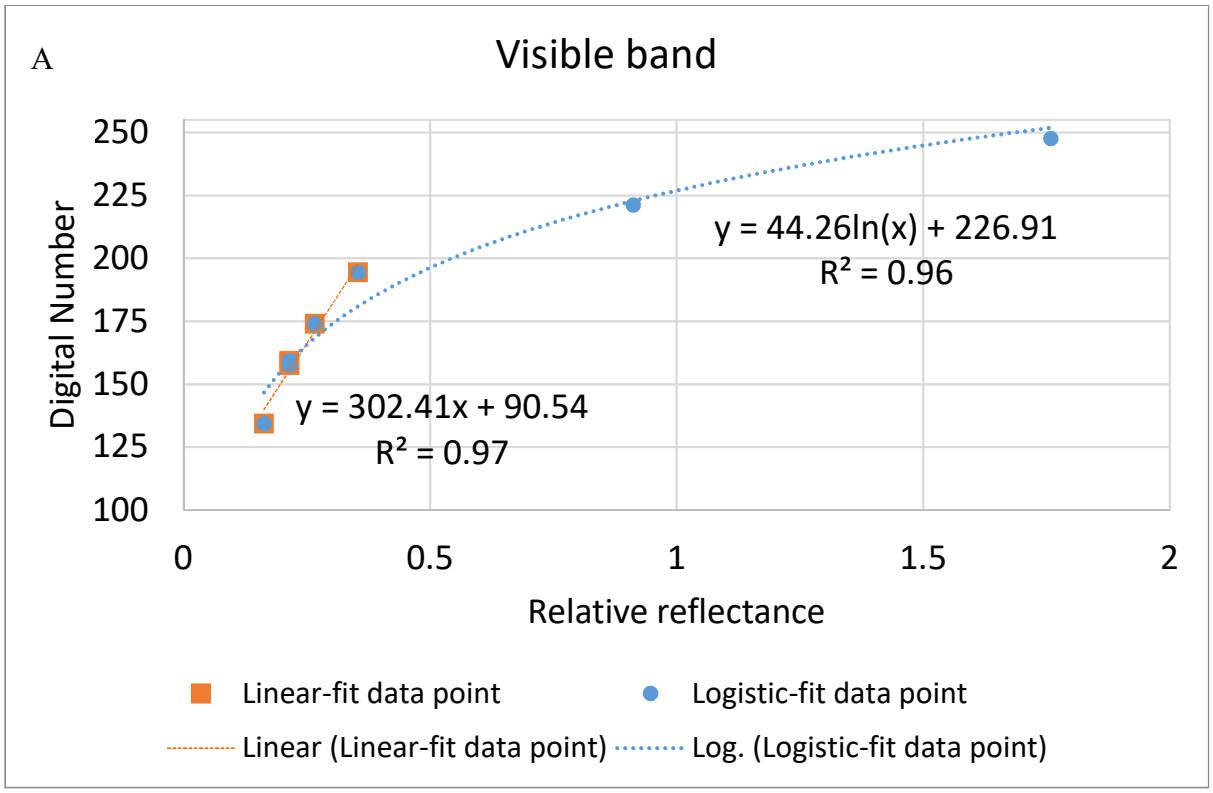

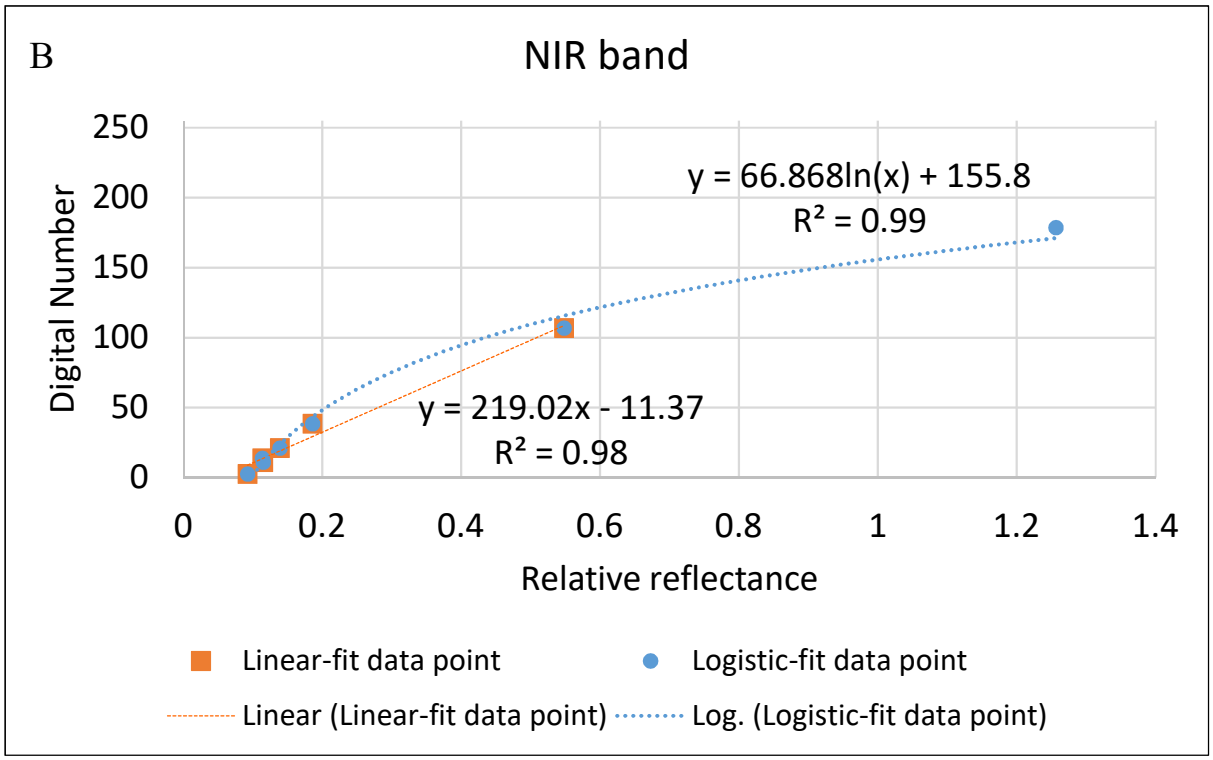

Figure A.3. Relationships between digital numbers of the modified Canon S100 and relative spectral reflectance of a hyperspectral imaging sensor in visible (blue and green) (A) and NIR (B) bands.

Appendix B - Additional Tables for Chapter 1

Figure B.1. Deficit to well-watered irrigation treatment according to 15, 30, 50, 65, 80, and 100% reference evapotranspiration (ET) replacement. Irrigation was applied three times a week by hand with a wand attached to a meter.

Table B.1. Daily analysis of irrigation treatment effects on $NDVI_{FS}$ (FieldScount) in 2015.

Treatment*	Date (2015)									
	6/22	6/25	7/13	7/22	7/28	7/31	8/7	8/11	8/20	8/31
100	0.88	0.87	0.88AB	0.89AB	0.87A	0.87A	0.87A	0.86A	0.83AB	0.85A
80	0.88	0.87	0.88B	0.88B	0.86A	0.87A	0.87A	0.86A	0.83AB	0.82A
65	0.89	0.88	0.89A	0.90AB	0.87A	0.88A	0.89A	0.88A	0.84A	0.83A
50	0.89	0.87	0.88AB	0.90A	0.86A	0.86A	0.87A	0.83A	0.81AB	0.77A
30	0.89	0.88	0.87B	0.89AB	0.86A	0.84A	0.84A	0.82A	0.77B	0.64B
15	0.89	0.87	0.86C	0.85C	0.76B	0.70B	0.55B	0.53B	0.42C	0.37C

* Percentage of evapotranspiration (ET) replacement. Irrigation treatments began as 25, 50, 75, 100, 125, and 150% ET on June 29; modified as 15, 30, 50, 65, 80 and 100% ET on to reflect shorter mowing height on July 17 (denoted by a vertical dashed line).

Table B.2. Daily analysis of irrigation treatment effects on soil volumetric water content (%) in 2015.

Treatment*	Date (2015)									
	6/22	6/25	7/13	7/22	7/28	7/31	8/7	8/11	8/20	8/31
100	49.1	47.4	51.4A	44.7A	45.4A	40.9A	48.0A	49.5A	46.1A	42.8A
80	48.6	47.3	50.7A	44.0A	44.6A	39.3A	46.5A	48.3AB	42.6A	40.8AB
65	46.5	48.6	51.0A	41.8A	45.0A	40.7A	49.5A	49.1AB	44.2A	38.2B
50	46.4	48.1	50.8A	46.2A	43.0A	39.3A	47.5A	45.5B	37.3B	28.7C
30	47.7	48.1	45.6B	40.9A	37.2B	29.2B	38.6B	33.2C	27.2C	19.3D
15	48.0	47.3	32.2C	27.0B	23.5C	19.5C	28.5C	24.8D	19.7D	17.6D

* Percentage of evapotranspiration (ET) replacement. Irrigation treatments began as 25, 50, 75, 100, 125, and 150% ET on June 29; modified as 15, 30, 50, 65, 80 and 100% ET on to reflect shorter mowing height on July 17 (denoted by a vertical dashed line).

Table B.3. Daily analysis of irrigation treatment effects on soil temperature (°C) in 2015.

Treatment*	Date (2015)									
	6/22	6/25	7/13	7/22	7/28	7/31	8/7	8/11	8/20	8/31
100	29.7	30.2	32.2	27.5A	30.8	29.8B	29.8AB	29.3	30.1	33.6B
80	29.0	30.4	32.0	27.3AB	30.8	29.9B	29.6BC	29.3	30.3	33.0B
65	29.4	29.9	32.0	27.2B	30.7	29.9B	29.1C	29.2	29.9	33.1B
50	29.5	30.1	32.2	27.2B	30.8	29.9B	29.6BC	29.5	31.0	33.5B
30	29.3	30.0	32.0	27.0B	30.7	30.1AB	29.2C	29.3	31.8	36.3A
15	29.4	29.9	32.8	27.2B	31.1	30.6A	30.3A	29.9	32.5	37.3A

* Percentage of evapotranspiration (ET) replacement. Irrigation treatments began as 25, 50, 75, 100, 125, and 150% ET on June 29; modified as 15, 30, 50, 65, 80 and 100% ET on to reflect shorter mowing height on July 17 (denoted by a vertical dashed line).

Table B.4. Daily analysis of irrigation treatment effects on visual quality in 2015.

Treatment*	Date (2015)									
	6/22	6/25	7/13	7/22	7/28	7/31	8/7	8/11	8/20	8/31
100	9.0	8.9	8.8A	8.0A	7.9A	7.9A	7.4A	7.8AB	7.2A	7.3A
80	9.0	8.9	7.8B	8.1A	7.7A	7.9A	7.3A	7.4AB	7.5A	6.8A
65	9.0	9.0	8.0AB	8.1A	8.1A	7.9A	7.5A	8.3A	7.8A	7.0A
50	9.0	9.0	7.5B	7.6A	7.4A	7.3A	6.9A	7.1B	5.5B	4.6B
30	9.0	9.0	7.5B	7.5A	6.3B	6.2B	5.5B	5.6C	4.4C	3.4C
15	9.0	8.9	6.0C	4.3B	3.0C	2.9C	2.6C	2.8D	2.2D	1.0D

* Percentage of evapotranspiration (ET) replacement. Irrigation treatments began as 25, 50, 75, 100, 125, and 150% ET on June 29; modified as 15, 30, 50, 65, 80 and 100% ET on to reflect shorter mowing height on July 17 (denoted by a vertical dashed line).

Table B.5. Daily analysis of irrigation treatment effects on Blue band in 2015.

Treatment*	Date (2015)									
	6/19	6/25	7/13	7/23	7/28	7/31	8/7	8/11	8/21	8/31
100	161.0	161.4	147.6	156.6	140.2AB	143.3	140.3	138.3AB	129.1B	127.9BC
80	161.4	162.8	148.0	155.7	140.0AB	142.1	139.8	136.9ABC	128.2B	127.6BC
65	158.3	165.5	145.4	154.5	137.2BC	141.2	136.4	132.5C	125.8B	124.7C
50	160.8	164.0	147.3	154.6	139.4AB	141.9	137.9	134.1BC	128.2B	130.7B
30	158.7	165.0	146.5	155.5	136.3C	141.5	137.0	132.8C	128.3B	132.9B
15	159.5	163.1	148.6	153.9	140.7A	141.5	141.9	141.2A	145.9A	152.1A

* Percentage of evapotranspiration (ET) replacement. Irrigation treatments began as 25, 50, 75, 100, 125, and 150% ET on June 29; modified as 15, 30, 50, 65, 80 and 100% ET on to reflect shorter mowing height on July 17 (denoted by a vertical dashed line).

Table B.6. Daily analysis of irrigation treatment effects on Green band in 2015.

Treatment*	Date (2015)									
	6/19	6/25	7/13	7/23	7/28	7/31	8/7	8/11	8/21	8/31
100	122.0	121.6	112.9	121.6A	110.3A	110.9A	107.6A	106.3A	97.9A	95.4A
80	121.8	122.2	113.2	121.0AB	110.1A	110.0A	107.1A	105.2AB	96.5AB	93.8AB
65	118.8	123.5	111.8	120.4AB	108.4B	109.9A	105.2A	102.9BC	95.0BC	91.3BC
50	121.1	122.7	112.2	120.1AB	109.0AB	109.4A	105.1A	102.2C	93.7C	91.3BC
30	119.6	123.8	111.8	120.1B	106.0C	107.3B	101.3B	97.9D	88.6D	88.8C
15	120.9	123.0	110.7	115.0C	101.9D	99.0C	94.3C	93.0E	92.7C	95.8A

* Percentage of evapotranspiration (ET) replacement. Irrigation treatments began as 25, 50, 75, 100, 125, and 150% ET on June 29; modified as 15, 30, 50, 65, 80 and 100% ET on to reflect shorter mowing height on July 17 (denoted by a vertical dashed line).

Table B.7. Daily analysis of irrigation treatment effects on NIR band in 2015.

Treatment*	Date (2015)									
	6/19	6/25	7/13	7/23	7/28	7/31	8/7	8/11	8/21	8/31
100	144.0	147.0	142.0AB	147.4AB	138.4A	139.3A	135.3A	136.0A	124.4A	121.2A
80	142.5	146.8	142.5AB	147.7AB	138.9A	139.3A	135.7A	135.9A	123.5A	118.3AB
65	141.4	147.8	144.0A	149.8A	139.9A	141.9A	137.0A	137.5A	124.4A	117.2B
50	142.8	147.2	141.9AB	147.5AB	136.8AB	137.9AB	132.8A	132.1A	117.3B	108.6C
30	142.1	148.3	141.3B	146.8B	133.8B	133.9B	124.9B	123.8B	106.1C	99.7D
15	143.3	148.4	136.3C	136.1C	118.4C	113.3C	98.4C	98.2C	89.9D	89.6E

* Percentage of evapotranspiration (ET) replacement. Irrigation treatments began as 25, 50, 75, 100, 125, and 150% ET on June 29; modified as 15, 30, 50, 65, 80 and 100% ET on to reflect shorter mowing height on July 17 (denoted by a vertical dashed line).

Table B.8. Daily analysis of irrigation treatment effects on NDVI Enhanced1 in 2015.

Treatment*	Date (2015)									
	6/19	6/25	7/13	7/23	7/28	7/31	8/7	8/11	8/21	8/31
100	-0.095	-0.092	-0.073AB	-0.076B	-0.06AB	-0.068AB	-0.072A	-0.066A	-0.075A	-0.083A
80	-0.099	-0.095	-0.073AB	-0.074AB	-0.059AB	-0.066AB	-0.070A	-0.063A	-0.076A	-0.092A
65	-0.098	-0.099	-0.064A	-0.067A	-0.050A	-0.057A	-0.060A	-0.049A	-0.068A	-0.089A
50	-0.098	-0.097	-0.073B	-0.072AB	-0.063AB	-0.069AB	-0.074A	-0.068A	-0.097B	-0.133B
30	-0.096	-0.096	-0.073AB	-0.076B	-0.064B	-0.080B	-0.096B	-0.090B	-0.137C	-0.170C
15	-0.094	-0.092	-0.092C	-0.102C	-0.121C	-0.143C	-0.191C	-0.192C	-0.230D	-0.242D

* Percentage of evapotranspiration (ET) replacement. Irrigation treatments began as 25, 50, 75, 100, 125, and 150% ET on June 29; modified as 15, 30, 50, 65, 80 and 100% ET on to reflect shorter mowing height on July 17 (denoted by a vertical dashed line).

Table B.9. Daily analysis of irrigation treatment effects on NDVI Enhanced2 in 2015.

Treatment*	Date (2015)									
	6/19	6/25	7/13	7/23	7/28	7/31	8/7	8/11	8/21	8/31
100	0.246	0.249	0.267AB	0.264B	0.279A	0.272AB	0.268A	0.273A	0.265A	0.257A
80	0.242	0.246	0.267AB	0.266AB	0.280A	0.274AB	0.27A	0.276A	0.264A	0.249A
65	0.244	0.243	0.275A	0.273A	0.289A	0.282A	0.279A	0.29A	0.271A	0.252A
50	0.243	0.244	0.266B	0.268AB	0.276A	0.271AB	0.266A	0.272A	0.244B	0.210B
30	0.245	0.245	0.267AB	0.264B	0.275A	0.260B	0.245B	0.251B	0.206C	0.173C
15	0.247	0.249	0.249C	0.240C	0.221B	0.200C	0.152C	0.150C	0.112D	0.099D

* Percentage of evapotranspiration (ET) replacement. Irrigation treatments began as 25, 50, 75, 100, 125, and 150% ET on June 29; modified as 15, 30, 50, 65, 80 and 100% ET on to reflect shorter mowing height on July 17 (denoted by a vertical dashed line).

Table B.10. Daily analysis of irrigation treatment effects on NDVI Enhanced3 in 2015.

Treatment*	Date (2015)									
	6/19	6/25	7/13	7/23	7/28	7/31	8/7	8/11	8/21	8/31
100	-0.325	-0.316	-0.294B	-0.307B	-0.288A	-0.292AB	-0.294AB	-0.285B	-0.292AB	-0.296A
80	-0.330	-0.320	-0.294B	-0.304B	-0.286A	-0.288AB	-0.290A	-0.281AB	-0.291AB	-0.303A
65	-0.324	-0.323	-0.282A	-0.295A	-0.274A	-0.278A	-0.276A	-0.263A	-0.279A	-0.296A
50	-0.327	-0.322	-0.293B	-0.301AB	-0.290A	-0.292AB	-0.293AB	-0.283AB	-0.309B	-0.343B
30	-0.324	-0.321	-0.293AB	-0.305B	-0.289A	-0.300B	-0.313B	-0.302B	-0.343C	-0.38C
15	-0.324	-0.317	-0.311C	-0.328C	-0.344B	-0.360C	-0.412C	-0.409C	-0.452D	-0.469D

* Percentage of evapotranspiration (ET) replacement. Irrigation treatments began as 25, 50, 75, 100, 125, and 150% ET on June 29; modified as 15, 30, 50, 65, 80 and 100% ET on to reflect shorter mowing height on July 17 (denoted by a vertical dashed line).

Table B.11. Daily analysis of irrigation treatment effects on Blue NDVI in 2015.

Treatment*	Date (2015)									
	6/19	6/25	7/13	7/23	7/28	7/31	8/7	8/11	8/21	8/31
100	-0.055	-0.047	-0.019B	-0.030B	-0.006A	-0.014AB	-0.018A	-0.008AB	-0.019AB	-0.027A
80	-0.062	-0.052	-0.019B	-0.026AB	-0.004A	-0.010AB	-0.014A	-0.004A	-0.019AB	-0.038A
65	-0.056	-0.056	-0.005A	-0.015A	0.010A	0.002A	0.002A	0.019A	-0.006A	-0.031A
50	-0.059	-0.054	-0.018B	-0.023AB	-0.009A	-0.015AB	-0.019A	-0.008AB	-0.045B	-0.092B
30	-0.055	-0.053	-0.018AB	-0.029B	-0.009A	-0.028B	-0.047B	-0.035B	-0.095C	-0.143C
15	-0.054	-0.047	-0.043C	-0.062C	-0.086B	-0.111C	-0.181C	-0.180C	-0.237D	-0.258D

* Percentage of evapotranspiration (ET) replacement. Irrigation treatments began as 25, 50, 75, 100, 125, and 150% ET on June 29; modified as 15, 30, 50, 65, 80 and 100% ET on to reflect shorter mowing height on July 17 (denoted by a vertical dashed line).

Table B.12. Daily analysis of irrigation treatment effects on Green NDVI in 2015.

Treatment*	Date (2015)									
	6/19	6/25	7/13	7/23	7/28	7/31	8/7	8/11	8/21	8/31
100	0.083	0.095	0.114B	0.096B	0.113B	0.114AB	0.114AB	0.123B	0.119AB	0.119A
80	0.078	0.091	0.115B	0.099B	0.115AB	0.118AB	0.118AB	0.128AB	0.123AB	0.116A
65	0.087	0.090	0.126A	0.109A	0.127A	0.127A	0.131A	0.144A	0.134A	0.124A
50	0.083	0.091	0.117AB	0.103AB	0.113B	0.115AB	0.116AB	0.128AB	0.112B	0.087B
30	0.086	0.090	0.117AB	0.100B	0.116AB	0.110B	0.104B	0.117B	0.090C	0.058C
15	0.085	0.094	0.103C	0.084C	0.075C	0.067C	0.021C	0.027C	-0.015D	-0.034D

* Percentage of evapotranspiration (ET) replacement. Irrigation treatments began as 25, 50, 75, 100, 125, and 150% ET on June 29; modified as 15, 30, 50, 65, 80 and 100% ET on to reflect shorter mowing height on July 17 (denoted by a vertical dashed line).

Table B.13. Daily analysis of irrigation treatment effects on GreenBlue VI in 2015.

Treatment*	Date (2015)									
	6/19	6/25	7/13	7/23	7/28	7/31	8/7	8/11	8/21	8/31
100	-0.138	-0.141A	-0.133A	-0.126AB	-0.119AB	-0.128A	-0.132A	-0.131A	-0.138A	-0.146A
80	-0.140	-0.142AB	-0.133A	-0.125AB	-0.119AB	-0.128A	-0.132A	-0.131A	-0.141A	-0.153AB
65	-0.143	-0.145B	-0.13A	-0.124A	-0.117A	-0.124A	-0.129A	-0.126A	-0.139A	-0.154B
50	-0.141	-0.144B	-0.135A	-0.126AB	-0.122AB	-0.130AB	-0.135A	-0.135A	-0.155B	-0.177C
30	-0.140	-0.142AB	-0.135A	-0.129B	-0.125B	-0.138B	-0.150B	-0.152B	-0.183C	-0.199D
15	-0.138	-0.14A	-0.146B	-0.145C	-0.160C	-0.177C	-0.201C	-0.206C	-0.223D	-0.227E

* Percentage of evapotranspiration (ET) replacement. Irrigation treatments began as 25, 50, 75, 100, 125, and 150% ET on June 29; modified as 15, 30, 50, 65, 80 and 100% ET on to reflect shorter mowing height on July 17 (denoted by a vertical dashed line).

Table B.14. Daily analysis of irrigation treatment effects on NIR BlueRatio VI in 2015.

Treatment*	Date (2015)									
	6/19	6/25	7/13	7/23	7/28	7/31	8/7	8/11	8/21	8/31
100	-17.0A	-14.4A	-5.6B	-9.2B	-1.8A	-3.9AB	-5.0A	-2.3BC	-4.7AB	-6.8A
80	-18.9A	-16.0AB	-5.4B	-8.0AB	-1.2A	-2.8AB	-4.0A	-1.0AB	-4.7AB	-9.3A
65	-17.0A	-17.6B	-1.5A	-4.7A	2.7A	0.7A	0.6A	5.0A	-1.4A	-7.4A
50	-17.9A	-16.8AB	-5.4B	-7.1AB	-2.6A	-4.1AB	-5.1A	-2.0ABC	-10.9B	-22.0B
30	-16.6A	-16.7AB	-5.2AB	-8.6B	-2.5A	-7.6B	-12.1B	-9.0C	-22.2C	-33.2C
15	-16.3A	-14.7A	-12.3C	-17.8C	-22.3B	-28.2C	-43.5C	-43.0D	-56.0D	-62.5D

* Percentage of evapotranspiration (ET) replacement. Irrigation treatments began as 25, 50, 75, 100, 125, and 150% ET on June 29; modified as 15, 30, 50, 65, 80 and 100% ET on to reflect shorter mowing height on July 17 (denoted by a vertical dashed line).

Table B.15. Daily analysis of irrigation treatment effects on NIR GreenDiff VI in 2015.

Treatment*	Date (2015)									
	6/19	6/25	7/13	7/23	7/28	7/31	8/7	8/11	8/21	8/31
100	-0.759	-0.728	-0.671B	-0.716B	-0.666AB	-0.669AB	-0.670AB	-0.647B	-0.659AB	-0.664A
80	-0.772	-0.738	-0.668B	-0.707B	-0.659AB	-0.658AB	-0.66AB	-0.633AB	-0.652AB	-0.678A
65	-0.750	-0.744	-0.638A	-0.681A	-0.626A	-0.631A	-0.622A	-0.586A	-0.622A	-0.656A
50	-0.762	-0.741	-0.664AB	-0.699AB	-0.667B	-0.666AB	-0.666AB	-0.635AB	-0.690B	-0.765B
30	-0.752	-0.742	-0.664AB	-0.706B	-0.661AB	-0.684B	-0.707B	-0.674B	-0.760C	-0.849C
15	-0.754	-0.730	-0.706C	-0.759C	-0.790C	-0.817C	-0.944C	-0.93C	-1.039D	-1.085D

* Percentage of evapotranspiration (ET) replacement. Irrigation treatments began as 25, 50, 75, 100, 125, and 150% ET on June 29; modified as 15, 30, 50, 65, 80 and 100% ET on to reflect shorter mowing height on July 17 (denoted by a vertical dashed line).

Table B.16. Daily analysis of irrigation treatment effects on $NDVI_{FS}$ (FieldScount) in 2016.

Treatment*	Date (2016)							
	6/30	7/7	7/15	7/22	7/28	8/03	8/10	8/29
100	0.76	0.79	0.78	0.80A	0.78A	0.80A	0.78A	0.72A
80	0.77	0.79	0.79	0.77A	0.71AB	0.73AB	0.71A	0.57B
65	0.76	0.80	0.79	0.74AB	0.70AB	0.73AB	0.69A	0.60AB
50	0.76	0.80	0.76	0.76A	0.63BC	0.68B	0.67A	0.50B
30	0.76	0.78	0.76	0.68BC	0.57CD	0.56C	0.50B	0.29C
15	0.76	0.77	0.76	0.62C	0.48D	0.43D	0.33C	0.22C

* Irrigation treatments began July 1.

Table B.17. Daily analysis of irrigation treatment effects on $NDVI_{RS}$ (RapidScan) in 2016.

Treatment*	Date (2016)							
	6/30	7/7	7/15	7/22	7/28	8/03	8/10	8/29
100	0.74	0.76	0.77A	0.77A	0.74A	0.74A	0.70A	0.58A
80	0.73	0.74	0.75AB	0.72AB	0.66AB	0.66AB	0.58B	0.41B
65	0.73	0.74	0.75AB	0.69B	0.63B	0.62B	0.55B	0.38B
50	0.74	0.75	0.75AB	0.70AB	0.62B	0.59B	0.53B	0.35BC
30	0.73	0.73	0.70BC	0.60C	0.49C	0.45C	0.39C	0.26BC
15	0.73	0.71	0.69C	0.58C	0.42C	0.36C	0.29C	0.23C

* Irrigation treatments began July 1.

Table B.18. Daily analysis of irrigation treatment effects on NDRE (RapidScan) in 2016.

Treatment*	Date (2016)							
	6/30	7/7	7/15	7/22	7/28	8/3	8/10	8/31
100	0.28	0.29	0.30	0.31A	0.28A	0.30A	0.28A	0.24A
80	0.28	0.29	0.28	0.28AB	0.25AB	0.27AB	0.23AB	0.17B
65	0.27	0.29	0.28	0.27BC	0.24B	0.26B	0.22B	0.16BC
50	0.28	0.29	0.28	0.27ABC	0.24B	0.25B	0.21BC	0.15BC
30	0.27	0.28	0.27	0.24CD	0.19C	0.19C	0.17CD	0.12BC
15	0.27	0.28	0.26	0.23D	0.17C	0.16C	0.13D	0.11C

* Irrigation treatments began July 1.

Table B.19. Daily analysis of irrigation treatment effects on red edge (RapidScan) in 2016.

Treatment*	Date (2016)							
	6/30	7/7	7/15	7/22	7/28	8/3	8/10	8/29
100	20.0	19.9	19.8	19.6D	20.0B	19.7C	20.0D	20.6C
80	20.1	19.9	19.9	20.0CD	20.6B	20.1BC	20.6CD	21.6B
65	20.1	19.9	20.0	20.1BC	20.5B	20.3BC	20.8C	21.7B
50	20.0	19.9	20.0	20.1BCD	20.6B	20.5B	21.0BC	21.9AB
30	20.1	20.0	20.2	20.6AB	21.3A	21.2A	21.7AB	22.4AB
15	20.1	20.1	20.2	20.7A	21.6A	21.7A	22.2A	22.6A

* Irrigation treatments began July 1.

Table B.20. Daily analysis of irrigation treatment effects on NIR_{RS} (RapidScan) in 2016.

Treatment*	Date (2016)							
	6/30	7/7	7/15	7/22	7/28	8/3	8/10	8/29
100	35.7	36.4	36.6	37.3A	35.8A	37.0A	35.6A	33.7A
80	35.4	36.0	35.9	35.9AB	34.1AB	35.3AB	33.3B	30.7B
65	35.3	36.0	35.7	35.1BC	33.6B	34.6B	32.8B	30.2BC
50	35.5	36.2	35.7	35.2BC	33.3BC	33.9B	32.2BC	29.7BC
30	35.2	35.7	34.9	33.5CD	31.3CD	31.5C	30.3CD	28.5BC
15	35.3	35.4	34.7	32.9D	30.4D	30.1C	28.8D	28.0C

* Irrigation treatments began July 1.

Table B.21. Daily analysis of irrigation treatment effects on red (RapidScan) in 2016.

Treatment*	Date (2016)							
	6/30	7/7	7/15	7/22	7/28	8/3	8/10	8/29
100	5.4	5.0	4.6C	4.8B	5.3C	5.6C	6.3C	8.9C
80	5.4	5.4	5.1C	5.9B	7.0BC	7.1BC	8.8BC	13.1B
65	5.5	5.4	5.2BC	6.4B	7.6B	8.0B	9.6B	13.7B
50	5.4	5.2	5.2BC	6.3B	7.6B	8.7B	10.0B	14.4AB
30	5.5	5.6	6.2AB	8.3A	10.7A	12.0A	13.3A	16.6AB
15	5.6	5.9	6.4A	8.8A	12.5A	14.2A	15.8A	17.6A

* Irrigation treatments began July 1.

Table B.22. Daily analysis of irrigation treatment effects on soil volumetric water content (%) in 2016.

Treatment*	Date (2016)							
	6/27	7/7	7/15	7/22	7/28	8/03	8/10	8/29
100	48.5	44.0	45.1A	37.4A	49.6A	44.1A	45.0A	43.0A
80	44.7	40.5	38.3AB	30.1ABC	43.6AB	36.7B	37.1B	42.9A
65	46.7	39.7	40.5AB	32.9AB	43.5AB	31.4B	33.6BC	38.3B
50	46.2	39.1	35.9ABC	28.9DBC	36.4BC	30.4B	27.7CD	30.5C
30	46.7	35.9	33.0BC	23.7CD	29.9CD	22.4C	23.8D	29.3C
15	46.4	34.4	27.3C	21.8D	26.4D	21.9C	20.1D	23.3D

* Irrigation treatments began July 1.

Table B.23. Daily analysis of irrigation treatment effects on soil temperature (°C) in 2016.

Treatment*	Date (2016)							
	6/27	7/7	7/15	7/22	7/28	8/3	8/10	8/29
100	31.7	32.0	29.2	32.5	30.7	26.8	27.8BC	30.0BC
80	31.8	32.1	29.2	32.6	30.7	26.7	27.7C	29.6C
65	31.8	32.4	29.1	32.6	31.0	26.8	28.0AB	29.9BC
50	31.6	32.2	29.4	32.8	30.8	26.7	27.8BC	29.9BC
30	31.8	32.0	29.4	33.1	31.3	26.6	27.9BC	30.3B
15	31.5	32.3	29.3	33.2	31.0	25.8	28.3A	31.2A

* Irrigation treatments began July 1.

Table B.24. Daily analysis of irrigation treatment effects on visual quality in 2016.

Treatment*	Date (2016)							
	6/29	7/7	7/15	7/22	7/28	8/03	8/10	8/29
100	6.6	7.3	7.8	7.5A	8.0A	8.1A	7.8A	6.6A
80	6.6	7.0	6.8	6.5AB	6.6AB	7.1AB	6.4AB	4.8AB
65	6.8	7.3	6.8	6.5AB	6.1B	6.5B	6.0B	4.8AB
50	6.6	7.0	6.3	5.5BC	5.6BC	6.0B	5.6B	3.8BC
30	6.6	6.5	5.8	4.5C	4.5CD	4.4C	4.0C	2.1CD
15	6.5	6.0	5.3	4.0C	3.6D	3.3C	2.3D	1.1D

* Irrigation treatments began July 1.

Table B.25. Daily analysis of irrigation treatment effects on Percentage Green Cover in 2016.

Treatment*	Date (2016)							
	6/27	7/7	7/15	7/22	7/28	8/03	8/10	8/29
100	85.6	90.6	92.7	94.3A	89.8A	89.6A	86.3A	67.9A
80	83.8	88.1	83.4	83.5A	67.4AB	74.2AB	55.8AB	29.8B
65	86.9	87.5	85.3	80.0A	59.5B	67.2AB	62.7A	27.7B
50	85.5	83.3	78.5	79.3A	58.4B	54.8B	60.2AB	19.0B
30	83.5	82.5	68.7	42.8B	20.5C	23.4C	30.5BC	4.9B
15	83.9	85.0	75.7	50.0B	10.5C	7.3C	2.7C	0.1B

* Irrigation treatments began July 1.

Table B.26. Daily analysis of irrigation treatment effects on Blue Band in 2016.

Treatment*	Date (2016)							
	6/28	7/07	7/15	7/22	7/28	8/3	8/10	8/29
100	136.2	144.1	147.9	129.5C	132.1C	133.6C	124.1C	141.8D
80	136.0	145.4	148.7	131.3BC	134.0BC	139.2BC	133.7BC	171.3BC
65	133.2	142.1	145.3	129.7C	132.2C	137.4BC	132.9BC	163.3CD
50	135.5	144.7	146.9	132.6BC	134.4BC	141.4B	136.6B	173.4ABC
30	134.7	143.9	145.8	137.2AB	139.1AB	151.2A	149.6A	190.6AB
15	135.0	145.0	147.1	139.2A	142.6A	155.7A	158.4A	194.5A

* Irrigation treatments began July 1.

Table B.27. Daily analysis of irrigation treatment effects on Green Band in 2016.

Treatment*	Date (2016)							
	6/28	7/07	7/15	7/22	7/28	8/3	8/10	8/29
100	98.7	111.5	112.4A	97.9	101.2A	101.5	93.7C	100.5C
80	98.6	112.2	111.9A	97.4	99.6AB	101.9	96.2BC	114.1AB
65	97.0	109.6	109.7AB	96.0	97.6BC	100.1	95.5BC	109.1BC
50	98.4	111.6	110.8A	97.8	98.3BC	101.7	96.8BC	114.2AB
30	97.6	109.8	107.6B	97.8	96.5C	103.7	100.7AB	122.4A
15	97.7	110.2	107.5B	98.0	96.6C	104.2	103.4A	123.1A

* Irrigation treatments began July 1.

Table B.28. Daily analysis of irrigation treatment effects on NIR Band in 2016.

Treatment*	Date (2016)							
	6/28	7/07	7/15	7/22	7/28	8/3	8/10	8/29
100	121.8	142.3	139.5A	125.3A	127.9A	126.8A	117.9A	115.4A
80	121.7	141.8	136.9A	121.2AB	120.8AB	119.3AB	110.2B	107.0B
65	120.5	139.2	135.3A	120.0B	118.2B	117.2B	109.5B	105.9BC
50	121.7	141.1	136.4A	120.5AB	117.2B	115.3B	107.3B	104.0BC
30	120.1	137.4	129.6B	114.1C	105.4C	104.6C	97.5C	98.8CD
15	120.2	137.2	128.1B	112.1C	100.8C	98.6C	90.1C	93.2D

* Irrigation treatments began July 1.

Table B.29. Daily analysis of irrigation treatment effects on NDVI Enhanced1 in 2016.

Treatment*	Date (2016)							
	6/28	7/07	7/15	7/22	7/28	8/3	8/10	8/29
100	-0.105	-0.064	-0.080A	-0.074A	-0.071A	-0.078A	-0.079A	-0.135A
80	-0.105	-0.068	-0.089AB	-0.091A	-0.098AB	-0.114AB	-0.128B	-0.210BC
65	-0.101	-0.067	-0.085A	-0.091A	-0.102AB	-0.117B	-0.129B	-0.204B
50	-0.104	-0.068	-0.086AB	-0.097A	-0.110B	-0.131B	-0.144B	-0.227BCD
30	-0.106	-0.076	-0.103BC	-0.128B	-0.159C	-0.184C	-0.202C	-0.265CD
15	-0.107	-0.079	-0.111C	-0.139B	-0.182C	-0.211C	-0.242C	-0.285D

* Irrigation treatments began July 1.

Table B.30. Daily analysis of irrigation treatment effects on NDVI Enhanced2 in 2016.

Treatment*	Date (2016)							
	6/28	7/07	7/15	7/22	7/28	8/3	8/10	8/29
100	0.236	0.276	0.260A	0.266A	0.269A	0.262A	0.261A	0.208A
80	0.237	0.272	0.252AB	0.250A	0.244AB	0.227AB	0.214B	0.131BC
65	0.240	0.273	0.256A	0.250A	0.240AB	0.225B	0.214B	0.138B
50	0.238	0.272	0.254AB	0.244A	0.232B	0.211B	0.199B	0.115BC
30	0.235	0.264	0.239BC	0.214B	0.184C	0.159C	0.141C	0.075CD
15	0.235	0.261	0.231C	0.203B	0.161C	0.131C	0.100C	0.053D

* Irrigation treatments began July 1.

Table B.31. Daily analysis of irrigation treatment effects on NDVI Enhanced3 in 2016.

Treatment*	Date (2016)							
	6/28	7/07	7/15	7/22	7/28	8/3	8/10	8/29
100	-0.317	-0.285	-0.302A	-0.289A	-0.292A	-0.299A	-0.298A	-0.354A
80	-0.317	-0.290	-0.311AB	-0.307A	-0.319AB	-0.338AB	-0.352B	-0.450BC
65	-0.313	-0.288	-0.307AB	-0.306A	-0.321AB	-0.340AB	-0.352B	-0.439B
50	-0.315	-0.290	-0.308AB	-0.313A	-0.330B	-0.356B	-0.370B	-0.468BC
30	-0.318	-0.297	-0.323BC	-0.346B	-0.382C	-0.418C	-0.438C	-0.519CD
15	-0.319	-0.301	-0.331C	-0.358B	-0.407C	-0.450C	-0.488C	-0.546D

* Irrigation treatments began July 1.

Table B.32. Daily analysis of irrigation treatment effects on Blue NDVI in 2016.

Treatment*	Date (2016)							
	6/28	7/07	7/15	7/22	7/28	8/3	8/10	8/29
100	-0.056	-0.006	-0.029A	-0.016A	-0.016A	-0.026A	-0.026A	-0.102A
80	-0.055	-0.013	-0.041AB	-0.040A	-0.052AB	-0.077AB	-0.097B	-0.226BC
65	-0.050	-0.010	-0.036AB	-0.039A	-0.056AB	-0.080AB	-0.096B	-0.212B
50	-0.054	-0.013	-0.037AB	-0.048A	-0.069B	-0.101B	-0.120B	-0.249BC
30	-0.057	-0.023	-0.059BC	-0.091B	-0.138C	-0.182C	-0.209C	-0.316CD
15	-0.058	-0.027	-0.069C	-0.107B	-0.171C	-0.224C	-0.275C	-0.352D

* Irrigation treatments began July 1.

Table B.33. Daily analysis of irrigation treatment effects on Green NDVI in 2016.

Treatment*	Date (2016)							
	6/28	7/07	7/15	7/22	7/28	8/3	8/10	8/29
100	0.105	0.122	0.108	0.123A	0.117A	0.111A	0.114A	0.070A
80	0.105	0.116	0.100	0.109A	0.095A	0.078AB	0.067AB	-0.032BC
65	0.108	0.119	0.104	0.111A	0.095A	0.078AB	0.068AB	-0.015B
50	0.106	0.117	0.103	0.104AB	0.088A	0.063B	0.051B	-0.046BC
30	0.103	0.112	0.092	0.077BC	0.043B	0.004C	-0.016C	-0.106CD
15	0.103	0.109	0.087	0.067C	0.022B	-0.028C	-0.068D	-0.138D

* Irrigation treatments began July 1.

Table B.34. Daily analysis of irrigation treatment effects on GreenBlue VI in 2016.

Treatment*	Date (2016)							
	6/28	7/07	7/15	7/22	7/28	8/3	8/10	8/29
100	-0.160	-0.128A	-0.136A	-0.139A	-0.132A	-0.137A	-0.140A	-0.170A
80	-0.160	-0.129A	-0.141A	-0.148A	-0.147AB	-0.155B	-0.163B	-0.198B
65	-0.157	-0.129A	-0.139A	-0.149A	-0.151B	-0.157B	-0.163B	-0.198B
50	-0.159	-0.129A	-0.140A	-0.151A	-0.155B	-0.163B	-0.170B	-0.205BC
30	-0.160	-0.134B	-0.151B	-0.167B	-0.180C	-0.186C	-0.195C	-0.218BC
15	-0.160	-0.136B	-0.155B	-0.174B	-0.192C	-0.198C	-0.210C	-0.225C

* Irrigation treatments began July 1.

Table B.35. Daily analysis of irrigation treatment effects on NIR BlueRatio VI in 2016.

Treatment*	Date (2016)							
	6/28	7/07	7/15	7/22	7/28	8/3	8/10	8/29
100	-14.4	-1.8	-8.4A	-4.2A	-4.1A	-6.8A	-6.2A	-26.4A
80	-14.3	-3.7	-11.8AB	-10.0A	-13.2AB	-19.9AB	-23.6AB	-64.4BC
65	-12.7	-3.0	-10.0AB	-9.7A	-14.0AB	-20.3AB	-23.4AB	-57.4B
50	-13.8	-3.6	-10.5AB	-12.1A	-17.2B	-26.1B	-29.3B	-69.4BC
30	-14.7	-6.4	-16.3BC	-23.1B	-33.7C	-46.6C	-52.1C	-91.9CD
15	-14.8	-7.8	-19.1C	-27.2B	-41.8C	-57.1C	-68.3C	-101.3D

* Irrigation treatments began July 1.

Table B.36. Daily analysis of irrigation treatment effects on NIR GreenDiff VI in 2016.

Treatment*	Date (2016)							
	6/28	7/07	7/15	7/22	7/28	8/3	8/10	8/29
100	-0.710	-0.647	-0.690	-0.650A	-0.664A	-0.681A	-0.674A	-0.808A
80	-0.709	-0.663	-0.713	-0.692A	-0.728A	-0.779AB	-0.812AB	-1.081BC
65	-0.699	-0.656	-0.701	-0.689A	-0.731A	-0.780AB	-0.809AB	-1.039B
50	-0.706	-0.661	-0.704	-0.708A	-0.754A	-0.824B	-0.857B	-1.124BC
30	-0.714	-0.678	-0.739	-0.787B	-0.881B	-0.989C	-1.042C	-1.281CD
15	-0.714	-0.686	-0.755	-0.816B	-0.942B	-1.074C	-1.183C	-1.362D

* Irrigation treatments began July 1.

Table B.37. Daily analysis of irrigation treatment effects on $NDVI_{FS}$ (FieldScount) in 2017.

Treatment*	Date (2017)							
	6/07	6/15	6/20	7/1	7/10	7/25	8/4	8/31
100	0.78	0.83BC	0.82A	0.83A	0.85A	0.84A	0.86A	0.81A
80	0.80	0.86A	0.84A	0.86A	0.84A	0.84A	0.86A	0.77A
65	0.78	0.83ABC	0.82A	0.84A	0.83A	0.81A	0.84A	0.79A
50	0.81	0.86AB	0.82A	0.84A	0.84A	0.77AB	0.82A	0.73A
30	0.80	0.84AB	0.81A	0.83A	0.75B	0.65BC	0.66B	0.56B
15	0.77	0.81C	0.74B	0.74B	0.66C	0.53C	0.52C	0.56B

* Irrigation treatments began June 9.

Table B.38. Daily analysis of irrigation treatment effects on $NDVI_{RS}$ (RapidScan) in 2017.

Treatment*	Date (2017)							
	6/07	6/15	6/20	7/1	7/10	7/25	8/4	8/31
100	0.74	0.78A	0.79AB	0.81A	0.83A	0.8A	0.82A	0.78A
80	0.77	0.81A	0.82A	0.83A	0.84A	0.8A	0.82A	0.71AB
65	0.75	0.78A	0.79AB	0.80AB	0.82A	0.76A	0.78A	0.75AB
50	0.76	0.80A	0.80AB	0.79AB	0.80A	0.70A	0.69AB	0.66B
30	0.77	0.79A	0.78B	0.74BC	0.69B	0.56B	0.56BC	0.53C
15	0.74	0.75B	0.73C	0.69C	0.62B	0.45B	0.43C	0.51C

* Irrigation treatments began June 9.

Table B.39. Daily analysis of irrigation treatment effects on NDRE (RapidScan) in 2017.

Treatment*	Date (2017)							
	6/07	6/15	6/20	7/1	7/10	7/25	8/4	8/31
100	0.28	0.30	0.31BC	0.33AB	0.34A	0.32A	0.33A	0.30A
80	0.30	0.33	0.33A	0.34A	0.35A	0.32A	0.33A	0.27AB
65	0.29	0.31	0.31ABC	0.33AB	0.33A	0.30A	0.31A	0.29AB
50	0.30	0.32	0.33AB	0.32AB	0.33A	0.27A	0.27A	0.25B
30	0.30	0.32	0.32ABC	0.31BC	0.28B	0.22B	0.21B	0.20C
15	0.28	0.30	0.29C	0.28C	0.25B	0.18B	0.16B	0.19C

* Irrigation treatments began June 9.

Table B.40. Daily analysis of irrigation treatment effects on red edge (RapidScan) in 2017.

Treatment*	Date (2017)							
	6/07	6/15	6/20	7/1	7/10	7/25	8/4	8/31
100	20.0	19.7	19.8AB	19.4BC	19.3B	19.5B	19.4C	19.7B
80	19.8	19.4	19.4C	19.2C	19.2B	19.4B	19.4C	20.1B
65	20.0	19.6	19.6ABC	19.4BC	19.3B	19.7B	19.7C	19.9B
50	19.8	19.5	19.4BC	19.5BC	19.3B	20.1B	20.2BC	20.4B
30	19.8	19.4	19.5ABC	19.7AB	20.0A	20.8A	21.0AB	21.2A
15	20.0	19.8	19.8A	20.0A	20.5A	21.4A	21.8A	21.2A

* Irrigation treatments began June 9.

Table B.41. Daily analysis of irrigation treatment effects on NIR_{RS} (RapidScan) in 2017.

Treatment*	Date (2017)							
	6/07	6/15	6/20	7/1	7/10	7/25	8/4	8/31
100	35.6	37.0BC	37.3BC	38.6AB	39.1A	38.1A	38.6A	36.7A
80	36.7	38.5A	38.6A	39.3A	39.6A	38.0A	38.6A	35.2AB
65	35.9	37.4ABC	37.3BC	38.3AB	38.7A	36.9AB	37.3AB	35.9AB
50	36.6	38.1AB	38.3AB	38.0AB	38.8A	35.3B	35.4B	34.2B
30	36.7	38.1AB	37.7ABC	37.3B	35.7B	32.7C	32.4C	31.7C
15	35.6	36.6C	36.4C	35.5C	33.9B	30.9C	30.1C	31.5C

* Irrigation treatments began June 9.

Table B.42. Daily analysis of irrigation treatment effects on red (RapidScan) in 2017.

Treatment*	Date (2017)							
	6/07	6/15	6/20	7/1	7/10	7/25	8/4	8/31
100	5.3	4.5B	4.4BC	3.9C	3.7B	4.2B	3.8C	4.5B
80	4.8	4.0B	3.9C	3.7C	3.5B	4.2B	3.9C	6.0B
65	5.1	4.6B	4.5BC	4.2C	3.9B	4.9B	4.5C	5.2B
50	4.9	4.3B	4.1BC	4.5BC	4.2B	6.2B	6.4BC	7.0B
30	4.7	4.4B	4.7B	5.5AB	6.5A	9.2A	9.2AB	9.8A
15	5.4	5.3A	5.6A	6.5A	8.0A	11.7A	12.1A	10.3A

* Irrigation treatments began June 9.

Table B.43. Daily analysis of irrigation treatment effects on visual quality in 2017.

Treatment*	Date (2017)							
	6/07	6/15	6/20	7/1	7/10	7/25	8/4	8/31
100	7.1	7.3	7.6	8.1A	8.6A	7.9A	8.3A	7.4A
80	8.0	8.0	8.8	8.6A	8.9A	8.5A	8.5A	5.6BC
65	7.3	7.6	7.9	7.8A	7.6AB	7.3A	7.8A	6.5AB
50	8.3	7.9	8.4	8.0A	7.3B	5.6B	6.0B	4.5CD
30	7.8	8.0	7.9	6.1B	5.1C	4.0C	4.5BC	3.4DE
15	7.1	6.6	6.9	5.6B	4.3C	3.1C	3.4C	2.8E

* Irrigation treatments began June 9.

Table B.44. Daily analysis of irrigation treatment effects on soil temperature (°C) in 2017.

Treatment*	Date (2017)							
	6/07	6/15	6/20	7/1	7/10	7/25	8/4	8/31
100	27.5	28.7ABC	25.7	27.0C	30.2C	30.8B	26.4B	25.0
80	27.4	28.2C	25.9	26.8C	30.2C	30.5B	26.4B	25.0
65	27.3	28.7AB	25.7	27.0BC	30.7BC	30.8B	26.3B	25.1
50	27.4	28.4BC	26.0	26.8C	30.5BC	31.1B	26.3B	25.3
30	27.4	28.9A	26.0	27.5AB	30.9B	31.7A	26.7A	25.4
15	27.2	28.8AB	26.0	28.0A	31.8A	31.9A	26.9A	25.7

* Irrigation treatments began June 9.

Table B.45. Daily analysis of irrigation treatment effects on soil volumetric water content (%) in 2017.

Treatment*	Date (2017)							
	6/07	6/15	6/20	7/1	7/10	7/25	8/4	8/31
100	45.4	45.2A	42.8A	41.7A	47.6A	42.5A	46.3A	38.8A
80	45.3	43.8A	42.3A	41.4A	46.9A	40.9A	43.9AB	34.4B
65	44.9	40.7A	38.5B	39.2A	47.0A	38.6A	44.5AB	34.9AB
50	45.2	40.9A	39.8AB	39.3A	44.0A	33.3B	41.4BC	28.1C
30	46.1	34.3B	27.9C	27.4B	34.2B	24.7C	37.1CD	22.0D
15	44.5	29.4C	24.9C	22.9C	27.0C	20.9C	33.4D	18.0D

* Irrigation treatments began June 9.

Table B.46. Daily analysis of irrigation treatment effects on Percentage Green Cover in 2017.

Treatment*	Date (2017)							
	6/07	6/15	6/20	7/1	7/10	7/25	8/4	8/31
100	82.5	90.5AB	91.2A	98.0A	97.7AB	96.4A	98.8A	89.3A
80	90.8	95.6A	95.8A	99.0A	99.1A	97.5A	99.5A	67.0AB
65	87.5	92.5A	94.1A	98.2A	97.6AB	95.7A	98.3A	85.5A
50	90.9	94.9A	95.6A	98.5A	98.4AB	88.3A	96.8A	64.9AB
30	92.0	93.8A	92.5A	90.7B	72.9BC	49.3B	57.3B	26.4C
15	83.0	84.5B	83.1B	85.2B	53.0C	36.8B	35.1B	38.2BC

* Irrigation treatments began June 9.

Table B.47. Daily analysis of irrigation treatment effects on Blue Band in 2017.

Treatment*	Date (2017)							
	6/07	6/15	6/20	7/1	7/10	7/25	8/4	8/31
100	193.8	208.4	208.5	197.3BC	189.2BC	202.0C	181.8B	204.1B
80	193.8	205.9	206.3	195.0C	187.3C	201.4C	180.4B	206.8B
65	195.2	206.4	207.5	198.6BC	189.9BC	202.6BC	182.8B	206.1B
50	193.7	204.9	207.1	199.0BC	188.9BC	203.4BC	183.0B	210.7B
30	193.0	203.5	206.3	201.0B	192.5B	210.8B	191.4B	222.1A
15	196.2	206.4	210.7	208.5A	202.8A	221.1A	206.6A	227.1A

* Irrigation treatments began June 9.

Table B.48. Daily analysis of irrigation treatment effects on Green Band in 2017.

Treatment*	Date (2017)							
	6/07	6/15	6/20	7/1	7/10	7/25	8/4	8/31
100	149.2	173.1A	172.6A	161.2	154.7AB	172.1	150.2	159.8
80	149.9	171.0AB	171.2A	158.9	152.4ABC	171.9	148.8	158.4
65	151.1	170.1BC	170.6A	161.5	154.3AB	171.9	150.0	158.8
50	149.1	168.1CD	169.6AB	159.8	151.7BC	169.3	147.8	156.2
30	150.1	166.2DE	166.9B	158.8	150.5C	170.3	148.2	158.5
15	151.3	165.5E	166.5B	160.6	155.0A	173.9	153.3	161.3

* Irrigation treatments began June 9.

Table B.49. Daily analysis of irrigation treatment effects on NIR Band in 2017.

Treatment*	Date (2017)							
	6/07	6/15	6/20	7/1	7/10	7/25	8/4	8/31
100	170.9	200.6AB	201.0AB	194.6A	191.2A	210.1AB	193.6A	185.7A
80	175.6	202.5A	203.2A	195.1A	190.4A	211.1A	193.8A	179.9AB
65	173.8	198.9BC	199.5B	193.8A	189.4A	208.7AB	191.3A	182.3A
50	173.8	198.9BC	199.6B	191.6A	186.2A	203.6B	185.8A	170.6B
30	176.2	197.3C	196.0C	187.2B	177.5B	194.3C	172.3B	157.3C
15	172.8	191.2D	189.4D	180.0C	171.7C	185.8D	160.4C	153.4C

* Irrigation treatments began June 9.

Table B.50. Daily analysis of irrigation treatment effects on NDVI Enhanced1 in 2017.

Treatment*	Date (2017)							
	6/07	6/15	6/20	7/1	7/10	7/25	8/4	8/31
100	-0.095	-0.055A	-0.055AB	-0.051A	-0.045A	-0.028A	-0.028A	-0.083A
80	-0.087	-0.049A	-0.048A	-0.048A	-0.044A	-0.025A	-0.026A	-0.1AB
65	-0.092	-0.056A	-0.057AB	-0.056A	-0.05A	-0.031A	-0.034A	-0.094AB
50	-0.091	-0.055A	-0.057AB	-0.062AB	-0.056A	-0.043A	-0.046A	-0.126B
30	-0.084	-0.056A	-0.064B	-0.075B	-0.08B	-0.072B	-0.088B	-0.169C
15	-0.095	-0.073B	-0.084C	-0.101C	-0.108C	-0.102C	-0.136C	-0.181C

* Irrigation treatments began June 9.

Table B.51. Daily analysis of irrigation treatment effects on NDVI Enhanced2 in 2017.

Treatment*	Date (2017)							
	6/07	6/15	6/20	7/1	7/10	7/25	8/4	8/31
100	0.246	0.284A	0.284AB	0.287A	0.293A	0.309A	0.308A	0.257A
80	0.254	0.289A	0.29A	0.29A	0.293A	0.311A	0.31A	0.241AB
65	0.249	0.283A	0.281AB	0.283A	0.288A	0.305A	0.303A	0.247AB
50	0.250	0.284A	0.281AB	0.277AB	0.283A	0.294A	0.292A	0.216B
30	0.257	0.282A	0.275B	0.265B	0.26B	0.267B	0.252B	0.174C
15	0.246	0.267B	0.256C	0.241C	0.234C	0.239C	0.207C	0.162C

* Irrigation treatments began June 9.

Table B.52. Daily analysis of irrigation treatment effects on NDVI Enhanced3 in 2017.

Treatment*	Date (2017)							
	6/07	6/15	6/20	7/1	7/10	7/25	8/4	8/31
100	-0.335	-0.311AB	-0.309A	-0.296A	-0.285A	-0.281A	-0.263A	-0.324A
80	-0.324	-0.301A	-0.300A	-0.289A	-0.282A	-0.277A	-0.259A	-0.340A
65	-0.332	-0.309A	-0.309A	-0.300AB	-0.290A	-0.284A	-0.270A	-0.334A
50	-0.327	-0.304A	-0.307A	-0.304AB	-0.293A	-0.293A	-0.281A	-0.365A
30	-0.321	-0.304A	-0.311A	-0.316B	-0.318B	-0.325B	-0.327B	-0.415B
15	-0.336	-0.321B	-0.332B	-0.344C	-0.351C	-0.360C	-0.382C	-0.433B

* Irrigation treatments began June 9.

Table B.53. Daily analysis of irrigation treatment effects on Blue NDVI in 2017.

Treatment*	Date (2017)							
	6/07	6/15	6/20	7/1	7/10	7/25	8/4	8/31
100	-0.063	-0.019A	-0.018AB	-0.007A	0.005A	0.02A	0.031A	-0.047A
80	-0.049	-0.008A	-0.007A	0.0002A	0.008A	0.024A	0.036A	-0.07AB
65	-0.058	-0.018A	-0.02AB	-0.012A	-0.001A	0.015A	0.023A	-0.061AB
50	-0.054	-0.015A	-0.018AB	-0.019AB	-0.007A	0.001A	0.008A	-0.105B
30	-0.045	-0.016A	-0.026B	-0.036B	-0.041B	-0.041B	-0.053B	-0.171C
15	-0.064	-0.038B	-0.053C	-0.073C	-0.083C	-0.086C	-0.125C	-0.193C

* Irrigation treatments began June 9.

Table B.54. Daily analysis of irrigation treatment effects on Green NDVI in 2017.

Treatment*	Date (2017)							
	6/07	6/15	6/20	7/1	7/10	7/25	8/4	8/31
100	0.068	0.074	0.076AB	0.094AB	0.105A	0.1A	0.126A	0.075A
80	0.079	0.084	0.086A	0.102A	0.111A	0.103A	0.131A	0.063A
65	0.07	0.078	0.078A	0.091AB	0.102A	0.097A	0.121A	0.069A
50	0.076	0.084	0.081A	0.09AB	0.102A	0.092AB	0.114AB	0.044A
30	0.08	0.085	0.080A	0.082B	0.082B	0.066B	0.074B	-0.004B
15	0.066	0.072	0.064B	0.057C	0.051C	0.033C	0.022C	-0.025B

* Irrigation treatments began June 9.

Table B.55. Daily analysis of irrigation treatment effects on GreenBlue VI in 2017.

Treatment*	Date (2017)							
	6/07	6/15	6/20	7/1	7/10	7/25	8/4	8/31
100	-0.13	-0.093A	-0.094AB	-0.101A	-0.100A	-0.080A	-0.095A	-0.122A
80	-0.128	-0.093A	-0.093A	-0.102A	-0.103AB	-0.079A	-0.096A	-0.133A
65	-0.127	-0.096AB	-0.098BC	-0.103AB	-0.103AB	-0.082AB	-0.099A	-0.13A
50	-0.13	-0.099B	-0.099C	-0.109B	-0.109B	-0.091B	-0.107A	-0.149B
30	-0.125	-0.101B	-0.106D	-0.117C	-0.122C	-0.106C	-0.127B	-0.167C
15	-0.129	-0.110C	-0.117E	-0.13D	-0.134D	-0.119D	-0.147C	-0.169C

* Irrigation treatments began June 9.

Table B.56. Daily analysis of irrigation treatment effects on NIR BlueRatio VI in 2017.

Treatment*	Date (2017)							
	6/07	6/15	6/20	7/1	7/10	7/25	8/4	8/31
100	-22.9	-7.8A	-7.5AB	-2.6A	1.9A	8.2A	11.8A	-18.4A
80	-18.2	-3.4A	-3.0A	0.1A	3.1A	9.7A	13.4A	-26.9AB
65	-21.5	-7.4A	-8AB	-4.7A	-0.5A	6.1A	8.5A	-23.8AB
50	-19.9	-6A	-7.5AB	-7.5AB	-2.7A	0.3A	2.9A	-40.0B
30	-16.8	-6.2A	-10.3B	-13.8B	-14.9B	-16.5B	-19.1B	-64.9C
15	-23.4	-15.1B	-21.3C	-28.5C	-31.1C	-35.2C	-46.2C	-73.7C

* Irrigation treatments began June 9.

Table B.57. Daily analysis of irrigation treatment effects on NIR GreenDiff VI in 2017.

Treatment*	Date (2017)							
	6/07	6/15	6/20	7/1	7/10	7/25	8/4	8/31
100	-0.799	-0.767	-0.760A	-0.710AB	-0.677A	-0.683A	-0.615A	-0.775A
80	-0.766	-0.735	-0.731A	-0.687A	-0.663A	-0.674A	-0.601A	-0.812A
65	-0.792	-0.755	-0.755A	-0.720AB	-0.688A	-0.692A	-0.631A	-0.795A
50	-0.775	-0.739	-0.747A	-0.725AB	-0.691A	-0.711A	-0.655AB	-0.872A
30	-0.762	-0.735	-0.752A	-0.753B	-0.755B	-0.796B	-0.778B	-1.012B
15	-0.803	-0.778	-0.804B	-0.830C	-0.848C	-0.898C	-0.935C	-1.075B

* Irrigation treatments began June 9.